PRACA DYPLOMOWA

Study of diffusion of fluorescent nanoparticles inside human cell cytoplasm

Thesis by

Krzysztof Szczepański

Prepared under the supervision of

Prof. Dr hab. Robert Hołyst

Within the International PhD Studies at the

Institute of Physical Chemistry Polish Academy of Sciences

Department of Soft Condensed Matter

Kasprzaka 44/52, 01-224 Warsaw

Warsaw, July 2018

Acknowledgments

This work would not have been created without the support of several people:

My supervisor, prof. Robert Hołyst, who constantly believed that things could be done and always had time for the discussion.

Dr Karina Kwapiszewska, with whom I shared the hardships of the biological investigations and who I always saw as my unofficial supervisor.

Dr Krzysztof Sozański, who introduced me to the fluorescence correlation spectroscopy and showed the patience of a saint in the face of endless questions and problems.

Dr Tomasz Kalwarczyk, who provided the theoretical support for this work and performed all the simulations mentioned here.

Additionally, roommates from 215: Karina, Krzysiek and Agnieszka, who provided constant support and kept me laughing (and probably also sane) throughout my whole adventure in the Institute.

Finally, other members of the Soft Matter Group, for all the discussions, suggestions and help. They created truly warm and inviting atmosphere. It was my pleasure to work with you all.

This work was supported by the National Science Centre

within the Symfonia Grant 2013/08/W/NZ1/00687

NATIONAL SCIENCE CENTRE
POLAND

List of publications

Kalwarczyk, T., Kwapiszewska, K., **Szczepański, K.**, Sozański, K., Szymański, J., Michalska, B., Patalas-Krawczyk, P., Duszyński, J. and Hołyst, R. (2017) Apparent Anomalous Diffusion in the Cytoplasm of Human Cells: The Effect of Probes' Polydispersity, *J. Phys. Chem. B*, 121(42), pp. 9831–9837. doi: 10.1021/acs.jpcb.7b07158.

Kwapiszewska, K., Kalwarczyk, T., Michalska, B., **Szczepański, K.**, Szymański, J., Duszyński, J. and Hołyst, R. (2017). Novel method of quantification of protein interactions in living cells, *FEBS Journal*, 284, pp. 198–199.

Michalska, B. M., Kwapiszewska, K., Szczepanowska, J., Kalwarczyk, T., Patalas-Krawczyk, P., **Szczepański, K.**, Hołyst, R., Duszyński, J. and Szymański, J. (2018) Insight into the fission mechanism by quantitative characterization of Drp1 protein distribution in the living cell, *Sci. Rep.*, 8(1), p. 8122. doi: 10.1038/s41598-018-26578-z.

Kwapiszewska, K., Kalwarczyk, T., Michalska, B., **Szczepański, K.**, Szymański, J., Patalas-Krawczyk, P., Andryszewski, T., Iwan, M., Duszyński, J., Hołyst, R. General method for quantification of oligomerization of proteins in living cells, (submitted)

Szczepański, K., Kwapiszewska, K., Hołyst, R. Mobility of green fluorescent protein in HeLa cytoplasm during cell cycle, (submitted)

Abstract

Living organisms are extremely complicated. We, as humanity, invest a great deal of time and money into the understanding of what makes us tick. Comprehension of human physiology cannot be achieved without a properly described function of the basic constituent of life – cell. Single cells function thanks to the organized action of many distinct systems. Inside of tiny cellular volume, hundreds of different processes take place. All of them need substrates and give products, often requiring a catalyst to function. Cells maintain the homeostasis – a state in which all life functions remain in a balance. Disruption of the homeostasis triggers dysfunction and disease. Great effort was put into elucidation how, why, and when things happen inside cells. All those questions were answered by the experiments made either on whole organism, or more conveniently in a test tube. Both of those approaches are not without flaw. We shifted our attention to systems that are the middle ground thanks to the rise of the cell cultures. Now, uniform characterisation of conditions inside cytosol is necessary. This thesis aims to provide a comprehensive description of viscosity – one of the physiological values of the key importance in the living cells. Viscosity impacts vast majority, if not all, of biochemical and biophysical processes.

The complexity of cellular structure and its physiology will be presented in introductory part of this work. Also, subjects of diffusion and viscosity will be discussed. Finally, fluorescence correlation spectroscopy will be thoroughly described. Following the introduction, meticulous description of experimental procedures will be presented. Then, in part devoted to presentation and discussion of results obtained, changes of viscosity depending on the size of particles moving inside the cytoplasm of model living cells will be described. This description will be extended into several cell types representing different cancerous and healthy tissues. Fluorescence correlation spectroscopy will prove to be efficient in the elucidation of the mechanism of oligomerization of dynamin-related protein 1. Finally, investigations concerning changes of viscosity of the cytoplasm of cells undergoing cell cycle is going to be presented. The work will end with a short summary.

Streszczenie

Organizmy żywe są niezwykle skomplikowane. Ludzkość inwestuje ogromną ilość czasu i pieniędzy w wyjaśnienie tego, co sprawia, że funkcjonujemy. Zrozumienie ludzkiej fizjologii nie może zostać osiągnięte bez właściwego opisu podstawowej jednostki życia – komórki. Komórki działają dzięki zorganizowanemu współgraniu wielu odrębnych układów. Wewnątrz ich niewielkiej objętości zachodzą setki procesów. Każdy z nich potrzebuje substratów oraz daje produkty, częstokroć w obecności katalizatora. Komórki utrzymują stan homeostazy, w którym wszystkie procesy życiowe pozostają w równowadze, a którego zaburzenie skutkuje chorobą. Ogromny wysiłek został włożony w wyjaśnienie, jak, dlaczego i kiedy procesy zachodzą w komórkach. Na wszystkie te pytania szukano odpowiedzi albo badając cały organizm, albo w czasie prostszych doświadczeń w probówce. Oba te podejścia nie są pozbawione wad. Wraz z rozwojem hodowli komórkowych, uwaga skupiła się na nich, jako pośrednim rozwiązaniu. Teraz jednorodny opis warunków panujących wewnątrz komórek jest wymagany. Obecna praca ma na celu stworzenie wyczerpującego opisu lepkości – jednej z głównych wielkości istotnych z perspektywy wnętrza żywych komórek. Lepkość wpływa na większość, jeśli nie wszystkie procesy biochemiczne i biofizyczne.

We wprowadzeniu do tej pracy przedstawiona zostanie złożoność struktur wewnątrzkomórkowych oraz fizjologii komórek. Dodatkowo zostaną poruszone tematy dyfuzji i lepkości. Wstęp zakończy dogłębny opis spektroskopii korelacji fluorescencji. Następnie skrupulatnie opisane zostaną wszystkie procedury eksperymentalne. W części poświęconej przedstawieniu i omówieniu otrzymanych wyników opisane zostaną zmiany lepkości w zależności od wielkości próbnika poruszającego się wewnątrz modelowych żywych komórek. Opis ten zostanie następnie poszerzony o kilka typów komórek reprezentujących zdrowe i nowotworowo zmienione tkanki. Spektroskopia korelacji fluorescencji zostanie dalej wykorzystana do opisu oligomeryzacji białka Drp1. Jako ostatnie zaprezentowane zostaną doświadczenia dotyczące zmian lepkości w komórkach w czasie cyklu komórkowego. Pracę zakończy krótkie podsumowanie.

Table of Contents

Introduction

1.1.Human cells

Humans (*Homo sapiens*) belong to the domain of Eukaryota. Eukaryotic cells store their genetic material in a separate compartment enclosed by membranes, called nucleus and partially in mitochondria. They evolved, according to endosymbiotic theory, from prokaryotic cells, which now remain in an unbreakable symbiotic relation with eukaryotic counterparts. This unique relation required the development of an efficient way of cooperation permitting a great deal of autonomy of compartments. Compartmentalisation is required for not only the need for taming the "external forces". Many processes taking place inside the cell are separated spatially. Compartments may serve as a safety measure, for example, when environment needed for a given process lies far from the physiological one and could be destructive (e.g. endocytosis and digestion). The elaborate internal cellular membrane system is necessary for the protein production and secretion. Apart from the organelles and the membranes also the cytoskeleton is present in eukaryotic cells. It forms the main trafficking routes inside the cytosol and also allows reshaping of cells and their movement. A huge variety of smaller cellular elements like vesicles, proteins, and their complexes are present in-between bigger components. Each of them has its destination, function, and permanence. This thesis aims to elucidate some of the processes constituting the life of a human cell.

1.1.1. Cell cultures

The human organism is an extremely complicated system with different levels of the organisation. Groups of organs maintain systems (like the respiratory or the digestive tract), while a single organ is composed of a number of different tissues. Cells are therefore involved in a huge network of interactions and interplays. Studies of such complicated systems are virtually impossible. The vast majority of knowledge about the cellular physiology is obtained by studying the isolated cells *in vitro* (Latin for "in glass"). Such studies are usually performed using the cell lines. The cell line is defined as a population of cells having the same genetic makeup descending from a single cell. Maintenance of the cell lines in a laboratory is called cell culture. Cells are grown under closely monitored conditions (osmotic pressure, pH, temperature, atmosphere composition). These cells are usually cultured in bottles as either an adherent monolayer or suspensions (depending on the cell type) in specialised media

(containing essential nutrients, growth factors, etc.) and in incubators (Alberts *et al.*, 2008).

Adherent cell cultures are the most commonly used method of conducting research concerning the eukaryotic cells because they are simple to handle Alas, they poorly reflect the conditions in which cells grow and function as a part of a tissue (*in vivo*, from Latin "within living"). The comparison of the conditions of *in vitro* and *in vivo* is shown in Table 1.

In vivo	*In vitro*
Three-dimensional protein scaffolding	Flat culture surface
Extracellular matrix with the ability to adsorb secretion products (e.g. growth factors)	Glass or polymer, native or modified
Presence of different kinds of cells in environment	Monocultures – no interactions between different cell types Co-cultures – restricted interactions
Numerous spatial connections between cells	No connections
Small inter-cell fluid volumes enabling paracrine signalling	Great volume of culture medium, paracrine signals diluted
A continuous supply of nutrients and oxygen, and removal of metabolites	Periodic exchange of culture medium
Constant, stable hydrodynamic stress	Static conditions during incubation and extremely high short-term stress during passages

Table 1. Comparison of the conditions of growth of cells in the organism (*in vivo*) and in the cell cultures (*in vitro*).

Modifications of cellular morphology and function are common in cell cultures. Changes between the conditions in the tissue and in the culture can even influence gene expression (Griffith and Swartz, 2006). But still, the standard cell cultures remain the main method of studying the cell physiology. Fortunately, usage of primary cell lines (cells shortly after isolation from healthy tissues) offers a partial solution to those problems (Guillouzo and Guguen-Guillouzo, 2008).

The meaning of the terms *in vivo* and *in vitro* can differ depending on the branch of science. In biochemistry for example *in vitro* denotes experiments and observations coming from the reactions performed in a test tube, while *in vivo* is used for analogous measurements done in cell cultures. Throughout this thesis this meaning, different from biological one will be used.

1.1.2. Structure of the cytoplasm

The interior of any eukaryotic cell is highly compartmentalised. Most cellular functions are separated in space and restricted to the specialised organelles. This restriction allows precise control of ongoing processes. The compartmentalisation also prevents interferences between enzymes needed in one part of a cell with biochemical pathways of another (Alberts *et al.*, 2008). The overall structure of the cytoplasm cannot be discussed without mentioning all its constituents. Schematic representation of the structure of the eukaryotic (mammalian) cell is shown in Figure 1.

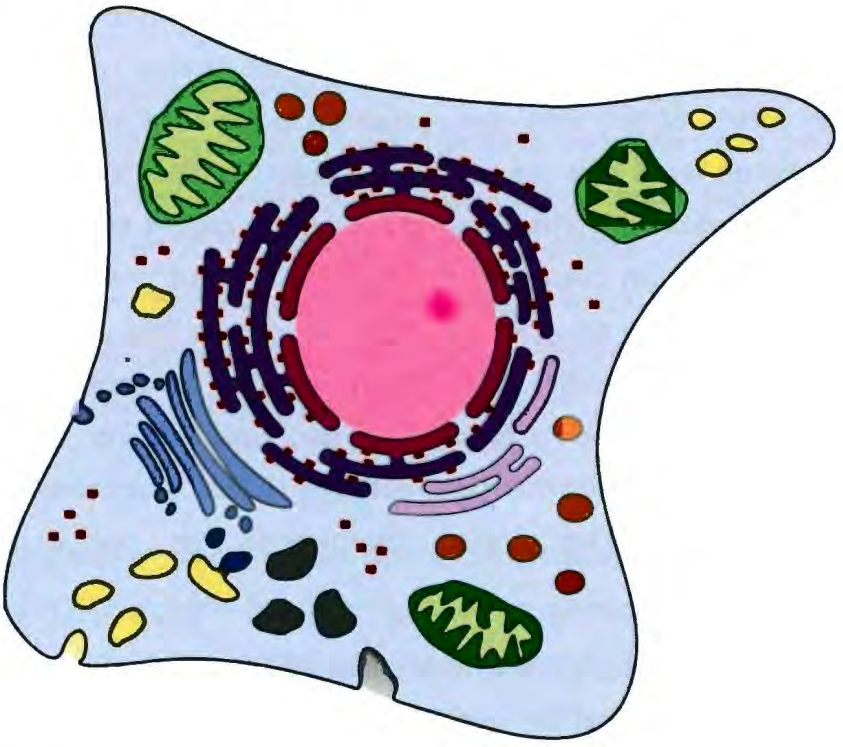

Figure 1. Structure of mammalian cell. All of the most important organelles (excluding cytoskeleton) are shown (detailed description is in the text):
Grey lines represent lipid bilayers (membranes) surrounding entire cell and individual organelles.
The nucleus (pink) – located in the middle of the cell stores DNA. Inside the nucleus, the nucleolus can be distinguished.

The nuclear envelope (dark pink) – a double membrane enclosing nuclear content. Outer nuclear membrane smoothly joins with the endoplasmic reticulum.
Rough endoplasmic reticulum (purple) – responsible for the synthesis, processing, and sorting of proteins. Richly decorated with ribosomes (red)
Smooth endoplasmic reticulum (light violet) – a place of lipid synthesis.
The Golgi apparatus (blue) – processes and sorts proteins produced on rough ER, and then secretes them inside secretory vesicles.
Endosomes – vesicles transporting either proteins produced by the cell (dark blue) or uptaken material from the outside (yellow).
Lysosomes (grey bodies) – responsible for the digestion of material.
Peroxisomes (orange) – detoxify various molecules and decompose fatty acids.
Mitochondria (green) – surrounded by a double lipid bilayer produce energy (in form of ATP) by the oxidation of glucose and fatty acids.

Nucleus

The nucleus is the biggest organelle taking up to 10 % of the total volume of the cell. It was the first organelle to be observed (by Antonie van Leeuwenhoek in 1719). This compartment of the cell concentrates vast majority of cell DNA (DNA is also present in mitochondria in human cells) and its function is focused around the DNA handling. Inside the nucleus, polymerases and other specialised enzymes transcribe information encoded inside nucleotide sequence into RNA. Other kinds of proteins are responsible for RNA strands modification to ensure the accuracy of the message conveyed by the RNA. In the nucleus additional structure can be distinguished, which is called the nucleolus, where tightly packed RNA/protein complexes are modified and prepared for shipment out of the nucleus to form ribosomes. DNA present in the nucleus is enclosed by the nuclear envelope together with the molecular machinery needed for its upkeep. The nuclear envelope is formed by two lipid bilayer membranes. The outer nuclear membrane is directly connected with the extensive network of the endoplasmic reticulum. The inner membrane is connected to DNA inside the nucleus.

Inside the nuclear membrane, there are huge protein complexes called the nuclear pores. Each of them is created by 50–100 different proteins called nucleoporins, which together create enormous (~125 million daltons) ring-like structures (Doye and Hurt, 1997). These complexes provide a way to exchange the material with the rest of the cell. This exchange is required for proper function of the nucleus. The nuclear pores are remarkably selective. They act as if they had a diameter of ~0.9 nm. Only the water, ions, small metabolites and globular proteins of less than ~60 kDa can freely diffuse through the channel

created by the nuclear pore complex. Thus small molecules can freely diffuse in and out of the nucleus. Movement of bigger molecules is subjected to the stringent control provided by the nuclear pores. Any big particle that should be transported across the nuclear envelope has either nuclear-localization signal (import into the nucleus) or nuclear-export signal (transport from the nucleus). These molecular tags allow transport through the nuclear pores. This process requires specialised groups of proteins – karyopharins (Lamond, 1998).

Endoplasmic reticulum

Endoplasmic reticulum (ER) is a vast network of interconnected membranes. ER constitutes more than a half of the total membranes present in a cell. It is a netlike labyrinth of tubules and flattened structures called the cisternae. Some crucial functions of the cell take place in this organelle. Two types of the endoplasmic reticulum can be distinguished depending on its function: smooth and rough. The smooth ER lacks the ribosomes and is the place where synthesis of phospholipids and fatty acids ensues. Rough ER is densely decorated with the ribosomes. Here, many plasma-membrane, organelle, extracellular and almost all secreted proteins are synthesised. Also, specialised excreted proteins (like antibodies and digestive enzymes) are produced on the rough ER. Maturation of around one-third of all proteins takes place inside the ER cisternae (Lodish *et al.*, 2000). The maturated proteins either destined to the membranes or for secretion are packed into transport vesicles (small structures consisting of liquid enclosed by a lipid membrane used for intercellular trafficking), which travel to the Golgi apparatus.

Golgi complex

The Golgi complex is a series of flat cisternae (stack) surrounded by membrane-enclosed vesicles. The main function of this organelle is processing and sorting of secreted and membrane proteins. Three regions in the Golgi cisternae stack can be distinguished: *cis*, *medial*, and *trans*. Transport vesicles coming from the ER merge with the *cis* region of the Golgi complex. Proteins travel through the *medial* to the *trans* region (Engel *et al.*, 2015). At each region different set of enzymes modify the proteins differently, according to their intended function and destination. Ready proteins are again packed into the vehicles, each intended for a specific region of the cell (e.g. membranes, lysosomes or other organelles).

Lysosomes

The lysosomes are vesicular organelles, which are primarily responsible for the intracellular digestion. Interior of the lysosomes is highly acidic, reaching pH of about 4.5–5.0 (cytoplasmic and nuclear pH is around 7.2). Low pH ensures optimal function of a huge variety of digestive enzymes (acid hydrolases). The lysosomes provide the cells with two modes of protection from the autodigestion: specialized membrane keeps harmful enzymes out of the cytoplasm, and even if those enzymes would leak out, higher pH would render them inactive (Cuervo and Dice, 1998).

Inside a single cell, several hundred of lysosomes can be present with varying sizes and shapes. Two kinds of lysosomes can be distinguished. Primary lysosomes are roughly spherical and do not contain the membrane or particulate debris. Secondary lysosomes are larger and irregularly shaped, as they result from the fusion of the primary lysosomes with other vesicles or membrane-bound organelles. Inside the secondary lysosomes digestion of mainly external material uptaken in the process of endocytosis takes place. Some cellular and nuclear proteins can be decomposed in the lysosomes, but the vast majority of them is rather degraded in the proteasomes, large multiprotein complexes present in the cytosol.

Endosomes

The Endosomes are structures originating from the *trans* Golgi membranes. Their main function is connected with endocytosis. Such process is observed when a relatively big particle (like virus or bacterium) is “swallowed” by the cell. During the endocytosis a portion of the plasma membrane invaginates into a pit, enclosing the particle inside. The created vesicle is joined with the endosome. In the early endosome first round of sorting of its content takes place. Some membrane proteins are recycled back to the cell membrane, others are transported to the late endosome for another round of segregation. The late endosome fuses with the lysosome forming the endolysosome, where digestion of the content begins.

Peroxisomes

The peroxisomes contain enzymes oxidizing various organic compounds without production of ATP. The oxidation by-products are utilized in other cellular

reactions. The peroxisomes are the main producer of the acetyl groups during oxidation of fatty acids. The acetyl groups are necessary for, among others, cholesterol synthesis (van der Zand *et al.*, 2006). Peroxisomes also degrade toxic compounds (mainly hydrogen peroxide, H_2O_2). These organelles are present in all animal cells with the exception of the red blood cells (De Duve, 1996).

Mitochondria

The mitochondria are surrounded by a double lipid bilayer, each layer with distinct composition and function. The mitochondria take up to 25 % of the cytoplasm volume. Their principal function is the ATP production during the aerobic metabolism.

The mitochondrion can be subdivided into four specialised compartments: outer and inner membranes, intermembrane space between them, and a matrix inside. Each of them has specific role and composition. The outer membrane is composed of lipids and proteins in almost equal parts. The proteins localised there are responsible for the synthesis of mitochondrial lipids, import of mitochondrial proteins and division and fusion of the organelle. The most abundant protein in mitochondria, porin, forms channels making the outer mitochondrial layer permeable to all molecules of 5 kDa or less.

The intermembrane space closely resembles the cytosol, thanks to the unrestricted motion of small molecules across the porin channels. The main function of the intermembrane space is tightly connected with the phosphorylation of nucleotides.

The mitochondrial inner membrane contains a number of different proteins which perform three interlocked functions. They carry out oxidation reactions of electron transport chain, production of ATP (by the ATP synthase), and sustain this gradient of H^+ ions across the membrane. The action of the ATP synthase is dependent on the electrochemical gradient of H^+. The inner membrane is therefore essentially impermeable to ions and small charged molecules. (Duchen, 2004). A surface of the internal membrane of the mitochondria is greatly increased thanks to a large number of interfoldings extending into the matrix. The mitochondrial inner membrane is composed of about 20 % lipid and 80 % protein.

The mitochondrial matrix consists of a highly concentrated mixture of proteins and mitochondrial DNA. In the mitochondrial matrix a machinery required for

the up-keeping and expression of the mitochondrial DNA is located, including specialized ribosomes and transport RNAs (tRNAs). Also, oxidation of pyruvate and fatty acids, and one of the most important cycles – citric acid cycle are located there (Anderson *et al.*, 1981). Thus, a large part of the energy generation process in the cell takes place in this compartment.

1.1.3. Dynamin-related protein 1

The mitochondria create a vast dynamic network of membranes that is continuously remodelled by the fusion and fission events. This remodelling plays an important role in few biological processes. The most important is the distribution of the mitochondria evenly between daughter cells during the cell division. The fusion process of damaged mitochondria with healthy ones is used to regenerate the former. The fission process I a method to get rid of defective part of mitochondria, which later are recycled by mitophagy. (Smirnova *et al.*, 2001; Twig *et al.*, 2008)

The dynamin-related protein 1 (Drp1) is the most important protein involved in the fission of the mitochondria. Drp1 belongs to the dynamin family present in mammals, worms, and flies (analogous protein Dnm1 is present in yeast) (Youle and van der Bliek, 2012). Drp1 has GTPase domain which allows to obtain energy necessary for its function. Drp1 has three abilities: 1) to self-oligomerise into helices surrounding mitochondrial outer layer, 2) to constrict upon nucleotide binding, 3) to trigger fission of membrane necks in a GTP-dependent manner (Antonny *et al.*, 2016). Drp1 is predominantly present in the cytosol in the form of dimers or tetramers. The tetramers can assembly into bigger polymers on the mitochondrial membranes. Drp1 assembles on the mitochondrial membranes in a form of polymer consisting of around 150 Drp1 monomers and performs the mitochondrial fission (Koirala *et al.*, 2013). This protein takes also part in the programmed cell death – apoptosis. The localisation pattern of Drp1 changes drastically on the onset of the apoptosis. The majority of Drp1 moves onto the mitochondrial membranes in preparation for the unrestricted mitochondria fragmentation (Montessuit *et al.*, 2010; Z. Wang *et al.*, 2012). It is one of the factors that kills the cells. Drp1 is also crucial for the apoptosis induction (Frank *et al.*, 2001).

1.1.4. Cytoskeleton

The cytoskeleton, an extensive network of interconnected polymers, dictates cell shape, supports its internal organization, and provides transport routes for other constituents of the cytoplasm. The cytoskeleton is often depicted as scaffolding or highway network inside the cell, but it is a far more dynamic structure. It constantly rearranges in response to external and internal stimuli, or during the lifetime of a cell. A schematic view of the whole cytoskeleton is shown in Figure 2.

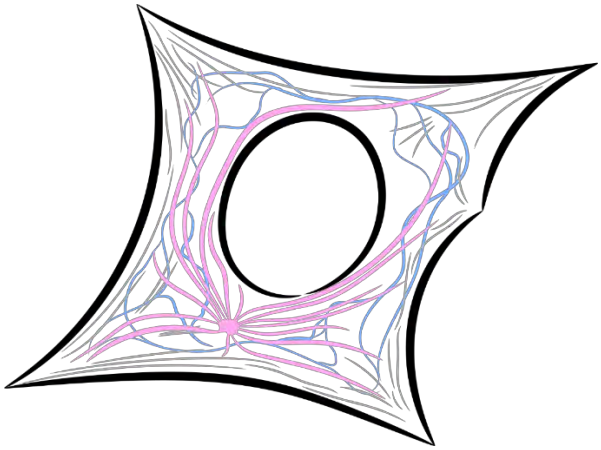

Figure 2. Schematic representation of the cytoskeleton. Microfilaments are shown in grey, intermediate filaments in blue, and microtubules in pink.

The cytoskeleton is created by the three types of filaments, each creating its own network: the microfilaments, intermediate filaments, and microtubules. The distinction between them is made on the basis of their diameter, arrangement, and type of the subunits. All of them interact with each other and also with different cellular components (Sodeik, 2000).

Microfilaments

The microfilaments, also called actin filaments, have a diameter ranging from 5 to 9 nm and length of the size of the cell (~few micrometres). They are created by a single protein, actin. Their main function is to provide the shape of the cell, and also to allow cell locomotion. Microfilaments are able to create flexible linear bundles, two-dimensional grids, and three-dimensional networks. The microfilaments are mainly located just beneath the cell membrane because their action is mainly connected with the reshaping of the cell.

Intermediate filaments

The intermediate filaments, contrary to the microfilaments and the microtubules, are composed of the very diverse and large family of proteins. The diameter of these structures is around 10 nm and length similar to the microfilaments. All of them create an internal network stretching from the nucleus to the cell membrane (and even beyond). In the cytosol, the intermediate filaments provide the cell with mechanical resistance. Inside the nucleus, a specialized group of the intermediate filaments called lamins is located. They form nuclear lamina – scaffolding just under the inner nuclear membrane supporting structure of the nucleus. Inside the epithelial cells, different kinds of the intermediate filaments extend to the outside of the cells (through membrane-bound structures called desmosomes and hemidesmosomes) mediating cell to cell adhesion and tissue formation.

Microtubules

The microtubules are not randomly spread throughout the cytoplasm. Instead, all of them radiate from a central structure, the centrosome. The microtubules are the biggest filaments (with an outer diameter of 25 nm) created by heterodimers of α- and β-tubulin. Microtubules are straight filaments, expressing polarity, meaning that their ends differ in dynamic properties (denoted as (+) and (–)). Usually, filaments originating from a single centrosome have their (+) ends directed towards the cell peripheries. They grow and shorten at the (+) ends. The undisturbed microtubular structure is necessary for proper endoplasmic reticulum and Golgi complexes formation. They also play a key role in the separation of the sister chromatids during the mitosis (the cell division is described in detail in section 1.1.7).

1.1.5. Cytoplasm as a crowded environment

The organelles and the cytoskeleton occupy a huge portion of the volume of the cell (over 60 %), but remaining space is not simply filled with water. The cytoplasm is a highly concentrated solution of thousands of different molecules. These small molecules (including proteins, nucleic acids, ions etc.) take between 5 and 40 % of the total cell volume, and their concentration can reach up to 400 mg/ml (Ellis and Minton, 2003). That is why the interior of the cell is considered crowded. The mean distance between proteins to approximately few nm. Such dense environment greatly impacts the speed of the diffusive transport (and

processes depending on diffusion) and also causes restriction of partitioning of molecules and organelles between the volume of the cell. The crowding gives rise to an unexpected binding interactions between molecules of the same kind and also unrelated ones (Luby-Phelps, 1999, 2013). The molecular crowding is accompanied by two typical components: steric (hard-core) interactions and chemical (soft) interactions divided into short range repulsion and longer ranged attraction. First of them is an effect of the size of a molecules, which cannot occupy the same volume in space. The second interaction is connected with the chemical character of two molecules (e.g. their charge). It is often less prominent. The molecular crowding is a ubiquitous phenomenon, as it is present in all cells (Ellis, 2001).

The simplest molecules (even water) are, to some extent, subject to the constraints of the molecular crowding. The cellular water is divided into two populations, with water molecules freely exchanging between them. Around 90 % of H_2O molecules belong to the bulk water freely diffusing in the volume of the cell. The rest 10 % is the fraction of water bound (interfacial) to molecules (Stadler *et al.*, 2008). Potma *et al.* (2001) studied the bulk water viscosity in mammalian cells. They observed, that cytoplasmic bulk water molecules have their mobility reduced by 70 % when compared to pure water. The interfacial water is present only in the case of fully synthesised, correctly folded and stabilized particles (Jasnin *et al.*, 2008).

The macromolecular crowding has the biggest effect on the reactions of proteins inside the cell. Protein folding and maintenance of the correct structure of proteins is promoted under the crowded conditions (Sasahara *et al.*, 2003; Hong and Gierasch, 2010). For example, the chaperone activity is increased in such conditions (Zimmerman and Harrison, 1987; van den Berg *et al.*, 1999). But overcrowding can lead to the formation of dysfunctional protein aggregates (Minton, 2000; Kinjo and Takada, 2002). The molecular crowding has a great impact on the speed of processes taking place inside the cell. Both increase and decrease in reaction rates have been observed in crowded solutions (Wenner and Bloomfield, 1999; Minton, 2006; Sasaki *et al.*, 2006; Ridgway *et al.*, 2008). Fast (diffusion-limited) reactions are slowed down, whereas slow (transition-limited) are accelerated by the crowding. The crowded environment can even help overcome an unfavourable environment for the reaction (Zimmerman and

Harrison, 1987) or allow reactions unavailable in the uncrowded conditions (Zimmerman and Pheiffer, 1983).

The molecular crowding influences stability of protein native structure through the hard-core and the soft interactions. First of them is always stabilizing while the second can be both stabilizing and destabilizing. The crowding promotes stabilization through the hard-core interactions since native conformations of proteins are usually more compact. Impact of the soft interactions is less uniform. Chemical repulsion stabilizes compact structures, while chemical attraction promotes exposure of more surface of the protein and its unfolding. The soft interactions are weaker and non-specific. But a great number of them can sometimes overcome steric interactions and permit or forbid a molecular process (Y. Wang *et al.*, 2012; Sarkar *et al.*, 2013).

The complexity of crowders influences cellular compartmentalization. A huge variety of species differing in shape, size, and flexibility can cause spontaneous demixing of molecules in the cell, or their condensation into stable droplet phases. Such effect, called the microcompartmentation, is believed to be crucial for sustaining the metabolism of the cell (Al-Habori, 1995; Walter and Brooks, 1995), although its effects are hard to predict (Long *et al.*, 2005).

1.1.6. Measurements of mobility inside living cells

Measurements of diffusion in the cell interior are performed with different techniques such as: single particle tracking (SPT), fluorescence recovery after photobleaching (FRAP), nuclear magnetic resonance (NMR) and fluorescence correlation spectroscopy (FCS). Each of the techniques has its advantages and disadvantages.

The single particle tracking determines a trajectory of single or very few fluorescent particles mainly in artificial and biological membranes (Schütz *et al.*, 1997). Three-dimensional trajectories are rarely addressed by the SPT. The SPT was used to track movements of the vesicles along the cytoskeleton in living cells (Levi *et al.*, 2005; Holtzer *et al.*, 2007) or expansion of a microtubule (Leduc *et al.*, 2013). All those works concerned directional movement along the cytoskeleton, so roughly two-dimensional movement. Robust three-dimensional tracing of a single particle movements inside the cell interior remains unachievable (Cognet *et al.*, 2014).

The nuclear magnetic resonance tracks movement of probes by monitoring the movement of hydrogen nuclei. Application of the NMR to studies of proteins is mainly limited by their rotational dynamics. This technique is restricted to studies of the small, freely tumbling proteins (Pielak *et al.*, 2009). Despite the limitations, Garcia-Perez *et al.* (1999) successfully applied pulse-field gradient spin-echo ^{1}H NMR to studies of the diffusion of small metabolites inside both artificial crowded systems and eukaryotic cells i.e. rat and chicken erythrocytes.

The fluorescence recovery after photobleaching (FRAP) measures the speed of influx of fluorescent tracer particles (recovery of fluorescence) into the previously photobleached region. It allows obtaining the diffusion coefficients of fluorescent or fluorescently labelled molecules. The FRAP experiments are accompanied by a careful analysis of data, because of two unwanted effects: incomplete fluorescence recovery and multi-component diffusion (Verkman, 2002). Distinguishing between slow and two-component diffusion is extremely hard in the FRAP experiments. Despite those restrictions, this technique was successfully applied to the studies of diffusion in different eukaryotic cells including HeLa cells (Lukacs *et al.*, 2000), Swiss 3T3 fibroblasts (Kao *et al.*, 1993), and muscle cells (Arrio-Dupont *et al.*, 2000).

The fluorescence correlation spectroscopy (FCS) is a technique commonly used for studying the diffusion of a wide range of particles. Most of the work described in this thesis was performed using this technique, so entire section (1.3) was devoted to an extensive description of the FCS and its application in studies of living cells.

1.1.7. Cell cycle in mammalian cells

The cells of every organism proliferate. The phenomenon associated with the proliferation is called the cell cycle. It is an orchestrated sequence of processes, which ensures generation of two daughter cells from a single mother cell. During the cell cycle, every component of the cell has to be carefully duplicated and then equally divided among two daughter cells. Overview of the cell cycle is shown in Figure 3.

Duplicated material (especially genetic) has to be an exact copy of the original. For this reason, cell cycle progression is tightly regulated and few control checkpoints during the cell cycle exist. A failure in the regulation mechanism leads to cancer. Few other diseases (e.g. Alzheimer's disease) are also connected

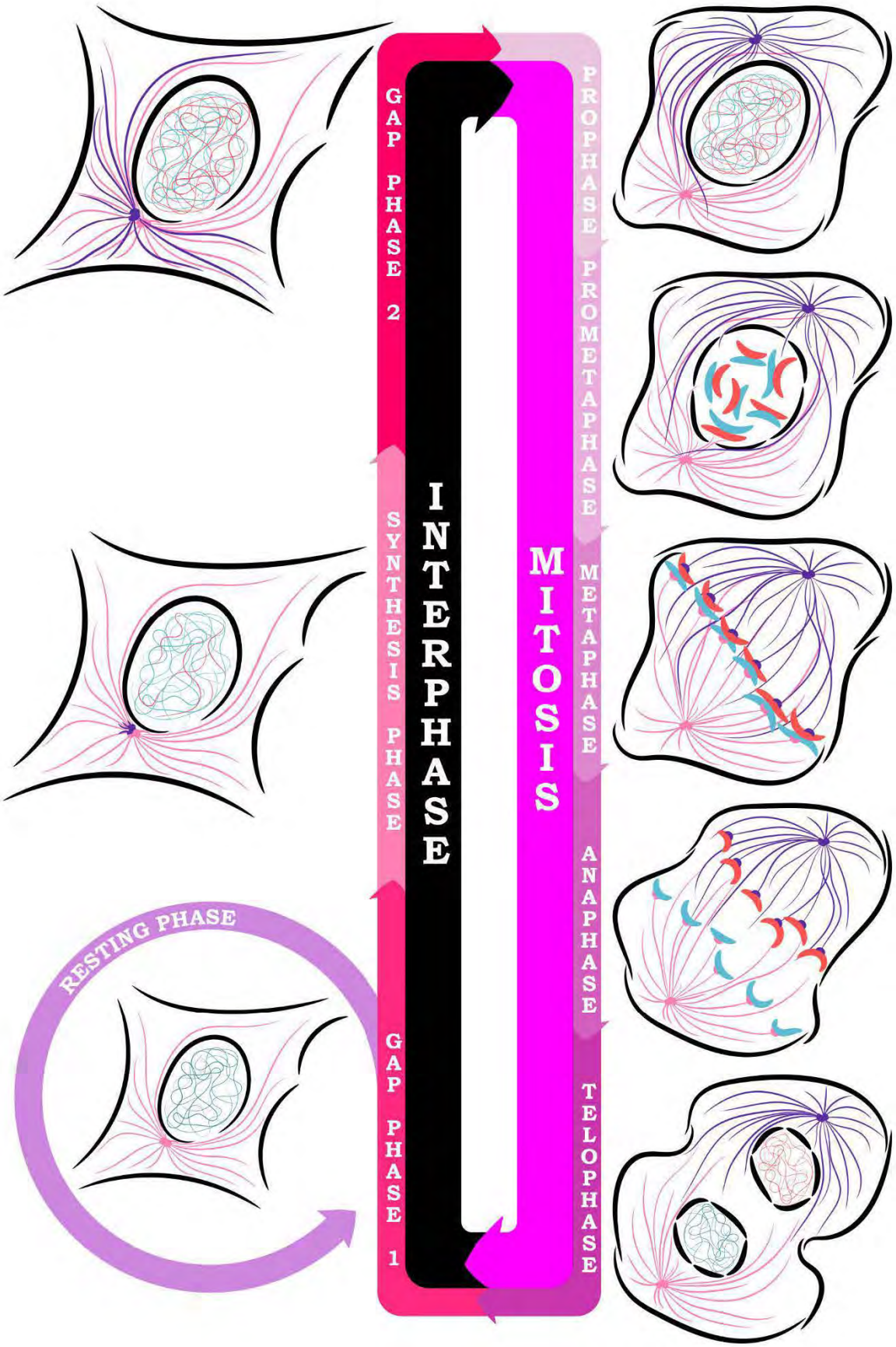

Figure 3. A simplified representation of the cell cycle in mammalian cells. Maternal and daughter DNA is shown in blue and red respectively, the microtubules in pink (maternal) and purple (daughter).

with the disruption of the cell cycle regulation (McShea *et al.*, 1997; Busser *et al.*, 1998).

The cell cycle is ubiquitous as it takes place in all single-cell organisms and in every somatic cell of multi-cellular ones. The cell cycle in eukaryotic cells is divided into four phases: first gap phase (G1), synthesis phase (S), second gap phase (G2) and mitosis (M). The tree first phases are jointly called the interphase, in which majority of cells exist. The fourth phase called the mitosis (M) can be subdivided into five consecutive stages: prophase, prometaphase, metaphase, anaphase, and telophase (Alberts *et al.*, 2008). During the mitosis two daughter cells are produced both being the exact copies of the mother cell. Additionally, there exists a specialised type of cell division called meiosis, during which genetic material of the parent cell is halved. This type of cell division is present only in sexually-reproducing eukaryotes and gives rise to the gametes.

Interphase

The interphase takes the overwhelming majority of the cell cycle. Human cells on average divide every 22-24 hours, of which the interphase takes 21-23.5. During the interphase a cell is growing and performing a designated function (for example as a part of the tissue). Also, during this phase a cell prepares for division by replicating its genetic material and duplicating cellular structures and other contents. The interphase is divided into three stages: the two gap phases (G1 and G2) and the synthesis of DNA phase (S) in between. During the first gap phase G1, the cell rapidly increase in size and synthesise a great amount of structural and functional proteins. In actively dividing cells it takes up to 8-10 hours, although the duration of this phase is subjected to wide variations (Puck and Steffen, 1963; Hahn *et al.*, 2009). From G1 phase cells can either commit to the DNA replication (and further division) or enter the resting phase called G0. During the G0 phase cells remain metabolically and physiologically active, which allows them to fulfil their designated role in the organism or in the tissue. An entrance into the G0 phase can be both reversible (quiescence) or irreversible (senescence or differentiation).

The synthesis phase (S phase) is devoted to the replication of the nuclear DNA. Each DNA fragment (chromosome) has to be replicated accurately, and the structure of the chromatin has to be reproduced. Apart from precise replication of the DNA, another factor is important. For one cycle every fragment of the

genetic material of the nucleus has to be copied exactly once. The S phase usually is the longest phase of the cell cycle, lasting up to 10-12 hours.

After the S phase, the second gap phase (G2) appears, during which a cell makes the final preparations to the division. This phase is short, lasting 4-5 hours. The microtubules begin to form the spindle and duplicate. During the G2 phase, organelles are duplicated. At the beginning of the interphase, all microtubules originate from a single structure – the centrosome. Just before the mitosis the centrosome is duplicated, and new microtubule network is created. Until the onset of the mitosis, both centrosomes remain in close proximity. For the mitosis, the duplication of the microtubule bundle is the most important.

Mitosis

After the S phase, there are two exact copies of the DNA. Those copies are called the sister chromatids (together they form single chromosome) and are connected to each other in the region known as the centromere. The mitosis begins with the prophase. During this phase, the chromosomes condense. Simultaneously, inside the cytosol, two centrosomes are separated and moved to the opposite poles of the cell. During the second stage of the mitosis (the prometaphase) abrupt breakdown of the nuclear envelope occurs. The nuclear membrane fragments do not disintegrate but are rather incorporated into the endoplasmic reticulum network. Additionally, during the prometaphase, the spindle microtubules bind to the chromosomes via the kinetochores (big protein complexes) localized in the centromere region. This binding to the spindle microtubules allows active movement of the chromosomes. To each of the chromosomes two microtubules are bound, one from every centrosome. At the third phase of the mitosis (the metaphase), the chromosomes in their most condensed form are aligned at the equator of the cell (the mitotic spindle). This is achieved by pulling of two centrosomes. Next, at the anaphase, the sister chromatids are pulled apart synchronously. As a result, two sets of the daughter chromosomes are created. Pulling of the daughter chromosomes is achieved by shortening of the kinetochore microtubules and simultaneous receding of the centrosomes. The final stage of the mitosis is called the telophase. In this phase, two sets of chromosomes arrive at the opposite poles of the cell and decondense. Around each set, the nuclear envelope is reassembled. This gives rise to the two daughter nuclei. On the cellular membrane surrounding equatorial plane, the contractile ring is formed by the filaments of

actin and myosin proteins. The cell division is finalized by contraction of this ring (the cytokinesis) when the cytoplasm is divided equally between the two daughter cells. The mitosis takes from 30 minutes up to 1 hour.

1.1.8. Cell cycle control mechanisms

The cell cycle requires a fine control. Inside the eukaryotic cells, a specialized class of proteins is devoted to the task. Those proteins are called cyclin-dependent kinases (CDKs). The level of the CDKs remains constant throughout the cell cycle. They activate and deactivate (by means of phosphorylation) a huge variety of other proteins in a timely fashion. The CDKs are regulated by other kinds of proteins, mainly cyclins (Schafer, 1998), which expression of which is restricted to definite phases. There exist four classes of cyclins: G1/S-cyclins, S-cyclins, M-cyclins, and G1-cyclins. Three first are indispensable for completion of the cell cycle. Fourth class (G1-cyclins) are accessory for the G1/S-cyclins and control initiation of the cell cycle. Each cyclin class forms complexes with the CDKs during a specific phase. The first complex is present throughout the whole G1 (G1-CDK), the second class only in late G1 and early S (G1/S-CDK). The third complex (S-CDK) is active from the restriction point (moment of commitment to the division) until the end of the mitosis, and final (M-CDK) from the late G2 to the end of the mitosis. Each of those complexes plays a specific function required for the cell cycle progression. Together, the CDKs and the cyclins create a robust, reliable, and adaptive system of control. This regulatory system is capable of working under a wide variety of conditions, even when partially damaged.

The control of the cell cycle is most prominent during three precise moments, which are called checkpoints. Cells are capable to stop progress through the cell cycle at each of them. The first of the checkpoints is known as the restriction point, localised inside the first gap phase. It is defined as the point of no return, any cell crossing it commits to the cell cycle and subsequent division. Crossing the restriction point requires favourable environment, and failure to do so places the cells in a quiescent state (Cappell *et al.*, 2016). The second checkpoint is localised at the end of the G2 phase (G2/S checkpoint). It is the final moment before the mitosis. Thus proper DNA replication needs to be completed at this point without errors. If any mistake occurs during the duplication of the genetic material, a signalling cascade triggered by such error

blocks progression until required corrections are made. The final control point is localised in the middle of the mitosis and is called the metaphase-to-anaphase transition checkpoint or simply the spindle checkpoint. At this point, a cell waits for the proper alignment of the chromosomes along the mitotic spindle. Until such alignment is obtained the cell is arrested in the metaphase (Vermeulen *et al.*, 2003). A proper function of all checkpoints is required to prevent any abnormalities during the cell cycle. Mutations of different checkpoint proteins are frequently observed in cancer (Anders *et al.*, 2011; Lu *et al.*, 2015).

Synchronization of cell cycle

Populations of cells synchronously progressing through the cell cycle can be achieved by two approaches: separation of the cells at a given stage of the cell cycle or synchronization of the population of cells. There are few methods illustrating those two approaches, each slightly different.

Mitotic shake-off is the simplest separation method. It is based on one of the properties of the adherent cells. When the cells enter the mitosis, they round up and are weakly bound to the culture surface. Such cells are easy to be taken from the culture surface by agitation. Free-floating cells are transferred to the new culture dish or flask. This method is a straightforward way to obtain cells in the M phase (Posakony *et al.*, 1977). The main drawback of this method is a low yield of cells (at any given time only around 5 % of the total cell count is undergoing the mitosis). The cells, which do not divide cannot be separated in this way.

Another approach to cell separation is countercurrent centrifugal elutriation (CCE). This method is based on the differences in size and density of the cells in each phase of the cell cycle. In principle, the cells should be twice as big during the G2 phase and the mitosis than at the beginning of the G1 phase. Cell suspensions are separated in a specially designed centrifuge rotor. During the CCE, the flow of the medium counters the centrifugal force exerted onto the sedimenting cells. The CCE can be successfully applied to both adherent and suspended cells and yields all phases of the cell cycle (Davis *et al.*, 2001). This procedure lasts several hours and cannot be applied to the types of cells which do not significantly change their size throughout the cell cycle.

The flow cytometry and cell sorting can be used for separation of cells based on one or few intracellular and/or surface properties, like DNA content, size of the cell or presence of molecular markers. The cells can be separated into the main phases: G1, S and G2/M. Unfortunately, application of the flow cytometry cannot yield completely separated cell populations, only enrichment is possible (Juan *et al.*, 2002).

As an alternative to the cell separation methods, synchronization of the whole culture can be utilised. The synchronization is obtained by either deprivation of important growth factor or addition of the external agent. Serum or amino acid starvation efficiently arrests the cell cycle. The cells devoid of crucial growth factors or "building blocks" of cellular components cannot pass restriction point localized in the G1 phase. This approach is restricted to the single phase (G1). Often cells devoid of nutrients exit the cell cycle altogether and enter the G0 phase, which is frequently observed in the primary cells. The cells synchronized by the starvation quickly lose synchrony. This method requires extremely long incubation times, reaching up to 48-72 hours (Davis *et al.*, 2001).

The contact inhibition (a regulatory mechanism keeping the cells growing in single monolayer) also allows for synchronization of the cells in the G1 phase. This approach is based on mechanism present in cells, with which cells respond to the density of the culture. This method does not trigger quiescence of the cells into the G0 phase. The contact inhibition mechanism is observed only in normal and few transformed cells, which makes its use limited to such cases. This method also takes a long time and synchrony of the cells is quickly lost (Davis *et al.*, 2001).

Different molecules can be applied for synchronization of the whole cell culture. Those molecules inhibit one of the paths of the cell cycle control in direct or indirect fashion. Several molecules with different targets are known. Their application into the medium allows to arrest the cell cycle at the desired stage. One of them, lovastatin, interferes with the cholesterol synthesis and action of the proteasome synchronizing the cells in the early G1 phase (Keyomarsi *et al.*, 1991). Mimosine, an inhibitor of the thymidine incorporation, blocks the cell cycle at the late G1 or G1/S transition (Zieve *et al.*, 1980; Krude, 1999). The microtubule polymerization inhibitors like vinblastine and nocodazole allow for the synchronization of cells at the G2/M border (Jordan *et al.*, 1992). All of these chemicals giving high degree of the synchronization of the cells, are

applicable in a great variety of the cell lines, and are simple to use. Unfortunately, they also manifest dose-dependent cytotoxicity, and even at low concentrations cause delays in the restart of the cell cycle machinery.

We used aphidicolin for the synchronization of HeLa cells. This compound is a mycotoxin obtained from fungi *Cephalosporium aphidicola* and *Nigrospora oryzae* (Spadari *et al.*, 1982). Aphidicolin stops the synthesis of the nuclear DNA and arrests the cell cycle at the G1/S border. Any cell that is in progress of DNA replication would also be arrested (with only partially replicated DNA). Non-dividing cells are unaffected. Aphidicolin is a specific inhibitor of DNA polymerases α and ε. It selectively blocks replication of only the nuclear DNA. Synthesis of the mitochondrial DNA is unaffected since it is conducted by different kind of polymerases. Aphidicolin binds near nucleotide-binding site, despite not sharing structural homology with deoxynucleotides. The action of aphidicolin selectively inhibits incorporation of cytosine by polymerase α. In the case of polymerase ε no such selectivity was observed (Baranovskiy *et al.*, 2014). The synchronization of the cell cycle caused by aphidicolin does not interfere with other processes present in the cell. Pedrali-Noy *et al.* (1980) proved, that the synthesis of polymerases α, β, and γ and of all nucleotides is unaffected during incubation of cells with the compound. They also showed, that after removal of this synchronization agent, cells restart cell cycle within 30 minutes. Aphidicolin can also have adverse effects. Prolonged exposure (over 48 hours) causes irreversible arrest of the cells in the S phase, or their death after removal of the compound (Borel *et al.*, 2002). Aphidicolin also induces gaps and breaks at the fragile sites in the chromosomes (Glover *et al.*, 1984).

1.1.9. Molecular foundations of cancer

Cancer is a generic term applied to a number of different diseases, which can affect any part of the body. Their common characteristic of cancer is a rapid generation of abnormal cells evading physiological control of growth and proliferation. The process leads to the transformation of healthy tissue into a malignant tumour. This process is called the neoplastic transformation. Eventually, those dysfunctional cells spread far beyond their original source in a process called metastasis. This aggressive invasion of the tumour cells into many tissues usually leads to the death of the affected organism. According to the World Health Organisation (data from 2015), the cancer is the second

leading cause of death in humans worldwide, after the cardiovascular diseases. Despite steadily decreasing mortality, nearly 1 in 6 deaths is still attributed to the cancer.

Most prevalent explanation of cancer is called the somatic mutation theory (SMT). The SMT states, that the cancer is a genetic disease caused by the microevolutionary process (Alberts *et al.*, 2008; Lodish *et al.*, 2013). The proliferation of cells is a controlled process. For a cell to acquire characteristics of cancer, several distortions of crucial supervisory pathways have to occur. In all types of cancer, two major groups of genes are dysfunctional: proto-oncogenes and tumour suppressor genes. The proto-oncogenes are responsible for promoting cell growth and proliferation. Alterations of their sequence transform them into oncogenes – hyperactive genes. The role of the suppressor genes is to restrict the growth of the cell. They are frequently inactive in cancer cells. Additional third class of genes is often accompanying mutations of the proto-oncogenes and the tumour suppressor genes. They are called caretaker genes. Their function is related to the genomic stability. Dysfunctional caretaker genes increase accumulation rate of mutations which speeds up cancer development.

Hallmarks of cancer

Many molecular effects are suspected to underlie the development of cancer (see: Figure 4.). Hanahan and Weinberg summarised them in 2000 and proposed six traits shared by all cancer cells. Those traits were called the hallmarks of cancer (Hanahan and Weinberg, 2000). Over the decade later the idea was revised by the authors. Two more hallmark traits and two additional (enabling) characteristics accompanying the cancer emergence were added (Hanahan and Weinberg, 2011). Those two works summarise all conceptual basics of the somatic mutation theory.

The hallmarks of cancer describe a distinctive and complementary set of ten traits that allow tumour onset and development. Presence of those characteristics is necessary for the metastasis (creation of secondary tumours).

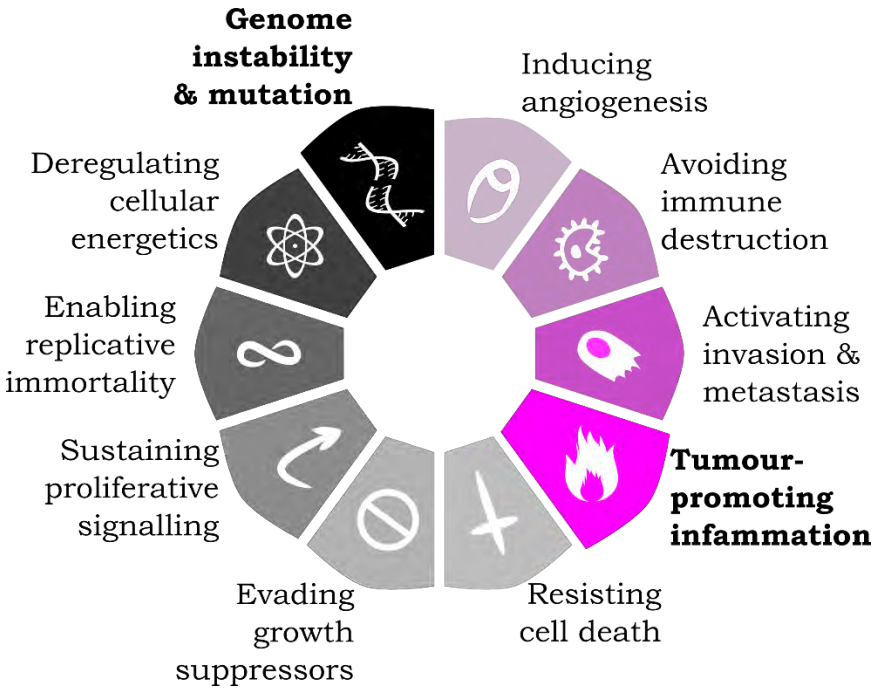

Figure 4. The hallmarks of cancer according to Hanahan and Weinberg. Two enabling characteristics are highlighted with bold typeface. The traits of cancerous cells impacting their nature in the cultures are shown in grey. The hallmarks that require the social context of the cell (i.e. their presence in tissues) are shown in pink. All ten traits are observed in the living organism. The division between those two groups of characteristics was done here for the purpose of clarification. In fact, all those traits are intertwined and influence each other.

Genome instability and mutation, and tumour-promoting inflammation are the "enabling characteristics" of cells developing cancer. These processes facilitate the neoplastic transformation but do not directly lead to cancer. In a normal tissue, the rate of acquiring mutations is extremely low thanks to the efficiency of DNA replication machinery and presence of multiple genome maintenance systems. The cancer cannot originate from a single mutation, instead, many changes are needed to disrupt the control mechanisms. Any change that increases error occurrence is favourable for the neoplasm development. The genome instability, therefore, promotes cancer. Increase of errors in the DNA duplication can be achieved by the breakdown of the genomic upkeep systems or by increased sensitivity to the mutagenic agents. There are two main targets of such changes. First is p53 protein, so-called "the guardian of the genome", responsible for the coordination of the DNA damage response. The second is the telomeric DNA, which protects chromosome integrity and imposes limits on the number of DNA replication rounds.

The tumour-promoting inflammation is the second “enabling” characteristic promoting tumour development, observed not in a single cell but in whole tissue or organism. Virtually every cancerous lesion attract an immune response. Usually, such action would prove beneficial for the organism. Paradoxically, this is disastrous in case of the development of tumour. The inflammation boosts the growth of the neoplasm by supplying to the tumour tissue large and diverse number of biomolecules such as the growth and survival factors. The inflammation also promotes the formation of new blood vessels.

The ability for unrestricted proliferation is the most prominent characteristic of the cancer cells. Thus, the majority of hallmarks develop ways in which unrestricted proliferations can be achieved. Neoplastic cells can sustain their own proliferative signalling. After acquiring the ability to produce growth factors for appropriate receptors on their own, cancer cells stimulate themselves. Alternatively, the cancer can signal surrounding normal cells of the tissue and stimulate increased production of the growth factors. Not always the presence of the growth factors is required. Mutations of growth factors receptors causing their constitutive activation are frequently described in human melanomas. Additionally, negative feedback loops that normally quench proliferative signals may be disrupted in the cancer. Without proper quenching the stimulations are prolonged.

Evasion of growth suppressors is the second hallmark of cancer. In healthy cells, dozens of various molecular pathways prevent excessive proliferation. Two major suppressors can be distinguished: p53 and pRb (retinoblastoma-associated) proteins. They are the central control nodes in the proliferation/senescence/death decision making. The action of those two proteins is frequently disrupted in cancers. Additionally, contact inhibition mechanism also prevents the abnormal proliferation. Cancerous cells divide even in populations of high density. The insensitivity of the cancerous cells to both the external and the internal suppression signals allows for their unrestricted division.

The resistance of cells to the apoptosis (programmed cell death) is the third hallmark of cancer. Properly functioning tissues maintain a balance between the proliferation and the apoptosis. The breakdown of this balance (either towards proliferation or apoptosis) leads to neoplastic transformation.

The fourth hallmark of cancer is the replicative immortality. Normal cells go through a limited number of replications (between 40 and 60). Then they enter non-proliferative (senescent) state in which they still retain viability and function. The senescence of the cells is usually connected with shortening of the telomeres (short tandem repeats of nucleotides localised at the ends of the chromosomes). The telomeres protect the DNA sequence from damage (during the replication short fragment of template DNA remains uncopied, leading to the shortening of the chromosomes). The shortening of the telomeres is often connected with the ageing of cells. Reactivation of the telomerase (the enzyme responsible for maintenance of the telomeres) was frequently attributed to the immortalization of cancer cells. The shortening of the telomeres and consequent destabilisation of the genomic DNA may also favour cancer progression.

Reprogramming of the energy metabolism is the final hallmark relevant in the cell cultures. Normally, cells obtain energy by catalysis of glucose under aerobic conditions. Cancer cells switch their glucose metabolism (glycolysis) to anaerobic conditions (Warburg *et al.*, 1927). In this case, the energy output is roughly 18 times lower than under the aerobic conditions, but such approach has great advantages for the development of cancer. In course of anaerobic catabolism, various intermediates are formed, which are subsequently used in the biosynthesis of nucleosides and amino acids. High level of the ATP molecules (energy carriers) triggers negative feedback loop inhibiting cellular growth, so the anaerobic glycolysis prevents this inhibition due to much lower energy (ATP) production. Such effect is also present in fast proliferating genetically normal cells (Pavlova and Thompson, 2016). The metabolism of the cancerous cells is faster although precise cause of such phenomenon is unknown. This allows faster replication of such cells. No data is available on whether physiological processes are hastened in the carcinogenesis.

Three remaining hallmarks of cancer are observed only in tumours inside living organisms. They are as follows: avoidance of the immune destruction, induction the angiogenesis, and activation of invasion and metastasis. The human immune system is extremely efficient at the detection and removal of abnormal cells so the neoplasm has to conceal itself at an early stage of development. For a tumour to grow also new blood vessels have to be recruited (oxygen and nutrients reach up to 100 μm into the human tissues). If cancer were to enter

the malignant state, it has to develop mechanism necessary for the transport and travel through the bloodstream.

In the context of the invasion and the metastasis, the idea of the circulating tumour cells (cancer stem cells) is discussed. These are cancer cells which, like normal stem cells, give rise to other, more specialised and “static” cell kinds. They form the new seat of the malignancy when transported through the bloodstream.

All of the hallmarks of cancer are intertwined. A single mutation of a crucial gene (for example in the gene encoding the p53 protein) disrupts few control pathways. The development of the cancer usually requires a succession of multiple mutations each slightly disrupting the cellular machinery. Not all cancers develop changes at the same pace or order, and not all of the hallmarks are always developed by a single tumour.

Tissue organization field theory

The somatic mutation theory of cancer is the most popular but it is not without flaw. Some experiments do not confirm its two core assumptions, that the cancer is a result of the defective control of the cell proliferation and, that default state of cells of multicellular animals is quiescence. Sonnenschein and Soto (2000) proposed the alternative tissue organisation field theory (TOFT). The TOFT is based on the assumption that the default state of cells is proliferation and motility and that tumours result from the defects of a tissue architecture. In series of their works, this pair of researchers challenged the somatic mutation theory (SMT) and its assumptions (Sonnenschein and Soto, 2013; Soto and Sonnenschein, 2014). Recently, the TOFT began to receive an increasing amount of recognition and its relation to the SMT is debated (Bedessem and Ruphy, 2015, 2017; Bizzarri and Cucina, 2016; Brücher and Jamall, 2016).

1.2.Diffusion and viscosity

The diffusion is a process in which matter spreads from one part of a system to another as a result of random motions of the molecules. The simplest illustration of this phenomenon is an observation of a droplet of a dye inside water. At the beginning, the dye is clearly separated from the rest of the liquid, but in time the molecules of the dye spread, which is visible as the change of

colour of water. After sufficient amount of time, diluted colour is evenly distributed throughout the whole volume. Overall, the diffusion can be considered as a phenomenon either described by the Fick's laws or with an atomistic approach illustrated as a random walk of diffusing molecules.

The first modern observation of the diffusive motion was done by the Dutch physician Jan Ingenhousz. In 1785 he observed small flickering of coal dust particles on the surface of alcohol. However, the earliest systematic description of diffusion phenomenon was performed by Thomas Graham. In his work with gasses, Graham (1829) performed the first quantitative experiments and provided data reliable enough to determine the diffusion coefficient (although the term "diffusion coefficient" was not established at that time). After these works, Graham performed experiments in liquids in which the diffusion proved to be three orders of magnitude smaller than in gases. Furthermore, Graham also noted that the diffusion rate seemed to slow down with time (Philibert, 2005).

1.2.1. Fick's laws

One of the possible ways to describe diffusion is to use mathematical apparatus created by Adolf Fick (1855). Fick assumed that the diffusion (the transport of mass) is analogous to the conduction of heat and electricity (already described by the Fourier's and Ohm's laws respectively). This approach gave rise to two equations, currently known as the Fick's laws.

The first Fick's law concerns situation when a concentration gradient is stable in time (the steady state). The law states that the diffusion flux J is proportional to the concentration gradient (Crank, 1975):

$$J = -D\frac{\partial c}{\partial x} \tag{1}$$

The diffusion flux J is the amount of substance crossing a unit area per unit time, c is the concentration of diffusing substance and x the space coordinate along the normal to the unit area. Finally, D is a proportionality factor, in Fick's original works denoted as k and described as "constant dependent upon the nature of the substances". Currently, this value is known as the collective diffusion coefficient. D is expressed in m^2*s^{-1} and is a basic measure of mobility of molecules.

The second Fick's law predicts changes of the concentration in time caused by diffusion. In the simplest, one-dimensional situation this law takes form of the partial derivative equation of the second order:

$$\frac{\partial c}{\partial t} = D\frac{\partial^2 c}{\partial x^2} \tag{2}$$

where t denotes time. In two or more dimensions the Laplacian must be used, which generalizes the above equation (Eq. 2) to:

$$\frac{\partial \varphi}{\partial t} = D\Delta\varphi \tag{3}$$

Fick also stated that the value of the diffusion coefficient increases with the temperature.

1.2.2. Brownian motion

The Fick's laws described the macroscopic transport of mass of many molecules due to the "thermodynamic force" imposed by the concentration gradient. But at the molecular level of description the diffusion of a single molecule is described as the random motion due to many collisions with molecules of the solvent. By following this random motion of a single particle we obtain the self-diffusion coefficient, while in the description of the Fick's laws we obtain the collective diffusion coefficient. Yet at the molecular level, both motions have the same atomistic origin.

The first quantitative description of the random walk of particles in fluids was done, independently from Graham, by Robert Brown. He recorded seemingly random movements of pollen of flower *Clarkia pulchella* under the microscope. Unexpectedly, this phenomenon was present not only in fresh but also in dried pollen irrespective of tested liquid (Brown, 1828). Later on, he expanded his studies to a great number of organic and inorganic substances, under the assumption that they could be ground to powder fine enough to be suspended in water. At the beginning of XIX century people believed that only animate matter can move, that is why a motion of unanimated matter surprised him (Brown, 1829).

The experiments made by Brown provided a lot of data, but no theoretical description of the observed phenomenon. This void was filled almost eighty years later independently by three scientists. In their works William Sutherland

(1905), Albert Einstein (1905) and Marian Smoluchowski (1906) provided necessary theoretical explanation for a phenomenon which was termed "Brownian motion" (side note: works of Einstein on Brownian motion, originally published in German, were translated and published as a book in 1956 which will be here cited further (Einstein and Fürth, 1956)).

At sufficiently long time the movements of particles undergoing Brownian motion seem random. Jean Perrin was able to track positions of small particles suspended in water (Perrin, 1913). Examples of such trajectories are shown in Figure 5.

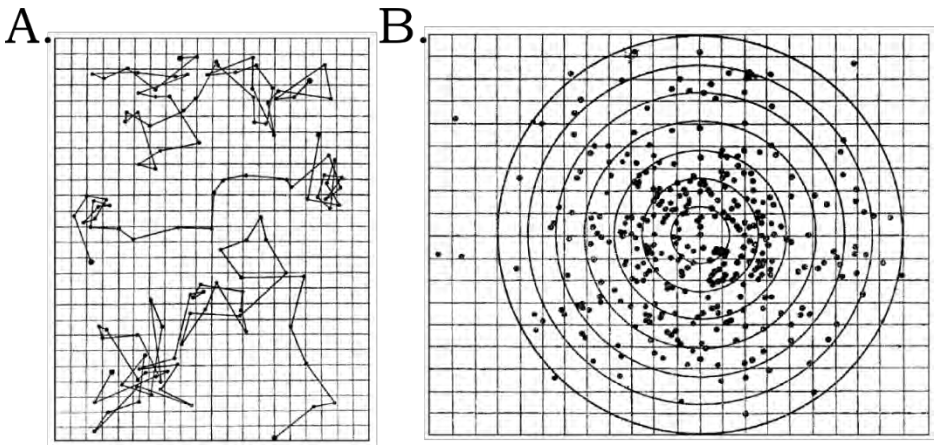

Figure 5. Random walk trajectories recorded by Jean Perrin. A. Three paths recorded for an individual particles. The positions were marked every 30 s. B. The distribution of positions in space recorded after every 30 s.

The Brownian movements of particles in the time scale of 30 s suggested that there existed sharp changes of the direction between steps. Einstein proved, that such mode of movement would require infinite force and proposed, that the Brownian motion is ballistic, meaning that particles travel along a smooth trajectory (Einstein and Fürth, 1956). This assumption was first proved by Li *et al.* (2010) for particles in the air and then by Huang *et al.* (2011) in the liquid water. The key factor proved to be time spacing between measurements. At extremely short time intervals (below nanoseconds for small particles) smooth ballistic motion is observed (Pusey, 2011). Only at longer time scales the Brownian trajectory looks random and in fact has the structure of fractal and looks the same irrespective of the time and length scale of observation. The total length of the trajectory is ill defined for the fractal objects, since it depends on the length scale of observation.

However, determination of the mobility can still be made from the mean square displacement (MSD):

$$MSD = \langle (r(t) - r(0))^2 \rangle \quad (4)$$

Here, $r(0)$ and $r(t)$ denote the initial position of a particle and the final one after time t respectively. Basing on the diffusion equations Einstein introduced the following equation:

$$MSD = \epsilon D t \quad (5)$$

where ϵ is a dimensionality parameter equal to 2, 4 or 6 for 1-, 2-, and 3-dimensional diffusion, respectively. This diffusion coefficient D is the same as the one used in the Fick's law in the limit of infinite dilution. Otherwise they can differ even by orders of magnitude, due to the interactions (attractive van der Waals or repulsive Coulomb interactions) between diffusing molecules. For attractive interactions between the molecules the collective diffusion coefficient from the Fick's law is smaller than the self-diffusion coefficient from the Einstein law. For repulsive interactions the former is larger than the latter. In this paper we determine the self-diffusion coefficient since we will work in the nM concentration range (high dilution) of the diffusing molecules.

1.2.3. Viscosity

The self-diffusion coefficient determined for a single molecule from its trajectory is inversely proportional to the viscosity of the liquid.

The viscosity is proportional to the resistance of a fluid (either a liquid or a gas) to flow. This resistance is measured in the following exemplary experiment. We take a system, where the uniform fluid is placed between two flat surfaces. One of them is immobile, while the second one is moving with constant velocity v. Such situation is depicted in Figure 6.

The movement of the upper surface causes the laminar flow of the liquid (assuming no edge effects). In such scenario, the liquid can be visualised as an assembly of layers of infinitesimal thickness stacked on top of each other. The momentum of the layers is transferred between them due to friction. On a molecular level, this is caused by random movements of particles along the y-axis, these molecules transfer with them x component of their momentum.

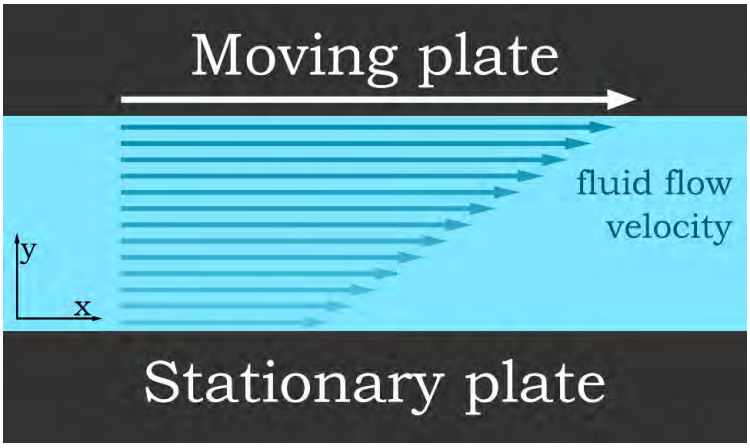

Figure 6. The idealized laminar flow between the stationary and moving plates. The top plate is moved along the x-axis with velocity v. As a result, the gradient of velocity inside the fluid appears along the y-direction. The velocity at the bottom plate can be zero for non-slip boundary conditions or can have a non-zero value for slip-boundary conditions.

As a consequence, the gradient of velocity perpendicular to the direction of the planes arises. This gradient is called the shear rate. Maintaining constant velocity of the upper plate (against losses coming from the friction) requires a force, which is proportional to the surface area of the upper plate where the force is exerted. The value of the force per unit area is the shear stress (τ_{shear}). Already Isaac Newton observed the relationship between the shear stress and the velocity gradient:

$$\tau_{shear} = \eta \frac{\partial v}{\partial y} \tag{6}$$

Here η denotes the dynamic viscosity of the liquid. Thus, η is the proportionality constant in the balance equation of the forces acting in the system. On the right hand of the equation we have the external force and on the left hand we have the drag force opposing the motion.

The dynamic viscosity is an important factor when describing fluid characteristics. On the basis of the dynamic viscosity, all fluids are divided into two groups: the Newtonian and non-Newtonian fluids. First of them is characterised by constant dynamic viscosity (at given temperature), independent of the shear stress. Liquids in this category obey the Newton's law of viscosity (Eq. 6). The behaviour of the non-Newtonian fluids deviates from those laws. This group can be further subdivided into shear thickening and shear thinning liquids. In former ones the viscosity increases with the shear stress (as example starch solution can be used, which is "resistant" when huge

force is applied, but flows easily when left undisturbed), in the latter the shear stress reduces the viscosity (e.g. strained (Greek) yogurt, which is thick when opened, but “liquefies” after stirring). Such deviations of the non-Newtonian fluids result from the interactions of various constituents of the liquid at a mesoscopic scale (intermediate between microscopic and macroscopic) (Panton, 2013).

1.2.4. Molecular dimensions description

Many different particles were used to study the diffusion in my PhD research. Among them, three main groups can be distinguished: proteins, dextrans and nanoparticles.

Both proteins and dextrans (complex branched sugars produced by bacteria) are long polymers (of amino acids and glucan, respectively). They can be described using either their mass or size. The proteins synthesised in cells have perfect monodispersity in terms of molecular mass, size and structure (both one dimensional described by the sequence of amino acids and 3D native structure formed in water). Dextrans are inherently polydisperse due to imperfect purification routes used by biochemists.

Currently, dextrans are obtained by their isolation from bacterial cultures. The purification methods are very powerful but still no perfect monodispersity of produced molecules can be achieved. Dextrans are usually described using the mean value of their weight measured by chromatographic methods. Number- or weight-average molecular mass (M_n and M_w respectively) can be expressed as:

$$M_n = \frac{\sum_i N_i M_i}{\sum_i N_i} \tag{7}$$

$$M_w = \frac{\sum_i N_i M_i^2}{\sum_i N_i M_i} \tag{8}$$

Here N_i denotes the number of chains of molecular weight M_i in the sample. The number average molecular mass (M_n) is the simplest arithmetic mean and its value can be obtained from the viscometry, gel permeation chromatography or nuclear magnetic resonance. The weight average (M_w) results from scattering experiments and its value is strongly dependent on the presence of big molecules. Those two values M_n and M_w often differ significantly (although relation $M_n \leq M_w$ is always true).

As a measure of uniformity of the sample, dispersity D_M is used. It is a ratio of weight- to the number-average molecular mass:

$$D_M = \frac{M_w}{M_n} \tag{9}$$

For a perfectly monodisperse polymer sample $D_M = 1$ and the higher this value is, the more polydisperse the sample is (Teraoka, 2002).

Commercially available probes are separated on the basis of weight. Also, the molecular masses of proteins are usually supplied. But, for the purpose of the experiments described in this work, not mass, but the size of polymers is of key importance. Schematic representation of a coil of polymer molecule and overview of all its dimensions is presented in Figure 7.

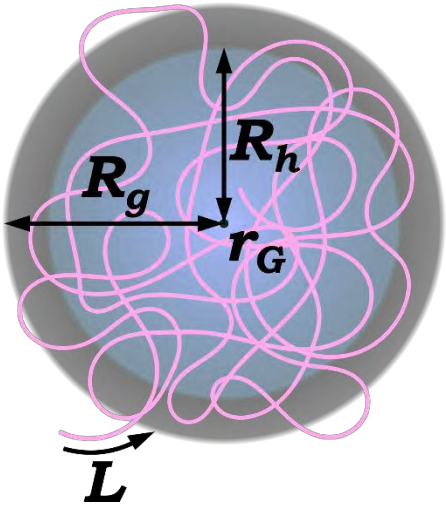

Figure 7. Schematic representation of characteristic values of a polymer chain (pink) in solution. L – the length of polymer along the chain (proportional to the molecular mass), r_G – the centre of mass, R_g – the radius of gyration, R_h – the hydrodynamic radius.

If the studied molecule is a homopolymer consisting of N monomers each of equal length l, then overall length of molecule L can be expressed as:

$$L = Nl \tag{10}$$

L is the length of fully extended polymer. In case of long, flexible molecules this value is often of little importance. Such polymers due to their internal entropy (determined from all possible conformations of a polymer chain) tend to reduce their size in solvents by adopting all possible conformations as shown in Figure 7. Then the radius of gyration tells us about the linear size of the volume occupied by a single polymer molecule (Doi and Edwards, 1986).

The radius of gyration R_g is the radius of a sphere in which total mass of polymer chain is supposed to be contained. Its square (R_g^2) is the second moment around the centre of the mass r_G. The centre of the mass is given by the equation:

$$r_G = \frac{1}{N+1}\sum_{i=0}^{N} r_i \tag{11}$$

where r_i is the distance of the monomer i (treated as a material point) from the centre of the mass. Now, the radius of gyration can be expressed as the mean squared displacement of all monomers from the centre of mass:

$$R_g = \sqrt{\frac{1}{N}\sum_{i=1}^{N}\langle(r_i - r_G)^2\rangle} \tag{12}$$

R_g is measured experimentally the static light scattering (Schärtl, 2010) and small-angle X-ray scattering (Eliezer *et al.*, 1995).

The second way to describe a polymer coil is to use the hydrodynamic radius R_h. This quantity is the radius of a hard sphere which would have the same diffusion coefficient as the investigated polymer molecule. The hydrodynamic radius includes not only size of the particle (with any shape- and flow-oriented deviations), but also hydration shell created by the surrounding solvent molecules. For the long linear polymers like dextrans, the hydrodynamic radius is always smaller than the radius of gyration (in compact protein structures opposite is true), although both radii are still of the same order of magnitude. With this approach, diffusing polymer coils are treated as perfect spheres with the radius equal to R_h.

1.2.5. Interplay of diffusion and viscosity

The self-diffusion coefficient describes the motion of single particles, while the viscosity describes macroscopic flows of fluids. The relationship between the self-diffusion coefficient and viscosity is described by the Stokes-Sutherland-Einstein equation.

$$D = \mu k_B T \tag{13}$$

Here D denotes the diffusion coefficient, μ is the mobility coefficient, k_B is Boltzmann constant, and T is the temperature in Kelvins. In case of a model system of a sphere, the mobility coefficient is given by:

$$\mu = \frac{1}{6\pi\eta r_P} \tag{14}$$

where r_P is the radius of the probe and η is the viscosity of the liquid. By substituting μ expressed in this way into Eq. 13, expression connecting the viscosity and the diffusion called the Stokes-Sutherland-Einstein (SSE) equation is obtained:

$$D = \frac{k_B T}{6\pi\eta r_P} \tag{15}$$

According to the original interpretation, the SSE equation is valid for fluids at given conditions, i.e. temperature, pressure and zero-shear conditions. The SSE equation is valid only for the diffusion of particles of sizes much larger than all the other constituents of the solution.

1.2.6. Viscosity of complex systems

The SSE equation is one of the fluctuation-dissipation relations (Frey and Kroy, 2005). The relation shows that fluctuations at equilibrium (given by the Brownian motion i.e. by the diffusion coefficient) are related to the dissipation of energy when a molecule subjected to the force moves at constant velocity in the liquid, having the mobility coefficient μ. Indeed, diffusion coefficient D and the friction present during the motion, and consequently also the viscosity η, are related in such way:

$$\frac{\eta}{\eta_0} = \frac{D_0}{D} \tag{16}$$

Here indices “0” denote values for the pure solvent. Unfortunately, this relation quickly proved to be apparently false in case of complex liquids (i.e. solutions containing macromolecules), when the size of diffusing molecule was smaller than characteristic sizes of the main components of the solution.

In the early fifties of the 20th century, Schachman and Harrington (1952) put above relation under question. In their work, they measured viscosity experienced by some probes using ultracentrifugation method. As probes they used big polystyrene beads, and two relatively small virus particles

(bacteriophage T3 and bushy stunt virus, BSV). Tested solvents were crowded by either fibrinogen (small protein) or DNA chains. The researchers observed no significant differences in the fibrinogen-enriched environment, but striking ones in the DNA solutions. When DNA was used as a crowder, sedimentation rate of small tracers did not differ significantly from that obtained in pure solvents. Surprisingly, measurements concerning huge particles showed much higher apparent viscosities. The authors hypothesised that the DNA particles form a mesh, through which small molecules travel relatively undisturbed, whereas in case of big ones this mesh had to rearrange or be transiently destroyed. This impeded big tracers' movement and increased apparent viscosity of the solution.

The dependence of the apparent viscosity on the size of the tracer was tested by numerous authors using different techniques. The ultracentrifugation (Langevin and Rondelez, 1978), the polyacrylamide gel electrophoresis (Rodbard and Chrambach, 1971), the fluorescence recovery after photobleaching (Wattenbarger *et al.*, 1992), the holographic interferometry (Kosar and Phillips, 1995), the capillary gel electrophoresis (Radko and Chrambach, 1996), and the fluorescence correlation spectroscopy (Zięba*cz et al.*, 2011) were all successfully applied in such investigations. All confirmed phenomenon first observed by Schachman and Harrington. The breakdown of the SSE equation was summarised by Odijk (2000). The breakthrough in the theoretical description came in the works of Hołyst et al. Hołyst *et al.* (2009) showed, that the SSE equation is valid providing one uses the scale-dependent viscosity, also termed "effective" and denoted as η_{eff}, which in large probe limit is equal to macroscopic viscosity η. Szymański *et al.* (2006), Hołyst *et al.* (2009), and Kalwarczyk *et al.* (2015) showed, that the effective viscosity is, in general, a stretched exponential function of the probe size, which is expressed as:

$$\eta_{eff} \propto \exp(r_P^a) \tag{17}$$

where a is a parameter of the order of unity (Sharma and Yashonath, 2006). The relationship between the viscosity and the diffusion in complex fluids is corrected to:

$$\frac{\eta_{eff}}{\eta_0} = \frac{D_0}{D} \tag{18}$$

All aforementioned studies concerning the apparent breakdown of the SSE equation were done using well-defined complex polymer solutions. Similar

investigations were also extended to other complex systems like hard-sphere-like colloids (Segrè *et al.*, 1995) or micellar solutions (Szymański *et al.*, 2006). Such approach also proved to be successful in protein solutions (Hou *et al.*, 2011; Kalwarczyk *et al.*, 2014) and even in bacterial (Elowitz *et al.*, 1999; Kalwarczyk *et al.*, 2012) and human cells (Lukacs *et al.*, 2000; Kalwarczyk *et al.*, 2011).

1.2.7. Viscosity scaling in living systems

The introduction of the effective viscosity properly characterized complex systems. The effect of probe radius on the effective viscosity of a system was undeniable, yet no theory could equally good describe both small and big tracers in living systems (Luby-Phelps *et al.*, 1986). The description of transport in living cells appeared the same as in all other complex liquids including polymer solutions (Kalwarczyk *et al.*, 2011).

Holyst *et al.* (2009) used the fluorescence correlation spectroscopy and capillary electrophoresis for the studies of polyethylene glycol solutions. In their work, they proposed two equations, which described the effective viscosity of complex liquids in two regimes: when the radius of the probe was much smaller than the radius of a crowder molecule and *vice versa* (nano- and macroscopic viscosity respectively). Kalwarczyk *et al.* (2011) expanded this idea. They introduced the notion of the effective hydrodynamic radius R_{eff} which is defined as:

$$R_{eff}^{-2} = R_h^{-2} + r_p^{-2} \tag{19}$$

In this relation, the hydrodynamic radius of the probe (r_p) and of the crowder (R_h) are connected. By introducing the term of the effective hydrodynamic radius, two relations describing extreme conditions (originally proposed by Holyst *et al.*) were successfully consolidated into the single one. The effective viscosity of a complex liquid η as a function of the hydrodynamic radius of the probe was described in the following form:

$$\eta = \eta_0 \exp\left[\left(\frac{R_{eff}}{\xi}\right)^a\right] \tag{20}$$

Here η_0 denotes the viscosity of the pure solvent, ξ is the correlation length understood as the average distance between the polymer (crowder) network nodes, and a is an exponent of the order of unity. Parameter a may vary depending on the system, but its physical meaning remains unknown (Odijk,

2000). The relation described by Kalwarczyk *et al.* is devoid of previously observed discontinuity and provides a smooth transition between the nano- and macroscale. The suggested criterion of crossover between those two regimes is simple: the probe experiences macroscopic viscosity when its effective hydrodynamic radius is much larger than the hydrodynamic radius of the crowder.

All those investigations led to the construction of the scaling formula describing the diffusion of probes in biological complex systems – the cytoplasm of cells. By combining formulas for R_{eff} and η, the universal scaling law was proposed:

$$\ln\left(\frac{\eta}{\eta_0}\right) = \ln(A) + \left(\frac{\xi^2}{R_h^2} + \frac{\xi^2}{r_p^2}\right)^{-a/2} \quad (21)$$

The description was expanded by adding parameter A, which is a constant of the order of 1. Such scaling law proved successful in the description of a plethora of literature data, concerning bacteria *E. coli* and cytoplasm of HeLa and Swiss 3T3 cells (Kalwarczyk *et al.*, 2011, 2012, 2015). Also, a great part of this work is based on this description of the diffusion in the cytoplasm of living cells.

1.3. Fluorescence correlation spectroscopy

The fluorescence correlation spectroscopy (FCS) is a non-invasive technique allowing observation of single or several molecules in a confined space. FCS analyses time-dependent fluctuations of intensity of signal coming from fluorescent species. Those fluctuations are a result of some dynamic process, usually translational diffusion of fluorescent probes moving in and out of small detection volume of the order of femtoliter (10^{-15} l). Such extreme confinement is achieved thanks to the confocal aperture. Fluorescence fluctuations measured by FCS can be translated to obtain diffusion coefficient of the studied probe and also its concentration.

1.3.1. Fluorescence

The fluorescence is the emission of light by a molecule after absorption of a quantum of electromagnetic radiation. The absorption of the radiation induces so-called “excited state” of higher energy than the ground state of the molecule. The relaxation of such high energy state is achieved through different scenarios,

one of which could be the emission of light. In the overwhelming majority of cases, emitted light is of longer wavelength than the radiation which excited the molecule. The fluorescence takes less than 10^{-8} s.

The first observations of fluorescence, described in the literature, were made in the XVI century. Bernardino de Sahagun and Nicolas Monardes simultaneously described peculiar features of bark extract coming from two species of trees: *Pterocarpus indicus* and *Eysenhardtia polystachya*. These extracts emitted light under alternating strength of illuminating visible light (Valeur and Berberan-Santos, 2011). The emission was commonly used for authentication of wood shipments. Later it was proved that one of the flavoid compounds (maltalin) present in these extracts was responsible for the fluorescence. The term fluorescence was not used until 1852. This word was first coined by Stokes in his work describing changes in the wavelength of light. It is analogous to the word opalescence – fluorescence originating from fluorspar (Stokes, 1852).

The fluorescence is a phenomenon of excitation and relaxation of a fluorescent species (fluorophores). A quantum of electromagnetic radiation is absorbed by the fluorophore, creating an excited singlet state (S_1). This excited state exists for a short time during which it undergoes series of non-radiative transitions. These transitions called internal conversion ends with the partial dissipation of absorbed energy and leaves molecule at the lowest vibrational energy of the excited state. From this state spontaneous emission of light takes place. Hence the fluorophore returns to the ground state (S_0). Overall illustration of the changes occurring in the fluorescence is presented at the Jablonski diagram (Figure 8. A.).

The fluorescence is not the only way of emission of energy from the excited molecule. Most of the time, an excess of energy (above the ground state) is dissipated into the environment as heat (photons in the infrared range of the electromagnetic radiation, responsible for the vibrations in the molecules). Also, another luminescent phenomenon – phosphorescence – can take place (Figure 8. B.). The phosphorescence results from the effect of intersystem crossing, meaning that the molecule assumes additional state (called the triplet state). Since this phenomenon requires a forbidden transition, the phosphorescent emission is delayed. The phosphorescence occurs usually in the range of microseconds or more (after the irradiation pulse) whereas the fluorescence under nanoseconds.

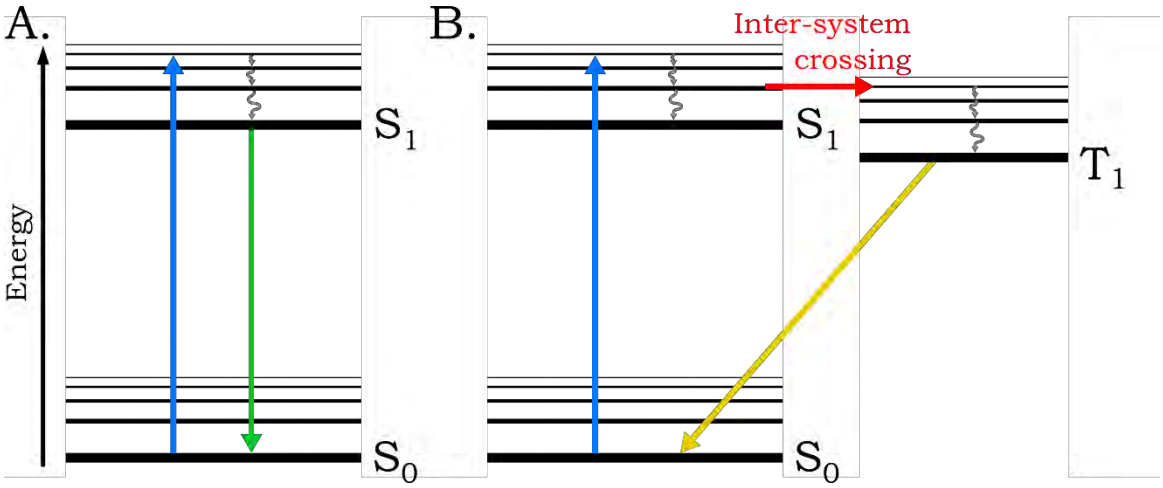

Figure 8. The Jablonski diagram for fluorescence (A) and phosphorescence (B). S_0 and S_1 represent the ground state and the first excited singlet states respectively, whereas T_1 corresponds to the triplet state. Thinner lines represent vibrational excited states.

The molecules have few ways of relaxation which is reflected in the quantum yield. This quantity is expressed as a probability of emitting quantum of light after excitation pulse. Furthermore, non-radiative transitions in excited molecules are the reason why the emitted light is shifted towards longer wavelengths when compared to exciting one. This difference in wavelengths of absorbed and excited lights is called the Stokes shift (Atkins and De Paula, 2010).

1.3.2. Biofluorescence

The biofluorescence is a physical phenomenon of the fluorescence observed in living organisms. It is most prevalent in marine organisms (both invertebrates, like corals, and vertebrates – fish) but also was observed in butterflies, parrots and flowers (Sparks *et al.*, 2014). Although its evolutionary purpose is still uncertain, it is suspected to play role in recognition and mating. The biofluorescence is currently extensively used in life sciences and medicine (e.g. Ingram *et al.*, 2013).

The most important fluorescent protein is the green fluorescent protein (GFP) coming from jellyfish *Aequorea victoria*. Since its discovery, it is the most intensively studied and used protein (Tsien, 1998). Native GFP has two excitation peaks (major at 395 nm and minor at 475 nm) and a single emission peak in the visible range (at 509 nm). It has relatively small, robust structure and it is easy to use. Numerous variants and applications of GFP were created.

Currently, over 200 modifications of the GFP are available (Stepanenko *et al.*, 2008). They can differ in the wavelength of emitted light, some are photoswitchable (capable of changing the wavelength of emitted light after the irradiation by a specific wavelength of light). GFP and its variants have been the subject of the astounding number of studies and applications (e.g. Chiu *et al.*, 1996; Feng *et al.*, 2000; Patterson, 2002). The importance of GFP in biology was ultimately recognized in 2008 when the Nobel Prize in Chemistry was awarded jointly to Osamu Shimomura, Martin Chalfie and Roger Y. Tsien "for the discovery and development of the green fluorescent protein, GFP".

The biofluorescence should not be mistaken with the bioluminescence. The bioluminescence (for example seen in fireflies) is a result of chemical reaction (in case of fireflies: oxidation of luciferin). This means that bioluminescence consumes energy reserves of an organism, while in case of biofluorescence required energy comes from an external source. The GFP is in a way connected to bioluminescence. Inside *A. victoria* excitation light needed for GFP fluorescence to occur comes from the luminescent reaction of aequorin with calcium ions. Hence, naturally occurring GFP light is, in fact, a result of resonant energy transfer phenomenon.

1.3.3. Introduction to FCS

The theory of fluorescence correlation spectroscopy (FCS) was created in the early seventies of the last century. In series of works Magde, Elson and Webb described formalism, various models and possible application of newly created method (Magde *et al.*, 1972, 1974; Elson and Magde, 1974). Those works were at that time performed under huge limitations since no aperture was able to truly meet the requirements of the theory. This hindrance was overcome in the nineties when a single-molecule detection limit was reached by Rigler and Eigen (Rigler *et al.*, 1993). In their works, they combined FCS with confocal microscopy. Together with growing accessibility of ultrasensitive detectors, this combination allowed the FCS to grow to its full potential. Currently, numerous variations stemming from original FCS idea exist (Macháň and Wohland, 2014): fluorescence cross-correlation spectroscopy (FCCS), which allows dual-colour measurements of two fluorescent species (Triffo *et al.*, 2012); stimulated emission depletion (STED FCS), which allows even further reduction of focal volume (Ringemann *et al.*, 2009), or raster image correlation spectroscopy

(RICS), which correlates the images taken by scanning the sample at fixed speed (Illaste *et al.*, 2012). With all its advancements the FCS can be successfully applied for a wide variety of problems. Most common use of the FCS is measurements of the diffusion coefficient. From such measurements, the FCS can be easily repurposed for determination of the hydrodynamic radii and the concentrations of molecules and complexes. Possible applications also extend to studies of kinetic rates of chemical reactions, complexation or oligomerization of particles and singlet-triplet dynamics (Haustein and Schwille, 2003). We successfully applied the FCS for the studies concerning crowding of the cell cytoplasm. We confirmed the existence of the lengthscale dependent viscosity in the cell cytoplasm. We also investigated the mechanism of oligomerization of the Drp1 protein, compared the nanoviscosity of cancerous and non-cancerous cells, and monitored structural changes of the cytoplasm during the cell cycle of human cell.

1.3.4. FCS experimental setup

Over 40 years of development of FCS have resulted in modern, commercially available and user-friendly setups. Original ideas have been supplemented with extensions which dramatically improved the reliability of obtained data. Currently, the confocal aperture is coupled with robust single photon counting systems. This system permits acquisition of fluctuations of fluorescence coming from species present in extremely small volumes. Schematic representation of the typical FCS instrumentation is presented in Figure 9.

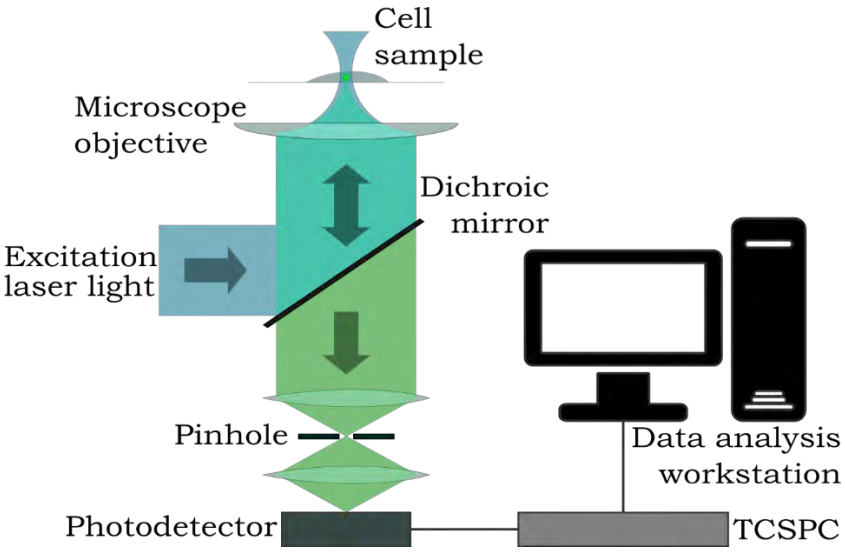

Figure 9. Standard FCS setup. TCSPC – time-correlated single-photon counting device.

The excitation light coming from a laser source is first reflected by a dichroic mirror and illuminates the sample. The illuminated part of the sample is called the focal volume. Precise focusing of the light is obtained thanks to the confocal objective with a high numerical aperture (NA>0.9). This value describes how many photons coming from the illuminated volume are collected by the objective. NA is defined by the following equation:

$$NA = n \sin\theta \tag{22}$$

Where n denotes the index of refraction of the medium surrounding the lens and θ is the maximal half-angle of the cone of the light entering the lens. Since NA of the objective needs to be high, air objectives cannot be applied (n of air is equal to 1). Usually, water ($n = 1.33$) or oil ($n > 1.5$) immersion objectives are used (Hell *et al.*, 1993).

The light coming from the laser source induces the fluorescence of the probes which are travelling through the focal volume. The emitted light is collected by the objective. Some of the excitation light is also reflected back but is cut off (partially) by the dichroic mirror. The separated fluorescent signal then travels through the pinhole. This element filters out-of-focus light. In the FCS the detection volume is limited to the range of femtoliters (10^{-15} l). Our equipment allowed the reduction of the focal volume up to ~0.2 fl.

The emitted light falls onto the set of wavelength filters. Here remnants of the reflected excitation beam and fluorescence of undesired wavelengths are blocked. These filters protect the fluorescent signal from being covered by the interferences. Also, filters protect the detectors from being overrun by the intense signals and blocked or even damaged.

The purified signal finally reaches the detectors. These devices quickly (high time resolution) and sensitively (high quantum efficiency) register incoming photons. As detectors, the single-photon avalanche diodes (SPADs) or photomultiplier tubes (PMTs) can be used. The former are usually characterized by lower quantum efficiencies and lower number of dark counts (false-positives) than the latter (Hess *et al.*, 2002). The detectors are coupled with the additional processing unit – the time-correlated single-photon counting module (TCSPC). This device adds a time stamp to each event of photon detection which allows further correlation and analysis of all data points by the dedicated software.

1.3.5. FCS theory

FCS is a technique that monitors fluctuations of fluorescent particles moving in and out of the focus of the confocal microscope. Direct counting of the number of particles is impossible, so the fluorescence intensity $I(t)$ of particles temporarily present in the focus is analysed instead. After the excitation, the fluorescent signal is emitted in the order of nanoseconds (10^{-9} s). Each excitation event produces photons emitted in random directions meaning that only a fraction of them will be collected by the objective. The number of detections and subsequent signals received is proportional to the number of particles present in the detection volume. This output is the fluorescence intensity $I(t)$. Fluctuations of intensity $\delta I(t)$ and overall intensity $I(t)$ are connected according to the formula:

$$I(t) = \langle I \rangle + \delta I(t) \tag{23}$$

Where $\langle I \rangle$ denotes average fluorescence. It is possible to extract fluctuation times from obtained signal using the autocorrelation function (ACF, here denoted as $G(t)$). It measures the self-similarity of the fluctuations at time t compared to itself after a lag time τ. The ACF is defined as follows:

$$G(t) = \frac{\langle \delta I(t) * \delta I(t+\tau) \rangle}{\langle I(t) \rangle^2} \tag{24}$$

The fluctuations of the fluorescence intensity $\delta I(t)$ compared to those measured after longer lag times $\delta I(t+\tau)$ do not show any self-similarity in the signal since fluctuations at those two times are caused by different particles. Hence, the autocorrelation is supposed to be small (near 0). When τ is small enough, that the fluctuations at the time t and $t+\tau$ originate from the same set of molecules, self-similarity (and autocorrelation) will be high. The ACF transforms data obtained in the real-time into the lag time domain (Lakowicz, 2006).

The calculations of ACF cannot be done without proper characterization of the detection volume. Usually, the geometry of the focal volume is approximated as a three-dimensional Gaussian, because the edges of the detection volume created by the illuminating laser are not sharp. Such shape can be imagined as an ellipsoid with w_0 and z_0 as shorter and longer radii respectively. Model of such structure is illustrated in Figure 10.

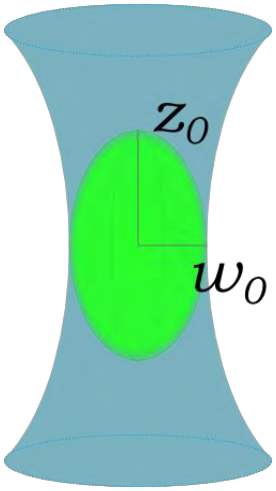

Figure 10. A schematic representation of the illumination spot in the FCS. The green area represents the focal volume with z_0 and w_0 denoting longer and shorter radii of the ellipsoid.

The effective volume of such ellipsoid can be calculated by the following equation:

$$V_{eff} = \pi^{3/2} * w_0^2 * z_0 \tag{25}$$

To obtain the diffusion coefficient and the number of particles, theoretical models conjugated with basic diffusion laws have to be applied. On their basis a relationship between the autocorrelation function, average retention time (diffusion time τ_D) of the fluorophore and the shape of the detection volume can be established:

$$G(\tau) = G(0) * \left(1 + \frac{\tau}{\tau_D}\right)^{-1} * \left(1 + \frac{\tau}{\kappa^2 \tau_D}\right)^{-1/2} \tag{26}$$

Here, $G(0)$ is the amplitude at $\tau = 0$ and is equal to the reciprocal of the average particle number inside the focal volume, N:

$$G(0) = \frac{1}{N} \tag{27}$$

Thus, $G(0)$, directly provides the concentration of fluorescent particles $C = N/V$ from the known size of the focal volume, V_{eff} (Eq. 25). The FCS is very sensitive to small number of molecules (see: Eq. 27) since the amplitude of the autocorrelation function decreases with N. Practically, for concentration decreasing below 0.1 nM the signal to noise ratio decreases so much, that it precludes accurate determination of $G(0)$. The main source of the noise is the autofluorescence of the environment and dark-photon (or ghost-photons) counts

in the photomultipliers. Although the $G(t)$ (Eq. 24) is independent of the brightness of a fluorophore, yet the signal intensity $I(t)$, and consequently the signal to noise ratio are proportional to the brightness of the molecules. For bright molecules, emitting a lot of photons, the signal to noise ratio is high and the measurements can be made even at concentrations lower than 0.1 nM.

κ is the quantity called the structure parameter. It is a measure of the elongation of the focal volume and is defined as (see: Figure 10):

$$\kappa = \frac{z_0}{w_0} \tag{28}$$

The mean distance covered by a freely diffusing molecule in a time τ is proportional to $\sim\sqrt{D\tau}$, therefore the molecule will cover the distance w_0 across the focal volume in time:

$$\tau_D = \frac{w_0^2}{4D} \tag{29}$$

For the known focal volume typically measured during the calibration of the FCS set-up, the diffusion coefficient of a fluorophore is readily obtained from Eq. 29, where the time τ_D is calculated from the fit of the autocorrelation function (Eq. 26) to the FCS experimental data (Elson, 2011).

The data obtained by the FCS can be easily misinterpreted. Although $G(0)$ is independent of the molecular brightness, the ACF can be distorted by any changes in the emission patterns. The simplest example of such phenomenon is photobleaching of probes. The photobleaching happens when the structure of the molecule is permanently altered in such way, that fluorescence is no longer possible. Using stable fluorophores and avoiding excessive laser power makes this affect practically non-existent.

The second problem is a more profound one. Fluorescent molecules can sometimes enter the triplet state. In the triplet state the molecules transiently lose the ability to emit photons. This phenomenon is registered as the blinking of the probes (at the time scale of the order of microseconds) and has an impact on the shape of the autocorrelation curve. The simplest ACF has to be expanded to take into account the triplet states and finally takes following the form (Dross *et al.*, 2009):

$$G(\tau) = G(0) * \left(1 + \frac{p}{1-p}\exp\left(\frac{-\tau}{\tau_t}\right)\right) * \left(1 + \frac{\tau}{\tau_D}\right)^{-1} * \left(1 + \frac{\tau}{\kappa^2\tau_D}\right)^{-1/2} \quad (30)$$

Here, p denotes the fraction of the particles present in the focus which are in the triplet state and τ_t is the lifetime of this state.

1.3.6. FCS in living systems

Under the diffraction-limited conditions, the detection volume of FCS reaches tenths of femtoliter. Such value is three to four orders of magnitude smaller than the average size of the eukaryotic cell. Therefore, FCS can be successfully applied inside the cells. The first application of FCS to such problems comes from the mid-seventies of the last century. Elson *et al.* measured the diffusion of fluorescently labelled lipids on membranes of rat myoblasts (Elson *et al.*, 1976). The first use of FCS coupled with confocal aperture comes from nineties when mobility of inert molecules microinjected into the cell cytosol was studied (Berland *et al.*, 1995; Brock *et al.*, 1998). Thanks to capabilities of the FCS questions concerning the diffusion and transport of molecules inside the cytoplasm, the nucleus or the membranes could be answered. A great diversity of approaches and modification of the original FCS idea exist. Many of them were developed as a mean to elucidate specific issues or phenomena taking place inside the living cells or even organisms.

Pioneering FCS studies on living organisms were conducted on membranes. First of all, the thickness of lipid bilayer (~4 nm) is around three orders of magnitude smaller than height of the focal volume. Therefore, diffusion of a probe in the membrane can be treated as two-dimensional. Also, usually membranes exhibit negligible autofluorescence, which improves the signal-to-noise ratio. Both of these factors facilitates data analysis (Hess *et al.*, 2002). The FCS helped solve several problems concerning the cell membrane architecture and protein binding reactions. For example, Gerken *et al.* (2010) measured selectivity of proteins to specific domains and role of cholesterol in this process. Similar experiments were performed by Lillemeier *et al.* (2010) and Mueller *et al.* (2011). These experiments are prone to artefacts that influence the data obtained. Due to slower diffusion (up to 50-fold; Dix and Verkman, 2008), probes in membranes are much more prone to photobleaching. The autofluorescence of the cells creates the unwanted background. Furthermore, the membranes could reshape in course of the experiment, dramatically

changing the observation area (Mütze *et al.*, 2011). Most of those issues are diminished by the introduction of the stimulated emission depletion (STED) systems.

Most of the works using the FCS for studies of biological phenomena concern the cell interior – the cytoplasm and the nucleus. Many studies compared diffusion of probes of different characteristics (biological character, size, interactions etc.). All these works confirm that internal environment of a living cell differs greatly from *in vitro* conditions. Protein-rich cell cytoplasm is commonly described as the crowded environment with diffusion times several times greater than in water (e.g. Seksek and Verkman, 1997; Elsner *et al.*, 2003; Mahen *et al.*, 2011). Thanks to capabilities of FCS, the structure and dynamics of the cytosol were successfully described. Also, the extent of the cytoplasm heterogeneity and its impact on the diffusion and interpretation of data has been thoroughly studied. Analogous FCS experiments were also conducted inside the cell nucleus. The chromatin network and its organisation were characterised in detail (e.g. Wachsmuth, Waldeck and Langowski, 2000; Gorisch, 2005; Bancaud *et al.*, 2009). Hinde *et al.* (2010; 2012; 2011) investigated the architecture of the chromatin. In the interphase nuclei, they discovered borders separating regions of high and low DNA concentrations. These borders proved to be entirely permeable to a small molecule (fluorescein), while protein (monomeric GFP) could cross them only in occasional bursts.

Currently, the most prominent use of the FCS extends to the studies of the complex formation of two biomolecules, or a biomolecule and a potential therapeutical agents. Such measurements are based on a significant decrease of the diffusion coefficient of the studied molecule after the binding to its molecular target, providing that the target is much larger than the molecule. Typically, the diffusion of small tracer (either fluorescent or fluorescently labelled) is first tested without interactions. In this way, the reference diffusion coefficient of freely diffusing molecule is obtained. Then, the data obtained for the diffusing molecule in the presence of the target provides the equilibrium constant for the complex formation. Unfortunately, this approach is limited by the ratio of sizes of the two components in the complex. In order to detect differences in the diffusion times, the fluorescent tracer has to be 1.5 to 2 times smaller than the second component (Haustein and Schwille, 2003). Hence, classical FCS is restricted to interactions of small molecules (or proteins) with

huge biological complexes. For example, Broderick *et al.* (2012) utilised this approach for the studies of interactions of a fluorescently labelled member of the cyclin-dependent kinases, Cdc45 protein, with CMG (Cdc45/Mcm2-7/GINS) complex. By comparing the diffusion rates of proteins of similar size, they showed that inside the nucleus the Cdc45 is a part of the protein complex. The size of this complex is significantly bigger than previously observed *in vitro*, suggesting that outside the nuclei it partially dissolves. In their work, they also confirmed that the investigated complex is transiently binding to the DNA. When using the FCS in the standard mode for the interaction studies, the interacting partner cannot be identified directly.

In the second possible approach, the evaluation of the molecular interactions is obtained by cross-correlations of signals coming from two molecules forming the complex, each labelled by the different fluorophore. This extension of the FCS technique is called the fluorescence cross-correlation spectroscopy (FCCS). The fractions of interacting molecules can be retrieved by the analysis of the autocorrelation functions for these two diffusing molecules. The FCCS removes limitations with regard to the size of the studied molecules. The improvement of range of applicability also increases the complexity of the data analysis. Three main artefacts can influence the reliability of the data obtained by the FCCS. The first is crosstalk between detection channels, which increases apparent cross-correlation. Statistical filtering solves this issue (Padilla-Parra *et al.*, 2011). The second is misalign of the effective detection volumes for respective channels. This effect lowers the apparent cross-correlation. Using a single wavelength for the excitation of both fluorophores offers a partial solution to this problem (Foo *et al.*, 2012). The third artefact is connected to the imperfect labelling of the probes. The probes devoid of the fluorescent tag or those with damaged fluorophores (e.g. as a result of photobleaching) can cause false interpretation of the data. The complexes containing such molecules can be interpreted as free molecules. The apparent fraction of interacting pairs will be lower than the actual one. To overcome this problem, great attention is required during the preparation of the sample. Also, appropriate maturation times of the fluorescent proteins must be assured (Hou *et al.*, 2014).

1.3.7. Problems concerning FCS in living cells

The FCS has many traits which make it a great technique for the studies of the diffusion and the interactions of the fluorescent molecules in the living cells. Small detection volume allows precise localization inside a specific region of the cell. To obtain optimal amplitudes of the autocorrelation curves, the nanomolar concentration of the fluorescent tracers is required. Such small numbers of the molecules prevent drastic alteration of the physiological conditions during the experiments. A broad variety of commercially available systems of FCS allows to choose the best one for a given problem. Despite its considerable advantages FCS still suffers from few limitations.

All fluorescence-based techniques inside the living cells have to deal with the issues of the autofluorescence of cells (decreasing the signal to noise ratio) and the photobleaching of tracers (influencing the quality of data obtained). Depending on the experimental conditions, a small concentration of probes can be a hindrance instead of an advantage, because of a weak signal. Plus, overall possible concentration of studied probe is narrow (10 pM-0.1 μM). During the measurements performed inside cells, limited pool of probes is available, making the decrease of the signal in time significant and unavoidable. Additionally, aggregation of the probes can occur, which results in lower than expected diffusion constants and influences the concentration measurements. Also, unspecific interactions of the tracers with big cellular structures are often present. This is especially common for standard dyes (e.g. rhodamines and cyanines) which are often lipophilic and therefore tend to bind to the cellular membranes (Dittrich *et al.*, 2001). This binding influences free diffusion inside of a cell and can render fluorophores more prone to the photobleaching. Next limitation comes from the acquisition time of the autocorrelation function, which must be greater than the time constant of investigated phenomenon. Also, excitation laser power may cause problems. To efficiently observe small, fast diffusing tracers high laser power is required. On the other hand when studying slowly moving huge complexes long acquisition time of data is necessary, so laser power should be limited to avoid extensive photobleaching. The final troublesome factor of the FCS measurements is a need for proper data fitting. Choice of a theoretical model is ambiguous and correct data interpretation may be problematic (Brock, 2006).

1.3.8. Models of diffusion in living cells

The autocorrelation curves obtained from the biological systems are usually fitted with the most appropriate physical model, either the one-component, two-component or anomalous diffusion. Rarely, the three-component model is applied. Also, blinking dynamics of the brightness of probes has to be included in the model. Commonly, more than one model is tested and, if similar results are obtained, simpler one is preferred (Kim *et al.*, 2007).

In the simplest case, the one-component model is used (Eq. 26). The model is applied to unhindered diffusion of a small, inert tracer inside a homogeneous medium. For example, the diffusion of Alexa Fluor 488 hydrazide (Kim *et al.*, 2007) or enhanced green fluorescent protein (EGFP) inside the cell cytosol (Wachsmuth *et al.*, 2000) is described by the model.

The diffusion of the biological molecules and their complexes in the cell cytoplasm cannot be described by the one-component diffusion model. The data obtained from the intracellular experiments are described using either multicomponent or anomalous diffusion models. The former describes the situation when two or more independently diffusing species are observed, each of them with its own characteristic diffusion coefficient. The general form of the multicomponent diffusion is expressed as:

$$G(\tau) = \sum_i G_i(0) * \left(1 + \frac{\tau}{\tau_i}\right)^{-1} * \left(1 + \frac{\tau}{\kappa^2 \tau_i}\right)^{-1/2} \quad (31)$$

where indices i denote the ith component. In the multicomponent diffusion model the data analysis is performed by fitting many parameters. In practice during fitting as many parameters as possible should be fixed. Their values should be derived from studies of isolated or non-interacting molecules. The bigger the number of free parameters the better the apparent fit, yet less reliable results.

The anomalous diffusion model is used for the description of the diffusion of molecules experiencing some sort of abnormalities. This model assumes the existence of an additional parameter α, which is added to the description of the diffusion:

$$G(\tau) = G(0) * \left(1 + \left(\frac{\tau}{\tau_D}\right)^{\alpha}\right)^{-1} * \left(1 + \frac{1}{\kappa^2}\left(\frac{\tau}{\tau_D}\right)^{\alpha}\right)^{-1/2} \quad (32)$$

The parameter α is a measure of the degree of alteration of motion created by the environment. Two kinds of anomalous diffusion can be distinguished. The first, when $\alpha < 1$ is called the subdiffusion, whereas the superdiffusion occurs when $\alpha > 1$. The subdiffusion corresponds to the situation when an environmental heterogeneity hinders the diffusion, either as result of the nonspecific interactions of a fluorescent probe or high concentration of the obstacles (in cellular conditions: the organelles, the cytoskeleton or the chromatin). This kind of movement is also observed for the crowded environments. The superdiffusion depicts situation when the movement is "assisted" by an additional force, e.g. active transport. The superdiffusion is scarcely observed in the cellular environment (Weiss, 2014).

The interior of a cell is highly heterogeneous. Wachsmuth *et al.* (2000) showed that movement of the enhanced green fluorescent protein (EGFP) in the cytosol can be described by the normal diffusion. When diffusion of the EGFP is traced inside the nucleus, anomality arise. This leads to the assumption that cellular organelles have a great impact on the diffusion. Furthermore, some extensions to the existing models were made, depending on experimental conditions. Gennerich and Schild (2000) proposed updated two- and three-dimensional models to describe the diffusion in the confined spaces. They tested their assumptions in the study of the dendrites of the neurons.

In their work Kalwarczyk *et al.* (2017) demonstrated, that apparent anomality can originate from the polydispersity of the probes. Through series of *in vitro*, *in vivo*, and *in silico* experiments they showed that the hydrodynamic drag of the fluorescently labelled dextrans introduced into the cell cytoplasm effectively broadens the distribution of their diffusion times. The hydrodynamic drag is a value that is exponentially dependent on the size of the probe. In consequence, the degree of (apparent) anomality of the diffusion deepens with the increasing probe polydispersity. Kalwarczyk *et al.* suggested that the anomalous diffusion may be the average of the interactions of the studied probes with the cell interior. Kalwarczyk *et al.* also showed that the EGFP is a monodisperse probe which movement can be successfully described by the one-component model.

Materials and methods

2.1.Cell culture handling

Cell sources

All cells were either provided by the Nencki Institute of Experimental Biology (Warsaw, Poland) or directly purchased from distributors. HeLa, A549, MCF-7, Hep G2, U2OS and Human primary small airway epithelial cells (HSAEC) come from American Type Culture Collection (ATCC; USA). HeLa-GFP inducible line was purchased from AMS Biotechnology (USA). HeLa Kyoto strain was a gift from Jan Ellenberg (EMBL Heidelberg) with the permission from Shuh Narumiya (Department of Pharmacology, Kyoto University Graduate School of Medicine, Japan). Human skin fibroblasts come from Coriell Institute for Medical Research (USA). Most important characteristics of the cell lines used in this thesis are presented in Table 2.

Cell line	Source	Character	Morphology
HeLa	Cervix	Cancerous	Epithelial
Hep G2	Liver	Cancerous	Epithelial
MCF-7	Breast	Cancerous	Epithelial
A549	Lung	Cancerous	Epithelial-like
U2OS	Bone	Cancerous	Epithelial
Fibroblasts	Skin	Normal	Mesenchymal
HSAEC	Lung	Normal	Epithelial

Table 2. Characterization of the cell lines used in the experiments.

Culture media

Majority of the cells (HeLa, HeLa Kyoto, A549, Hep G2, U2OS, skin fibroblasts) were cultivated according to the standard protocol. Culture medium contained Dulbecco's modified Eagle's medium (DMEM; Institute of Immunology and Experimental Technology, Poland) with 10 % heat-inactivated foetal bovine serum (FBS), L-glutamine (2 mM), penicillin (100 mg/ml) and streptomycin (100 mg/ml). All supplementary components of the basic medium were purchased from Sigma-Aldrich (USA). The medium was further enriched with 0.01 mg/ml of insulin (Sigma-Aldrich, USA) for MCF-7 cells or with 1 % MEM non-essential amino acid solution (Sigma-Aldrich, USA) for HeLa-GFP line. The culture of the HSAEC was performed according to the specialized protocol provided by their supplier. Only dedicated reagents were used.

Culture conditions

On daily basis, all cells were cultivated in 25 cm^2 culture bottles (Greiner Bio-One GmbH, Austria) at 37°C in a 5 % CO_2 humidified atmosphere. Passages were performed every two-three days (cells at 70-90 % confluence) according to the standard protocol (unless stated otherwise). For the probe introduction and subsequent FCS measurements, all cells were grown on 35 mm thin glass bottom CELLview Cell Culture Dishes (Greiner Bio-One GmbH, Austria) up to 80 % confluence. For the transfection procedure on 8-chamber coverglass Lab-Tek slides (Thermo Fisher Scientific, USA). For other experiments, the cells were cultured on the standard 35 mm dishes (Sarstedt, Germany).

Standard passage protocol

Used medium was first aspirated from the culture bottles. Then cells were washed with 1 ml of phosphate buffered saline (PBS) without $MgCl_2$ and $CaCl_2$ (Sigma-Aldrich, USA). The PBS washing allowed to remove any residual medium. PBS was devoid of bivalent ions which inhibit the action of the trypsin. Then 0.5 ml of 0.25 % trypsin-EDTA solution (Thermo Fisher Scientific, USA) was added. The flasks were then shortly incubated at 37°C. This caused cells to detach from the surface of the flask. After the incubation bottles were gently tapped and rinsed with 2 ml of fresh medium. Depending on the cell line 0.5-1 ml of the cell suspension was left in or transferred to the new flask (culture plastics were changed each third passage). Finally, 4 ml of fresh appropriate medium was added.

Passage of HSAEC

As previously mentioned, the passage of the HSAEC was performed according to the supplier's protocol using only dedicated media (all from ATCC, USA). First, spent medium was removed and cells were gently rinsed with 3ml of D-PBS. Then 1 ml of trypsin-EDTA solution was added, spread onto the whole surface of the bottle and its excess aspirated. Afterwards, the cells were observed under the microscope and as soon as they started to detach and pull away, the flask was gently tapped from several sides. After the majority of cells seemed detached, 1 ml of trypsin neutralizing solution was added. The dissociated cells were collected into a conical tube and set aside. Next, 3 ml of D-PBS was added to the culture bottle to collect any residual cells. The cell suspension was joined with D-PBS and centrifuged at 150 x g for 5 min. The solution was then

aspirated. The cell pellet was resuspended in 1 ml of fresh culture medium and 0.5 ml was transferred to a new flask. Finally, 4 ml of culture medium was added.

Microinjection

For the microinjection experiments, the cells were grown on the 35 mm glass bottom dishes prior to the probe introduction. The microinjection was performed using Femtojet system (Eppendorf, Germany), with glass capillaries fabricated in the micropipette puller P-1000 (Sutter Instrument, USA). The capillaries had the outer diameter smaller than 1 μm. Each capillary was loaded with 3 μl of the solution of either fluorescently labelled dextran (Dex; all from Sigma-Aldrich, USA) or custom synthesized silica nanoparticles (NP; Siliquan, Poland). Table 3. shows the most important characteristics of all the fluorescent probes used in the experiments.

Probe name	r_p [nm]	c [μM]	Method of introduction
Calcein-AM	0.65	2	Cellular uptake
Dex-4.4 kDa	1.3 ± 0.2	9/0.09	Microinjection/pinocytosis
EGFP	2.5	-	Stable expression
Dex-20 kDa	3.8 ± 0.3	40	Microinjection
Dex-40 kDa	4.9 ± 0.5	10	Microinjection
Dex-75 kDa	5.6 ± 0.5	5	Microinjection
Dex-155 kDa	8.6 ± 0.7	9/9	Microinjection/pinocytosis
NP S34	20.6	1	Microinjection
NP S43	33.5	1	Microinjection
NP S42	50.0	1	Microinjection

Table 3. Characteristics of the probes used in all the experiments. r_p – the hydrodynamic radius of the probe measured in water by the FCS; c – the concentration of the solution used for the microinjection. (±) denotes standard deviation.

Approximately 300 cells were injected during one session. The injection pressure was equal to 160 hPa, the injection time to 0.2 s, and the compensation pressure to 30 hPa. Just prior to the FCS measurements culture medium was replaced by PBS containing Ca^{2+} and Mg^{2+} ions.

Pinocytosis

As a faster, more robust method of introduction of two fluorescent dextrans (4.4 kDa and 155 kDa) commercially available approach was used (Influx Pinocytic Cell-Loading Reagent; Thermo Fisher Scientific, USA). Prior to the pinocytosis procedure, all required media were prepared in accordance with manufacturer's protocol. First, the hypertonic solution was prepared. It consisted of 20 µl of loading solution with the addition of 2 µl of the fluorescent probe solution (0.4 µl/ml and 1.5 mg/ml for Dex-4.4 kDa and Dex-155 kDa respectively). This solution was incubated at 37°C. The cells were grown in the culture flask and prepared as for the standard passage. Spent media was aspirated, cells were washed with PBS, and 1 ml of trypsin was added. After short incubation detached cells were suspended in 5 ml of fresh medium. Then the suspension was centrifuged (3500 rpm; 5 min) and the supernatant removed. Cells were suspended in 1 ml of medium, transferred to Eppendorf tube and centrifuged again (2500 rpm; 1 min). The supernatant was removed again. Then, previously prepared loading solution was added and the cells were incubated (37°C; 10 min). Next, 1 ml of hypotonic medium was added to the cell suspension and cells were transferred to the test tube containing additional 2 ml of hypotonic medium. The suspension was divided equally into 3 Eppendorf tubes, incubated (37°C; 1.5 min), and centrifuged (2500 rpm; 1 min). The medium was aspirated. Cells were finally suspended in 2 ml of fresh, appropriate culture media and transferred onto 35 mm glass bottom dishes. Before measurements cells were allowed to grow for 24 hours.

Introduction of other probes

Calcein was introduced into the cell cytoplasm by adding 2 µl of solution (2 µM) of its non-fluorescent derivative Calcein-AM (Sigma-Aldrich, USA) to the culture media and incubating for 10 min. After molecule was uptaken by the cells, the acetomethyl ester was hydrolysed by intracellular esterases producing fluorescent molecule. Prior to the FCS measurements, the culture medium was replaced by PBS.

The EGFP was constantly expressed in the cell line stably transfected with the appropriate plasmid. Normally, expression of protein would have to be induced, but for our FCS measurements, the level of the EGFP resulting from the promoter leakage was sufficient.

Introduction of Drp1 mutants

All EGFP-Drp1 mutant-carrying plasmids (K668E, G363D, C505A) were prepared by Bernadeta Michalska from the Nencki Institute of Experimental Biology (Warsaw, Poland) as described elsewhere (Michalska *et al.*, 2018). Ready-made appropriate plasmids were introduced into the HeLa Kyoto strain through the transfection. For this JetPRIME reagent (Polyplus Transfection, France) was used according to the manufacturer's protocol. Prior to the transfection cells were at 30 % confluency on 8-chamber Lab-Tek slides. First, 0.5 µg of appropriate plasmid DNA was mixed with 50 µl of the jetPRIME buffer, vortexed (10 s) and spun down. Then 1 µl of the jetPRIME reagent was added. The whole solution was vortexed again (10 s) and incubated for 10 min at room temperature. After that, the transfection mix was added into the medium in a single chamber. Cells were allowed to grow for 24 h prior to experiments.

Cell cycle synchronization

The synchronization of the cell cycle in HeLa GFP line was done using the aphidicolin. Ready-made solution (1 mg/ml) was purchased from Sigma-Aldrich (USA). Prior to the FCS measurements, the synchronized cells were grown on the 35 mm glass bottom dishes. For the cell counting and the flow cytometry six-well plates (Greiner Bio-One GmbH, Austria) were used instead. After the seeding, cells were allowed to adhere for 24 hours and then 5 µg of the aphidicolin per 1 ml of culture media was added. After 24 h of incubation, the medium containing the aphidicolin was removed and replaced with fresh one. Cells prepared in this way were subjected to further analyses.

2.2. Experimental techniques

Fluorescence correlation spectroscopy

The FCS measurements were performed using commercially available setup. It consisted of a confocal microscope (Nikon Eclipse TE2000U, Nikon, Japan) paired with the Pico Harp 300 TCSPC module (PicoQuant, Germany). During all the experiments stable temperature (36 ± 0.5°C) and atmosphere of the necessary humidity and composition was provided by the climate chamber (Okolab, Italy). Pulse diode lasers (PicoQuant LDH-D-C-485; 485 nm and PicoQuant LDH-D-TA-560B; 561 nm) driven by Sepia II module (all from PicoQuant, Germany) were used as the light sources. To avoid excessive

photobleaching of probes and phototoxicity in cells, low laser power (5-20 μW) was maintained. The observation of probes was performed using 60x (NA 1.2) objective with water immersion. The fluorescence signal was collected by the single photon avalanche diodes (MPD and PerkinElmer, USA). Each series of the measurements was preceded by a calibration step. A ~5 nM solution of either rhodamine 110 (λ_{ex}= 488 nm) or rhodamine B (λ_{ex}= 543 nm; both from Sigma-Aldrich, USA) in PBS with 2.5 $\%_{wt}$ glucose (Sigma-Aldrich; USA) was used for the calibration, depending on the probe used. The diffusion coefficient of 560 or 508 $\mu m^2/s$ (for rhodamine 110 and rhodamine B respectively) was used for the correction collar adjustments and the calculation of the size of the focal volume. This approach allowed to avoid the refractive index mismatch. Cells were selected for the measurements basing on the intensity of fluorescence. Those having too many or too few fluorescent particles were not suitable for the FCS measurements. During the measurements, the detection volume was positioned in a homogenous area of the cell cytoplasm. Regions of higher or lower fluorescence intensity were avoided. The number and duration of a single measurement per cell were adjusted depending on the kind of probe and the type of experiment. The acquisition of data was controlled via SymPhoTime 64 software (PicoQuant, Germany). The fluorescence lifetime filtering was used to improve the signal to noise ratio and eliminate the afterpulsing effect from the autocorrelation curves.

FCS for nanoviscosity curves

At least 5 measurements, each lasting 60 s, were taken in one spot for smaller probes (i.e. all probes apart from the calcein and the nanoparticles). Data acquisition for the calcein was limited to 30 s. For big nanoparticles a single measurement of 10 minutes duration was taken per cell. For each probe, two independent experimental runs were carried out, each consisting of at least 10 cells.

FCS of Drp1 variants

The experiment concerning the EGFP-Drp1 variants (3 mutant and wild-type protein) was performed in the same way as for nanoviscosity. For each cell, 10 consecutive measurements with the acquisition time of 30 s were performed. At least 8 cells for every variant were studied.

FCS of synchronized cells

In this experiment, 5 consecutive measurements, each lasting 60 s, were taken per cell. This experiment was repeated for the two separate rounds of the synchronization. Also, the start of the measurement in each cell was noted (in relation to the time of the aphidicolin removal). The whole experiment covered 30 hours from the restart of the cell cycle. All obtained results were grouped in the 30 min time periods, all of which consisted of at least 5 cells.

Data fitting

The fitting of the autocorrelation curves was performed using QuickFit 3.0 software (Division Biophysics of Macromolecules, German Cancer Research Centre, Germany). Depending on the probe type, different modules were used. This approach is based on the investigations of Kalwarczyk et al. (2017). The autocorrelation curve for the calcein and the EGFP were fitted using the one-component free diffusion model with FCS Correlation Curve Fitting Plugin, function FCS: 3D Normal Diffusion, Levenberg-Marquard fit (without box constraints). For the dextrans anomalous diffusion fit with FCS Correlation Curve Fitting Plugin, function FCS: 3D Anomalous Diffusion, Levenberg-Marquard fit (without box constraints), and for the nanoparticles two-component free diffusion model with FCS Correlation Curve Fitting Plugin, function FCS: 3D Normal Diffusion, Levenberg-Marquard fit (without box constraints) was applied. During the fitting of data from the nanoparticles, the first component was fixed with $T = 19.7$ μs, $\alpha = 0.84$ and $\rho = 0.14$ (T – the time of diffusion, α – the anomality parameter and ρ – the fraction of this component). The existence of this component was derived from the measurements in water. We hypothesize, that it is connected with the unusual photophysics of the rhodamine B tightly packed within the core of the nanoparticles.

We used Gnuplot 5.0 software to fit the autocorrelation functions obtained during the Drp1 oligomerization experiments. The two-component model was applied for studies of the mutant Drp1 proteins (Eq. 31). The model had to be expanded by adding an additional component for the EGFP blinking for the G363D and C505A (dimerizing) mutants. This approach was based on previous works (Haupts *et al.*, 1998; Capoulade *et al.*, 2011). For the monomeric K668E mutant blinking component was indistinguishable from the signal. The blinking

time of the EGFP is approximately 150 µs whereas the diffusion times of the protein oscillated around 550 µs. Finally, fitting of the data from the measurements of the EGFP-Drp1 (wild type) was performed with three component diffusion model. During the fitting amplitudes and the diffusion time of the bound component were treated as parameters. In accordance with the limitations of the fitting algorithm, diffusion times of the dimer and the tetramer were fixed based on the results obtained for the mutant variants of Drp1.

Hydrodynamic calculations and modelling

All calculations of the hydrodynamic radii of proteins (EGFP and Drp1-EGFP variants) were performed using HYDROPRO software (Ortega *et al.*, 2011). The diffusion coefficients in water (D_0) at the temperature of 37°C and the viscosity of 0.69 mPas were obtained based on the available structural data (RCSB Protein Data Bank and EM Data Bank). The sizes of respective oligomers were calculated from appropriate diffusion coefficients in water D_0 using the Einstein-Stokes equation (Eq. 15) and expressed as the hydrodynamic radii. The models of the hydrodynamic radii of the Drp1 and GFP-Drp1 were created basing on the Drp1 (4BEJ) and the GFP (1EMA) structures obtained from the protein data bank (PDB). Data concerning the EGFP and EGFP-tagged ferritin were acquired using the same approach. The structure of the GFP-Drp1 was obtained in UCSF Chimera software (Resource for Biocomputing, Visualization, and Informatics (RBVI), University of California, USA) and saved in the .pdb format for calculations in HYDROPRO software. Four monomers of the Drp1 present in the 4BEJ asymmetric unit of the 4BEJ structure were used as the tetramer model. The biological assembly was used as the model of the dimer and the single Drp1 molecule from the dimer was the model of the monomer. Monte Carlo simulations, in detail described elsewhere (Kwapiszewska *et al.*, work under revision), were made utilising Mcell simulator (Stiles *et al.*, 1996; Schutter, 2001; Kerr *et al.*, 2008) supported by CellBlender 1.1 and FERNET Toolkit (Angiolini *et al.*, 2015)

Flow cytometry

The cells for the flow cytometry analysis were grown on the 35 mm standard culture plates (Greiner Bio-One GmbH, Austria). The cells were synchronized according to the protocol described above. Prior to cell collection 70 $\%_{vol}$ ethanol (POCH, Poland) was prepared and cooled in the refrigerator (-20°C). The

medium from above the culture was collected and stored for further use. The cells were then washed with 0.5 ml of PBS (PBS was also collected). Next, 0.5 ml of trypsin-EDTA solution was added and incubated for few minutes. The action of trypsin was quenched using 1 ml of previously collected medium. The detached cells were collected. All collected fluids (culture media, PBS and washing media) were joined and centrifuged (3500 rpm; 5 min). The supernatant was aspirated. The cells were washed with 1 ml of fresh PBS and centrifuged again. PBS was removed and cells were suspended in 0.5 ml of new PBS. Then, using plastic Pasteur pipette, the cell suspension was vigorously injected into 5 ml of the previously prepared ethanol solution. This protocol allowed fixation of samples. Using this procedure 2 separate repetitions of the synchronized cells were collected in the characteristic timestamps (0, 1.5, 4, 8, 12, and 24 hours after removal of aphidicolin). Also, three unsynchronized control samples were prepared. All samples were investigated by Dr Mirosława Koronkiewicz at the National Medicine Institute (Warsaw, Poland). Just before the flow cytometric measurements appropriate staining solution was added (Triton X-100, propidium iodide, RNase). The DNA content in the cells was measured using BD FACSCanto II apparatus (BD Biosciences, USA). The data analysis was done employing FCS Express 4 (De Novo Software, USA).

Cell size measurements

For the cell count measurements, the cells were prepared as described above. The number of cells was determined by the Countess™ II FL Automated Cell Counter (Thermo Fisher Scientific, USA). After the detachment of cells from culture dishes, 10 µl of the cell suspension was mixed with 10 µl of 0.4 % trypan blue solution (Thermo Fisher Scientific, USA). Then, 10 µl of the stained cell suspension was transferred onto the dedicated cell counting slides. After 30 s the slides were put into the apparatus. The cell counting was performed automatically. Objects of the diameter less than 5 µm were excluded as possible debris. For each sample, three measurements were taken (two independent runs were always conducted) and averaged.

Results and discussion

3.1. Length-scale dependent viscosity in the cell cytoplasm

The study of the length-scale dependent viscosity of the HeLa cells cytoplasm was conducted. The phenomenon was described by Hołyst *et al.* (2009) Kalwarczyk *et al.* (2011), and Tabaka *et al.* (2014). The measurements of the diffusion coefficient in the cytoplasm of the mammalian cells, used by Kalwarczyk *et al.* and Tabaka *et al* were obtained from the literature. The literature data were based on the measurements of sometimes ill characterized probes, by many different techniques in different temperatures and culture conditions. Thus, there was a need to make proper, accurate and precise measurements of the length-scale dependent viscosity in the cytoplasm of cells at the fixed physiological temperature, using well characterized probes, cell cultures and growth medium. The results presented in this sub-chapter were obtained in such conditions for the HeLa cell line.

Non-linear diffusion in the cytoplasm of HeLa cells

We performed the FCS measurements for the different types of fluorescent probes inside the living HeLa cells. The probes were all inert for the interior of the cell, and covered a wide range of sizes, from ~nm in diameter to ~100-200 nm. We fitted the obtained data according to the model of the length-scale dependent viscosity (Eq. 21). Results are summarised in Figure 11. Also, in Table 6. (section 3.3) all the results obtained for the probes used in every cell line tested are summarised.

The data obtained by us support the model of the length-scale dependent viscosity of the cell cytoplasm. The smallest probes experience the viscosity similar to that of water solution. With the increasing size of the tracer, the relative viscosity changes from the nanoviscosity for the small objects, through a non-linear increase for the moderate-sized ones, reaching a plateau (signifying the macroviscosity) for the biggest objects. One additional big nanoparticle (with a radius of 100 nm) was also introduced to HeLa cells. The results for this probe are not shown on the plot, as it did not exhibit free diffusion. Under the microscope, it was seen as immobile spots inside the cytoplasm of the cells. We hypothesise, that this particles are bigger than the average distance between the

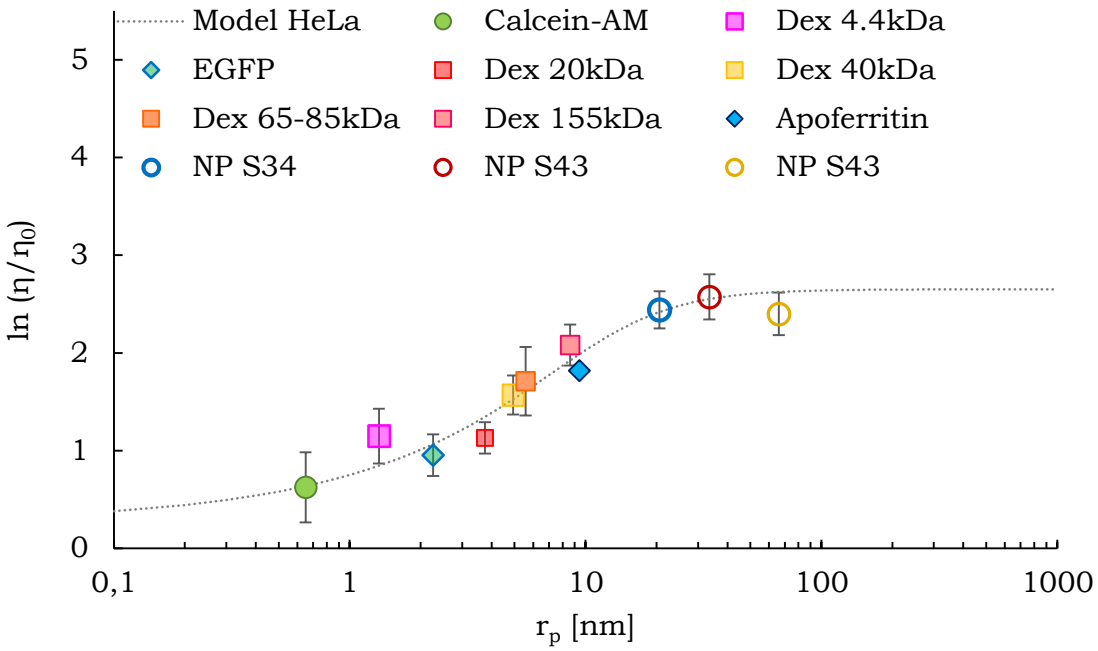

Figure 11. The relative viscosity inside the HeLa cell cytoplasm as a function of the probe radius r_p at 37°C. The viscosity measured in water (η) is divided by the viscosity experienced by the probe in the cytoplasm (η_0), r_p denotes the size of the probe. Error bars denote standard deviation.

nodes of the cytoskeleton network. Those probes are stuck as their size is greater than the openings in the meshwork. Any movement registered for such trapped particles would reflect the reshaping of the cytoskeleton. This assumption is partially supported by the literature data and will be further addressed for other cell lines (section 3.4).

Our systematic approach to the quantitative measurements of the diffusion inside the living HeLa cells presented here remains largely isolated. Only a few works tackled this issue but lacked deeper analysis of the results obtained. Verkman and his collaborators performed similar investigations concerning the diffusion of the DNA fragments of various lengths (Lukacs *et al.*, 2000; Dauty and Verkman, 2005). They also noticed the interplay of the size of a probe and the speed of diffusion. However, they did not propose any theoretical explanation for their observations. The DNA cannot be assumed to be an inert probe, so interactions between the DNA and the cytoplasmic content could not be ruled out. Reuel *et al.* (2012) tracked the movements of the carbon nanotubes of different sizes. They observed different modes of movement (normal and confined diffusion, and also active transport) without clear dependence of the size of the diffusing particle. The carbon nanotubes have a

huge aspect ratio (length to width) and during the diffusion experience translational and rotational motion. Therefore, the overall viscosity measured using the carbon nanotubes is most probably higher than that of a globular probe of similar size. Also, stiff prolonged structures (like the nanotubes tested) are extremely rare in the physiological conditions and poorly reflect the *in vivo* conditions.

The molecular crowding influences the folding of proteins (Sasahara *et al.*, 2003; Hong and Gierasch, 2010). It also influences the kinetic rates of enzymatic reactions (Wenner and Bloomfield, 1999; Minton, 2006; Sasaki *et al.*, 2006). So, local changes of the viscosity could influence the processes taking place inside cells at the specific regions of the cytoplasm.

"Typical" human protein (monomeric, excluding complexes) has a diameter of ~2 nm (Zhdanov, 2009) and size of ~50 kDa (Hendil *et al.*, 2002; Finka *et al.*, 2015). So, the majority of the mammalian proteins most probably localise in the region of the biggest slope of the model presented in our work. Therefore, in this size regime the most prone to the changes of the local viscosity. We measured two proteins: the EGFP (2.5 nm, 26.9 kDa) and the apoferritin (9.43 nm, 474 kDa). We hypothesise, that inside living human cells, the activity of proteins may be modulated through the changes of the nanoviscosity of their immediate surroundings. This hypothesis is further supported by the notion, that in the mammalian cells the DNA expression is controlled through changes of condensation of chromatin (Alberts *et al.*, 2008; Lodish *et al.*, 2013) and also directly impacted by changes of molecular crowding (Morelli *et al.*, 2011).

3.2. Oligomerization of Drp1 protein

We wanted to test the model of the length-scale dependent viscosity in the cytoplasm of living cells. We chose the oligomerization of the dynamin-related protein 1 (Drp1). The Drp1 forms dimers and tetramers, which then assembly on the mitochondrial outer membrane (Koirala *et al.*, 2013), but it was unknown whether the tetrameric form of Drp1 exists in the cytoplasm or is formed directly on membranes (Antonny *et al.*, 2016). We used a set of the mutant (monomeric K668E, dimeric G363D and C505A) and the wild-type Drp1 proteins tagged with the EGFP to investigate this scientific problem.

Theoretical calculations for the Drp1 forms

The hydrodynamic radii of monomers, dimers, and tetramers were calculated. Additionally, from the model constructed by us (see: section 3.1) expected values of the diffusion coefficient (D_{HeLa}) of every Drp1 form were determined. The results are summarised in Table 4.

Drp1	r_p [nm]	D_{HeLa} [μm²/s]	D_X [μm²/s]
Monomer	4.74	15.1 ± 0.5	28.9
Dimer	6.41	9.1 ± 0.5	21.4
Tetramer	8.43	5.7 ± 0.4	16.3

Table 4. Hydrodynamic characterisation of the Drp1 forms. D_{HeLa} – the diffusion coefficient calculated from the length-scale dependent model. For comparison we added the theoretical value of the diffusion coefficient widely used in biological studies. D_X – the diffusion coefficient assuming the constant viscosity of the cytoplasm. (±) denotes standard deviation.

Apart from the calculations based on our model, a set of additional values of the diffusion coefficients predicted according to the commonly assumed constant viscosity model is also presented (D_X). According to the constant viscosity model, the viscosity experienced by the EGFP protein is equal to 2.34 (Nenninger *et al.*, 2010; Mika and Poolman, 2011). Two observations come from such calculations. The first, that assumption of the constant viscosity leads to a serious miscalculation of the predicted diffusion coefficients, reaching up to the almost 3-fold difference for the tetramer. The second observation is, that in the case of the constant viscosity model the difference between the diffusion coefficients of different forms of the Drp1 would be too small to be distinguished by the FCS or similar techniques, possibly discouraging any effort to elucidate the issue of the Drp1 oligomerization. Whereas, in the real system (under the length-scale dependent viscosity) these differences are big enough for the distinction between the Drp1 oligomers.

Determination of the diffusion coefficients of the Drp1 variants

For the verification of the theoretical values, the FCS measurements were done for every variant of the Drp1-EGFP fusion protein. The first mutant, K668E, should be unable to oligomerise and thus be present inside the cell cytoplasm as monomers (Fröhlich *et al.*, 2013). The FCS curves were successfully fitted with the two-component diffusion model (Eq. 31, $i = 2$). The major component was equal to 15.54 ± 0.13 μm²/s and lies well in the predicted range

(15.1 ± 0.5 μm²/s) for the monomeric Drp1-EGFP. The second component was highly variable but always remained in the millisecond regime. It was also consistently present in a low fraction of ~20 %. This second component originates from the unspecific interactions of the Drp1 with the membranes or with other proteins. The second mutant, G363D, creates dimers but lacks the affinity to the mitochondrial membrane (Chang *et al.*, 2010; Strack and Cribbs, 2012). The average diffusion time of the main component measured for this mutant corresponded well with our predictions (9.14 ± 0.18 vs. 9.1 ± 0.5 μm²/s). The third Drp1 variant tested, C505A, was able to participate in the fission of mitochondria (Macdonald *et al.*, 2014). Our measurements confirmed both predictions for this mutant. The diffusion coefficient had similar value to the theoretical one (for this dimer we obtained the value of 8.85 ± 0.12 μm²/s). We also observed a significantly reduced fraction of the freely diffusing dimers (which confirms increased affinity to the mitochondrial membranes). For the G363D-Drp1 around 67 % of the dimers were freely diffusing, while for the C505A-Drp1 only 44 %. All our measurements confirmed the model of the length-scale dependent diffusion inside living cells.

Finally, we tested the wild-type Drp1-EGFP variant. Unfortunately, the two-component model was no longer applicable, so we used the three-component model instead (Eq. 31, $i = 3$). Basing on our results from the mutant Drp1 variants, and their good conformity with the model, we used the previously calculated diffusion coefficients of the dimer and the tetramer and fixed their values in the fit (the third component was composed by the additional unknown fraction with long diffusion times). The amplitudes of all those fractions were treated as free parameters (also the diffusion time of long component was free). In this way, we obtained the amplitudes of the dimer and the tetramer equal to 0.34 and 0.15 respectively. We assumed, that all oligomers exhibit the identical brightness (explained in the next paragraph). We established the ratio of the cytosolic dimers to tetramers as 7:3. The summary of all the results is presented in Table 5.

Variant	D_{FCS} [µm²/s]	Amplitude	Phenotype
K668E	15.54 ± 0.13	0.80 ± 0.09	monomer, low membrane affinity
G363D	9.14 ± 0.18	0.67 ± 0.10	dimer, low membrane affinity
C505A	8.85 ± 0.12	0.44 ± 0.12	dimer, higher membrane affinity
Wild-type	9.1 ± 0.50	0.34 ± 0.09	dimer and tetramer, high membrane affinity
	5.7 ± 0.40	0.15 ± 0.05	

Table 5. A summary of all characteristics of the Drp1-EGFP variants. D_{FCS} denotes the diffusion coefficient obtained for a given variant (or set values in case of the wild-type). The amplitude of the FCS curve is proportional to the relative concentration of the given component. (±) denotes standard deviation.

Brightness of the Drp1 oligomers

The intensity of the fluorescent probe is proportional to the molecular brightness of the probe. In the case of a mixture of various probes of different brightness, also the FCS autocorrelation function depends on their relative brightness (Kalwarczyk *et al.*, 2017). So, for the determination of the relative quantities of components in the mixture of different probes the brightness must not be neglected. If the Drp1 dimers or tetramers consisted of more than one fluorescently labelled monomer, the changes of contributions of each component to the FCS signal would be distorted. Four EGFP tags in tetramers and two in dimers would result in the relative contribution of the tetramer to the amplitude of the FCS autocorrelation function 4 times bigger than expected solely on its concentration.

During the experiments concerning the Drp1 oligomerization, we introduced the plasmids encoding tagged variants of the Drp1 into the cells expressing the native functional protein. The concentration of the endogenous Drp1 in HeLa cells is approximately 0.6 mM (Michalska *et al.*, 2018). The concentration of the fluorescently tagged Drp1 can be calculated from the FCS autocorrelation curve amplitude (the amplitude is equal to $1/N$, where N is the number of fluorescent objects in the focal volume). The concentrations of fluorescent particles were calculated using the following formula:

$$C = \frac{N}{N_A \pi h w_0^2} \tag{33}$$

where N_A is the Avogadro constant, h is the height of the detection volume (assumed to be constant in all experiments and equal to $1*10^{-6}$ m, see:

Figure 12.) and w_0 is the radius of the focal volume (for each experiment established separately). The concentration of the fluorescent particles obtained in such way ranged from 42 to 125 nM. The error in the determination of N is smaller than 5 %. We further assumed, that the bigger oligomers of the Drp1 were immobile in the timescale of the conducted FCS measurements and do not contribute to the FCS signal. Those huge entities were visible as immobile bright spots.

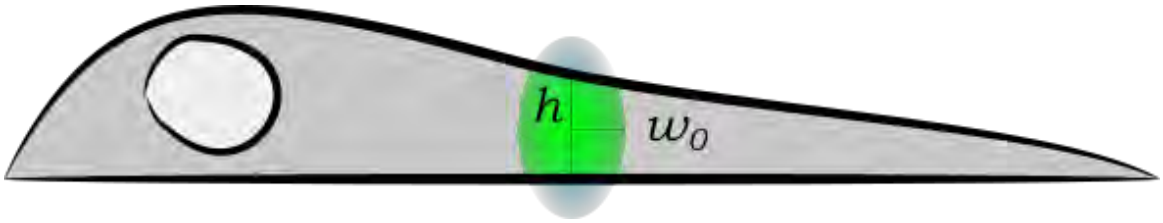

Figure 12. The geometry of the focal volume inside an adherent cell. The standard focal volume is slightly higher than the cytoplasmic region of the adherent cell, so it can be approximated as a cylinder with height h and radius w_0.

By relating the amounts of the endogenous and the introduced Drp1 we obtained the fraction of the fluorescent EGFP-Drp1. It ranged from 7 to 22 % (on average 12 ± 4 %). This shows, that there is an excess of the endogenous Drp1 inside the examined cells. Furthermore, the EGFP tag poses a steric limitation when two labelled monomers are concerned, which promotes assembly of the oligomers with only single tag. Taking into consideration all of those observations, we assumed that all fluorescent entities have an equal brightness corresponding to the single EGFP molecule.

Kinetics of the Drp1 oligomerization

We observed the presence of both dimers and tetramers in cells expressing the fluorescent wild-type Drp1 (but not the monomers). We propose the three-step oligomerization mechanism. First, dimers are formed from the Drp1 monomers, then dimers bind forming tetramers, and lastly, the creation of the membrane-bound complexes based on the tetramers occurs. We proved, that the quantification of dimer and tetramer fraction is possible, so also the calculation of the equilibrium constant for the process of formation of tetramers from dimers can be calculated. Unfortunately, two other steps are beyond the FCS capabilities. The formation of the dimers from monomers is much faster than time resolution of the FCS measurements, whereas binding of bigger oligomers

to the mitochondrial membranes cannot be distinguished from the unspecific interactions of the Drp1 with other cytosolic content.

K_D is defined as the "dissociation equilibrium constant" of a protein-protein complex (Pollard, 2010). In our experiments, it is calculated from the following equation:

$$K_D = \frac{C_{FCS}}{p} * \frac{A_{dimer}^2}{A_{tetramer}} \quad (34)$$

Here, C_{FCS} denotes the concentration of the detected molecules (i.e. the expression level of the fluorescent Drp1), p is the fraction of the Drp1-EGFP to the overall Drp1 amount, and A_{dimer} and $A_{tetramer}$ are, respectively, the amplitudes of the dimer and the tetramer. In this way, the K_D of the dimer-tetramer formation was established for each cell tested. Our results (summarised in Figure 13. A.) ranged from 0.16 to 2.5 μM, with the average of 0.66 ± 0.53 μM. Obtained values of the K_D point to the moderate-high affinity of the dimer-dimer interactions, which could have been expected for such reaction. Up to date, no literature reference for our results exists. To confirm, that the reaction takes place at the equilibrium conditions, we checked whether the expression levels of the Drp1-EGFP affects the K_D. No clear trend was visible (Figure 13. B.). In spite of the relatively large heterogeneity of the population, in the majority of cells the dimer-dimer affinity is high (K_D < 1 μM).

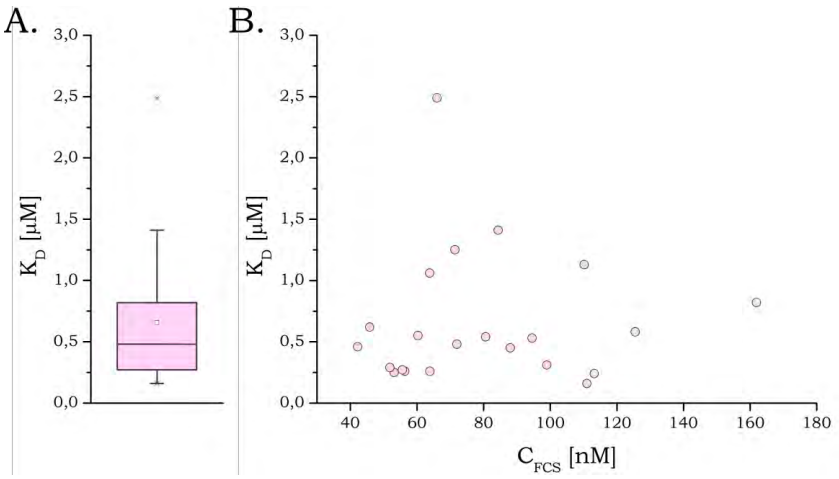

Figure 13. (A) Box plot representing distributions of the K_D of the tetramerization of the Drp1 in HeLa cells. The small square represents mean value, box – inter-quantile range with the median inside, and the whiskers – 1st and 4th quadrille. The crosses (x) denote 99 and 1% of all the results and the dashes (-) maximal and minimal values obtained. (B) The K_D plotted against the concentration of the wild-type Drp1-EGFP. No correlation between those two values exists.

The final confirmation of the obtained results was achieved through the Monte Carlo simulations. The physical values coming from our investigations were input into the simulator. We obtained a set of the autocorrelation curves, closely matching those coming from our experiments. An exemplary comparison is shown in Figure 14. The average amplitude values acquired by the fitting of the simulated curves with the length-scale dependent viscosity model (Eq. 21) were similar to the experimental ones (0.36 ± 0.06, 0.16 ± 0.11, and 0.48 ± 0.06 vs. 0.34 ± 0.09, 0.15 ± 0.05, and 0.51 ± 0.1 for the dimer, tetramer and large fluorescent fraction, respectively). This agreement further supports the introduced interpretation of the data.

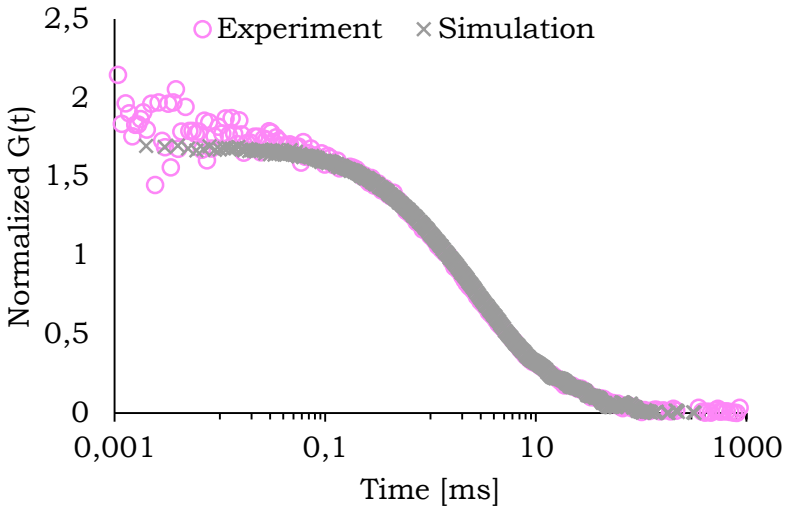

Figure 14. The comparison of the experimental and the simulated FCS curves. The experimental points are represented as circles, while the simulated data as crosses. Nearly perfect correspondence is observed. The discrepancies for times less than 0.1 ms come from the EGFP blinking, which was not simulated.

Oligomerization of the Drp1 protein in HeLa cells

During the conducted experiments we were able to measure the diffusion coefficients of different oligomers of the Drp1 protein inside the cytoplasm of the living HeLa cells. By doing so, we confirmed the reliability of the model of the length-scale dependent viscosity of the cytosol. Furthermore, we proposed a model of the oligomerization of the Drp1 protein. First, the dimers are created from the monomers, which later bind forming the tetramers and then larger, membrane-bound entities. We were also able to calculate the dissociation equilibrium constant for the process of formation of tetramers from dimers. Few works are similar to ours. Often much more problematic double-labelled

approach utilising the Förster resonance energy transfer (FRET) is applied (Phillip *et al.*, 2012), or the numerical analysis of the interactions is omitted whatsoever (Maertens *et al.*, 2005). Using the FCS Ohrt *et al.* (2008) studied the formation of the multicomponent RNA-induced-silencing complex (RISC) in the living human cells, and were able to show the differences in the size of this structure in the cytoplasm and the nucleus. Our work is among the pioneering investigations quantitatively tackling the issue of the protein-protein interactions *in vivo*.

3.3. Viscosity in cancerous versus non-cancerous cells

Kalwarczyk *et al.* (2011) suggested, that nanoviscosity may differ depending on cell type, tissue and/or organism. Kalwarczyk *et al.* summarised the literature data and created distinct models for human HeLa cells and also murine Swiss 3T3 cell line. We made comparative studies of the length-scale dependent viscosity in different human cell lines. We hypothesised, that healthy and cancerous cells would have clearly visible differences. We also tested the cells coming from different tissues and playing various roles in the organism.

Nanoviscosity in human cells

The HeLa cells are model cancerous human cells. Similarly, skin fibroblasts are regarded as a model of healthy cells. Therefore we determined the viscosity in both cell lines using the same probes and the same techniques. We also used two cell lines from the same tissue (lung). A549 and HSAEC represent cancerous and healthy lung epithelium, respectively. We characterised both of them to a moderate extent. We also chose U2OS, (bone cell line) as an additional (cancerous) control for fibroblasts. Both of those cell lines are part of the connective tissue. We also tested two additional cancerous lines coming from the breast (MCF-7) and the liver (Hep G2) as the confirmation of obtained results. The summary of all our results is presented in Figure 15. and in Table 6.

Probe	r_p [nm]	HeLa	Fibroblasts	HepG2	MCF-7	A549	U2OS	HSAEC
Calcein-AM	0.65	281 ± 99	89.04 ± 13.71	390.53 ± 60.15	446.95 ± 31.69	240.79 ± 95.34		339 ± 65
Dex-4.4 kDa	1.33	79 ± 21	54.44 ± 17.83				106.21 ± 24.08	89.16 ± 20.37
EGFP	2.50	56 ± 11	21.18 ± 10.31					
Dex-20 kDa	3.75	28.0 ± 4.5	17.19 ± 6.90					
Dex-40 kDa	4.93	13.8 ± 3.0	15.55 ± 7.81			17.76 ± 2.72		
Dex-75 kDa	5.57	11.0 ± 4.0	13.75 ± 2.55					
Dex-155 kDa	8.60	4.9 ± 2.0	7.23 ± 1.52	10.38 ± 2.90	11.60 ± 1.48	8.53 ± 0.70	9.29 ± 3.10	6.64 ± 2.55
Apoferritin*	9.43	5.5						
NP S34	20.60	1.38 ± 0.28	2.18 ± 0.72				1.63 ± 0.34	
NP S43	33.50	0.75 ± 0.21	0.53 ± 0.33			0.85 ± 0.17		
NP S42	50.00	0.44 ± 0.08						

Table 6. The summary of all the FCS measurements performed. The values in the table are shown as the average diffusion coefficient D [$\mu m^2/s$] obtained in the cell cytoplasm. The fibroblasts and the HSAEC are untransformed cell lines, others are immortalised cancerous cells. (±) denotes the standard deviation. *Results for the apoferritin in the HeLa cells were obtained under the same experimental conditions by Dr Jędrzej Szymański from the Nencki Institute of Experimental Biology.

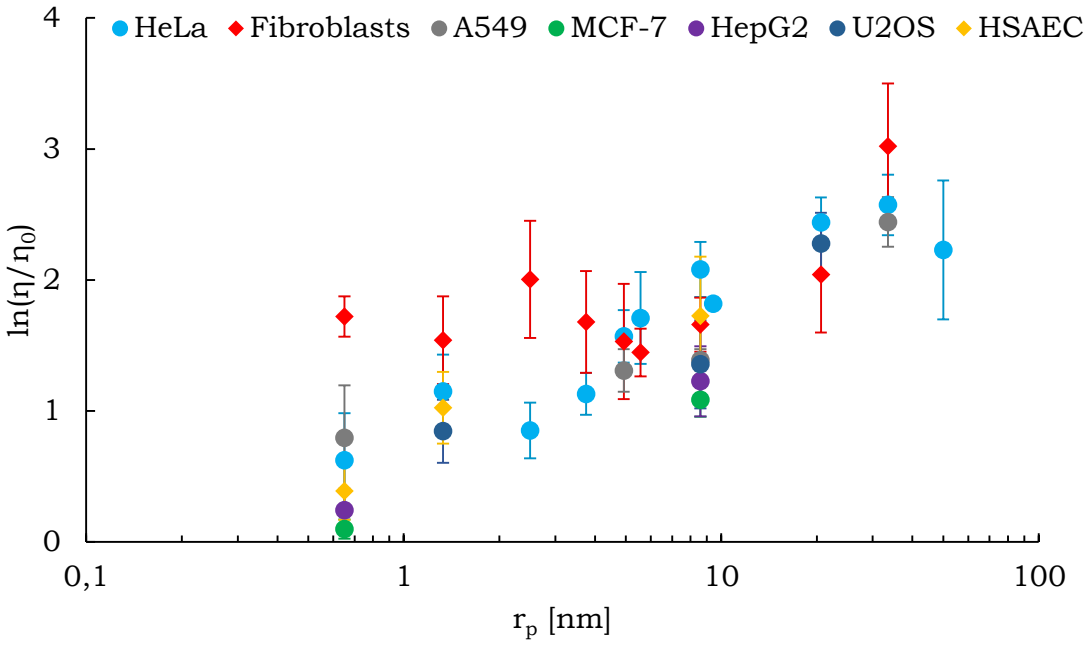

Figure 15. Comparison of the nanoviscosity measured by FCS in different cell lines The values are shown as $\ln(\eta/\eta_0)$, where η and η_0 denote the viscosity obtained in the cell cytoplasm and in water respectively. Circles represent cancerous and diamonds healthy cell lines. Error bars denote standard deviation.

We started the comparison of the viscosity in these cell lines by the FCS measurements of model healthy cells – fibroblasts. They were used as a healthy control for the experiments performed on the HeLa cells. These two cell lines show obvious differences in their viscosities. In HeLa cells, the relative viscosity is changing throughout whole tested range of probes, extending from the nanoviscosity region for the smallest probes to the macroviscosity regime for the biggest, with the moderate, steep change in-between them. In the fibroblasts, no such change is visible. Apart from the biggest probe tested (with the radius of 50 nm), all data points seem to indicate, that the viscosity of the cytoplasm of the fibroblasts is constant, irrespective of the size of the tracer (or this change is only slight). This might indicate, that the viscosity of the cytoplasm of cancerous and healthy cells differ, yet the data for the other cell lines disprove this assumption. Our results for Hep G2, MCF-7, and A549 (all cancerous epithelial cell lines, as HeLa is) closely resemble those of HeLa cells, which was expected. But the viscosity values obtained in the second healthy cell line, HSAEC, fall in line with cancerous cells, rather than healthy fibroblasts. This suggests, that the difference between the fibroblasts and other cell lines does not come from them being cancerous or not.

All of the cells mentioned up to this point (apart from fibroblasts) come from the epithelium (the outer layer of the organ), we checked whether this is the reason for the observed discrepancies. Thus, we tested U2OS cells, like fibroblasts, come from the connective tissue (bone in case of U2OS). The results for U2OS were similar to those for the HeLa line. We conclude, that this unusual viscosity of the fibroblasts is the result of the organisation of the cytoplasm. Every cell line tested is adherent, meaning that they grow attached to the surface of a culture dish. Still, only the fibroblasts show distinct spindle-like shape (suggesting a much more organised cytoskeleton), while the other cell lines grow exhibiting a fried egg-like shape. Comparison of the fibroblasts and the HeLa cells is shown in Figure 16. (every other cell line had the shape similar to the HeLa cells).

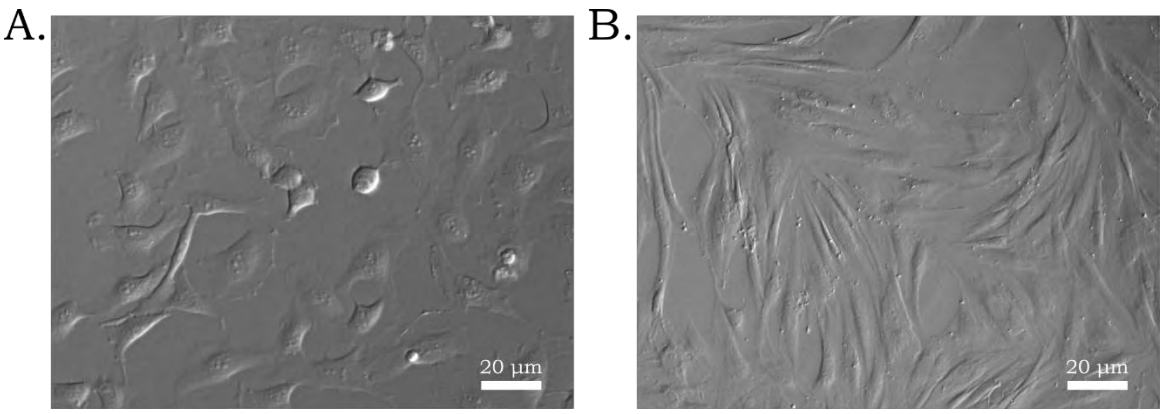

Figure 16. A microscopic pictures of the HeLa cells (A) and the fibroblasts (B).

The additional proof confirming our predictions of the differences of the viscosity observed in the fibroblasts and the other cells as resulting from the internal architecture of the cytoskeleton comes from the observations made for the biggest nanoparticles. In the HeLa cells, the nanoparticles of the radius of 100 nm were immobile, probably because they were bigger than the openings in the actin meshwork. In the fibroblasts, already smaller nanoparticles (radius of 50 nm) were immobile. This is in line with the literature data. The distance between the nodes of the actin mesh is slightly bigger than 50 nm (Luby-Phelps *et al.*, 1986; Janson *et al.*, 1996). Both of those works measured this value in the fibroblasts. We hypothesise, that openings in the mesh size in the HeLa cells are at least twice as big.

Length-scale dependent viscosity of the cytoplasm of human cells

We showed how the effective viscosity of the cytoplasm changes with the size of the probes in different human cells. The majority of the cell lines tested exhibit similar trend in the viscosity. Only the fibroblasts differ from the other cells, most probably due to a much more organized actin cytoskeleton. Our work thoroughly describes the phenomenon of the length-scale dependent viscosity of the human cells. Although no analogous works were done before, there are some investigations in similar areas. For example, the optical tweezers were used as a method for probing the mechanical properties of the cytosol. Hu *et al.* showed that the size of a particle (and also its speed) influences the response of the cytoplasm during the tracer dragging (Hu *et al.*, 2017). Guo *et al.* compared benign and malignant cancerous cells (Guo *et al.*, 2014). They showed reduced stiffness of the cell and increased traction forces in the cells of malignant cancer. A comparison of the different cell types (including both cancerous and healthy ones) was done by Guigas, Kalla and Weiss (2007a, 2007b). In their works, they used the fluorescently tagged gold nanoparticles for the FCS measurements. The results they obtained were highly inconclusive, once they reported no difference in the viscosities of the cancerous and healthy liver cells (Guigas *et al.*, 2007b), and once they observed some differences (Guigas *et al.*, 2007a). Probably these inconsistencies result from poor characterisation of their probe. They used colloidal gold covered with a layer of fluorescent dye. They observed anomalous diffusion, but from our experience it follows, that probably they released free dye into the cytoplasm together with the nanoparticles.

3.4. Changes of viscosity during the cell cycle

Final series of experiments addressed the issue of possible changes of the viscosity of the cytoplasm of living cells during the cell cycle. During the cell cycle, huge structural changes take place. We used the synchronised population of HeLa cells constantly expressing the EGFP (enhanced green fluorescent protein) for the studies of this issue.

Synchronization of the HeLa cells

The efficiency of synchronisation of the HeLa cells by the addition of aphidicolin was tested. The aphidicolin blocks cell cycle progression at the G1/S border but also can induce irreversible arrest of the cell cycle (Pedrali-Noy *et al.*, 1980;

Borel *et al.*, 2002). We selected a few representative times (0, 1.5, 4, 8, 12, and 24 hours after aphidicolin removal) for the control of the experiment. The cells at the given time were collected and subjected to the flow cytometry analysis. The vast majority of the cells (up to 90 %) progressed through the cell cycle in the synchronised fashion. Figure 17. shows that cells properly resume their progression through the cell cycle (seen as the doubling of the DNA content) after the removal of the aphidicolin. 24 hours later the distribution of cells matches that of an unsynchronized control. Our results are in agreement with

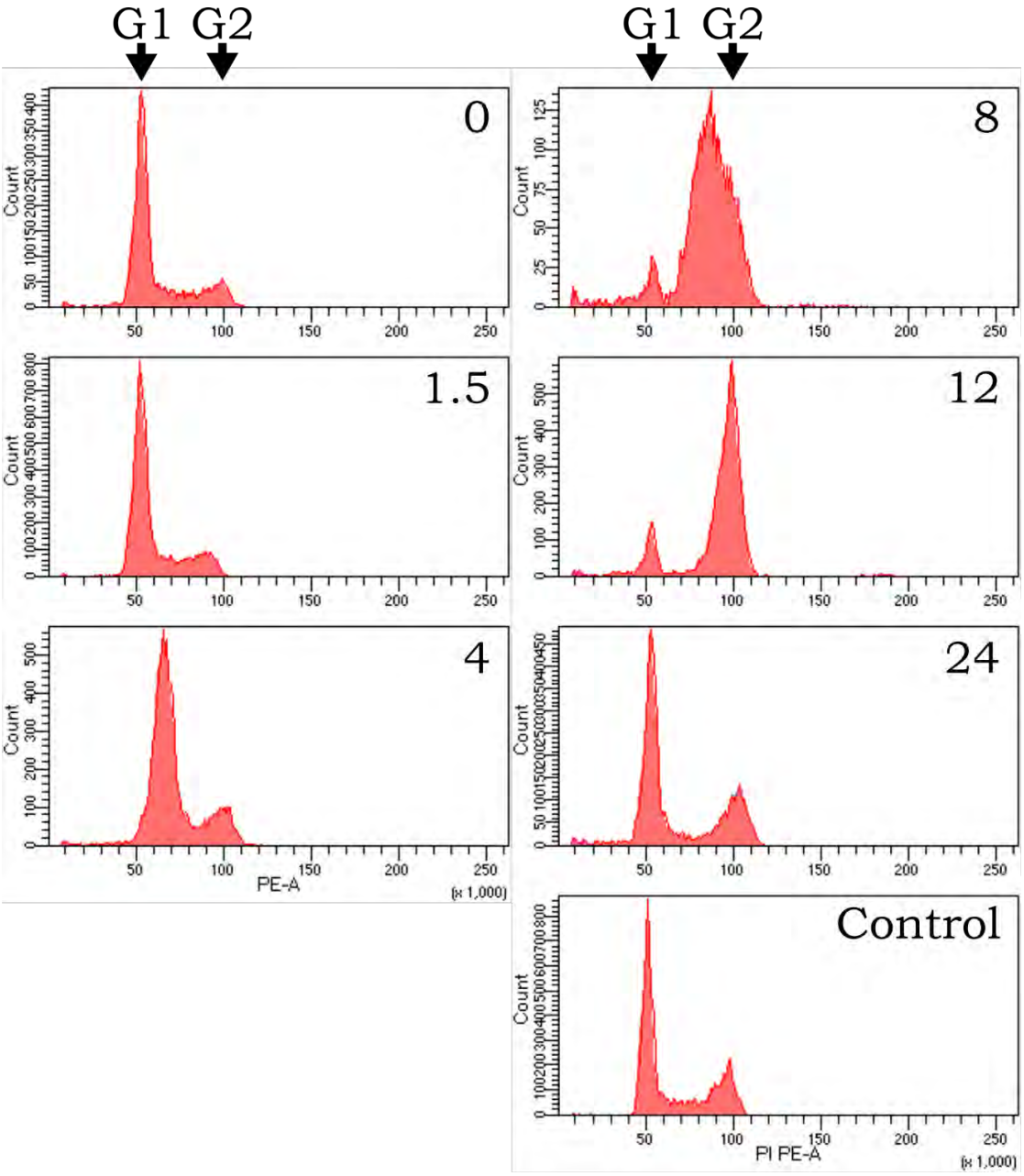

Figure 17. Progression through the cell cycle in the synchronized HeLa cells. Graphs show the content of fluorescently labelled DNA. The arrows indicate the peaks characteristic for the diploid and the tetraploid cells (cells in G1 and G2 phases respectively).

the literature data (Pedrali-Noy *et al.*, 1980), and prove that aphidicolin efficiently synchronizes cells and does not exhibit any cytotoxic properties.

Diffusion of the EGFP during the cell cycle

During the cell cycle, huge structural changes take place inside the cytoplasm of the cell since it prepares its division and thus doubles all biomolecules inside. We hypothesise, that such huge changes would have an impact on the viscosity of the cytoplasm. We monitored the relative diffusion (with respect to the diffusion in water) of the enhanced green fluorescent protein (EGFP) during the cell cycle of HeLa cells during the cell cycle. The localisation of the EGFP inside the HeLa cells during the main phases of the cell cycle is shown in Figure 18. A. The graph summarising obtained results is shown in Figure 18.

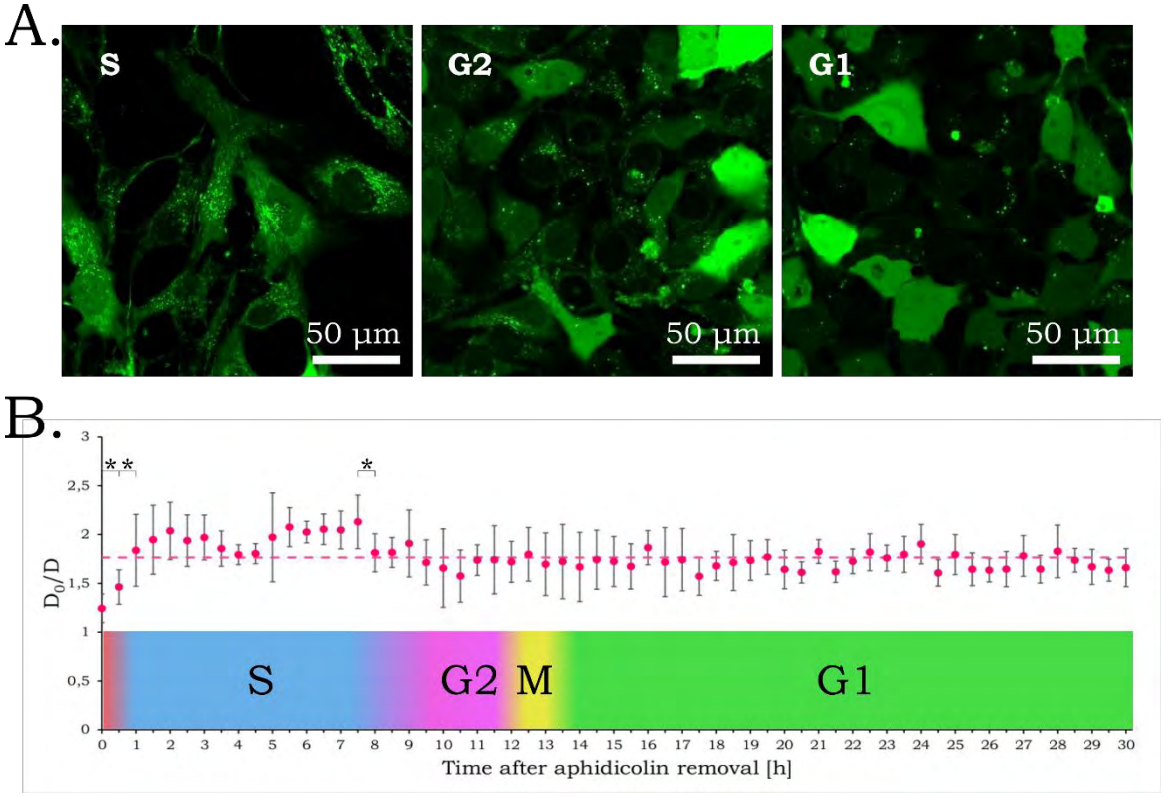

Figure 18. (A) The localisation of the EGFP in the HeLa cells at a given phase of the cell cycle (1.5, 10, and 14 hours after the aphidicolin removal for the S, G2, and G1 phases respectively). (B) The changes of the relative viscosity 1/D of EGFP with respect to water $1/D_0$ measured in the HeLa cells cytoplasm. The points represent the mean values taken from at least 5 cells with the error bars denoting the standard deviation. The dashed line represents the mean value of the whole experiment (D_0/D = 1.76). The asterisks (*) mark statistically significant changes between the points according to the unpaired Student's t-test, $P<0.05$. The coloured bar signifies the approximate duration of each phase of the cell cycle.

To our surprise, obtained results suggested a different scenario, than we initially assumed. Immediately after aphidicolin removal, a brief lag phase was observed. It was expected since the cell cycle progression needs time to restart. After the full restart of the DNA replication system, during the S phase, the relative viscosity of the cytoplasm (expressed as the ratio of the diffusion coefficient of the EGFP in water (D_0) to that measured in the cytoplasm (D)) increased noticeably. The hydrodynamic radius of the EGFP (2.3 nm) was calculated using HYDROPRO software, and the value of diffusion coefficient of the EGFP in water (128 $\mu m^2/s$) from the Stokes-Einstein equation (Eq. 15). Shortly after the DNA replication, the relative viscosity drops and remains constant (D_0/D = 1.76) throughout the rest of the cell cycle. This mean value does not change between cells before and after the division. Although precise identification of mitosis was impossible, we assumed, that the division of the cells occurred around 12 hours after the aphidicolin removal. Thus, cells before 12 hours were treated as "mother" and after as "daughters". Unfortunately, the inability to pinpoint the mitosis precluded observations of any changes of the viscosity of the cytosol during the transient disappearance of the cell nucleus. The diffusion of the EGFP in the cells during the division was measured by Pawar *et al.* and no changes were observed (Pawar *et al.*, 2014). The average value of the relative diffusion coefficient of the EGFP in the synchronised HeLa cells is around 30 % smaller than that obtained in the unsynchronized cells (1.76 vs. 2.29). This indicates that the aphidicolin synchronization has previously undescribed, inhibitory effect onto the physiology of HeLa cells.

Impact of the aphidicolin

The impact of the aphidicolin synchronization was unexpected, so we studied this effect further. We measured the size of synchronised cells at the same times as previously and compared them to the unsynchronized controls. The comparison (in form of the box plots) is summarised in Figure 19.

Our results show, that 24 hours of incubation with the aphidicolin causes an overall decrease in the size of cells. We also observed a small, statistically significant increase of the cell size with time. The effect of the aphidicolin is not reversed even after 24 hours of the unrestricted growth (which corresponds to one generation of the undisturbed development). According to the literature data, aphidicolin does not influence any cellular processes apart from the DNA replication, yet its effect on the cell physiology is prominent.

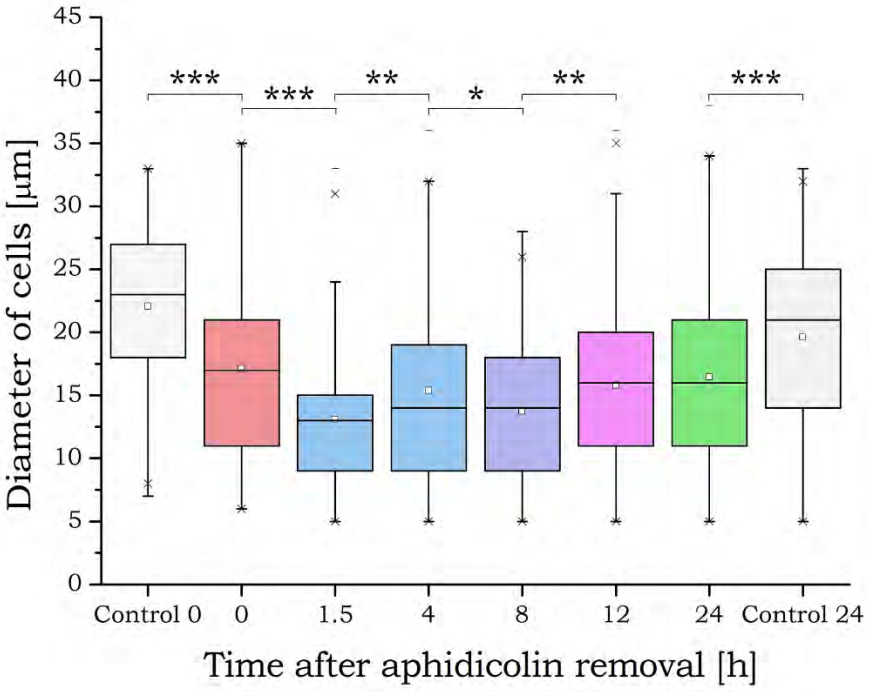

Figure 19. The changes in the sizes of HeLa cells after the incubation with the aphidicolin. The results are shown as the box plots with the small squares representing the mean value, the boxes – inter-quantile range with the median inside, and the whiskers – 1st and 4th quadrille. The crosses (x) denote 99 and 1% of all the results and the dashes (-) the maximal and the minimal values obtained. Statistical significance: unpaired Student's t-test. Single asterisks (*) denote significant (P<0.05), double (**) very significant (P<0.005), and triple (***) extremely significant (P<0.0005) statistical changes. The colours of bars are related to that of the cell cycle progression from Figure 18. B.

Changes of viscosity during HeLa cell cycle – discussion

We monitored the viscosity of the cytoplasm during the cell cycle of HeLa cells. Our approach is the most thorough presented in the literature. Liang *et al.* (2009) also studied the viscosity of the cytoplasm. They focused their attention only on the three interphase phases (G1, S, and G2). They also noted slight change of the viscosity during the S phase. However, they show the opposite effect. In their experiments, the viscosity of the cytosol of cells during the DNA replication decreases. We assume, that this difference originates from their method of synchronization. For each of the timestamps studied they utilised a different method/agent, each with a different molecular target (the mimosine for the G1 phase, the thymidine block for the G1/S boundary, and the colchicine for the G2 phase). We show that the synchronization can have an unpredictable effect, which has to be taken into consideration. It seems plausible, that every perturbation of the cell cycle could give rise to changes in the physiological

condition of the treated cells. Our approach utilizing a single agent for the synchronization seems to be more appropriate.

On the first glance, the results we obtained are surprising. We anticipated, that enormous changes of the structure and composition of the cytosol of living cells undergoing the cell cycle would have an impact on the diffusion rates of the cellular constituents. Basing on the literature data (Pedrali-Noy *et al.*, 1980; Spadari *et al.*, 1982), we assumed that the cells synchronized with the aphidicolin would function normally (except for the influence on the DNA synthesis). However, our results suggested a different scenario. During the cell cycle, only transient increase of the viscosity of the cytoplasm is present during the S phase. In human cells, the DNA replication is tightly connected to the well-being of the whole cell. Kung *et al.* (1993) proved that in the HeLa cells the inhibition of the DNA synthesis causes a down-regulation of the protein production which arrests the cell growth. Such action prevents the accumulation of abnormal levels of the regulatory proteins, which would otherwise cause great disruptions of the regulatory pathways. So, the action of every synchronizing agent has to be considered as cytotoxic. The cell cycle arrest "toxicity" comes not from the direct action of synchronizing agents, but rather from the alterations of the ratio of the cell size to the DNA content (Kung, Sherwood, *et al.*, 1990; Kung, Zetterberg, *et al.*, 1990). This assumption is further supported by the similar experiments concerning mitochondria. Posakony *et al.* (1977) shown, that corresponding phenomena of a stable ratio of the cell size to the volume of mitochondria in the undisturbed cells is tightly controlled throughout the cell cycle.

Considering the cytosol as a crowded environment favours the existence of the stable physiological nanoviscosity. The majority of processes taking place inside the cells are diffusion-dependent, so their speed depends also on the viscosity of the environment. The extent of these changes was described in many works (e.g. Minton, 2001; Sasaki *et al.*, 2006, 2007). But, not only are the diffusion-limited reactions dependent on a stable value of the viscosity. The active transport may be also influenced. Sozański *et al.* (2015) showed, that kinesin-1, one of the most robust and powerful transport proteins is highly susceptible to the local changes of the nanoviscosity. The kinesin is stopped at the microtubule when the nanoviscosity exceeds 5 times the water viscosity. Taken together, all of these results favour the maintenance of the stable physiological

viscosity of the cytoplasm. We, therefore, hypothesise that inside the cells there exists an unknown mechanism responsible for the sustaining of the nanoviscosity at a constant level. This mechanism ensures that drastic disturbances of the viscosity of the cytoplasm are avoided.

The aphidicolin binds only to the dCTP (deoxycytidine triphosphate) binding site and in this way stops the action of the DNA polymerase (Baranovskiy *et al.*, 2014). Apart from the molecular target of the aphidicolin, no data about the fate of aphidicolin inside the cytosol and its clearance is available. Basing on our results we can only hypothesise. We observed, that the cells synchronized by the aphidicolin have significantly reduced size and viscosity of cytosol when compared to the untreated control. This effect is more prominent shortly after the removal of the cell cycle block. Two possible scenarios of the action of the aphidicolin can be imagined. The aphidicolin binds to the DNA polymerase molecules only transiently. Despite the expunge of the aphidicolin, the influx of the new ones from the medium (where an excess of the aphidicolin is present) creates an equilibrium between the movements in and out of the cells. This causes the replication apparatuses to be efficiently stopped on the DNA strands. After the removal of the excess of the synchronization agent from the medium, the remaining molecules are quickly removed and the DNA replication resumes. In the second scenario, the DNA polymerases are permanently blocked by the aphidicolin. Then, the deactivated polymerase molecules are detached from the DNA and destroyed. New polymerase molecules are constantly being synthesised, but are also rapidly blocked by the influx of the aphidicolin from the media. Wahl *et al.* (1988) and Zeng *et al.* (1994) already described such equilibrium of the creation and the destruction of the DNA polymerases. The DNA replication restarts as soon as the active population of the polymerases is restored. Both of those scenarios have a common result – the DNA replication is efficiently blocked by the aphidicolin presence. Helmrich *et al.* (2011) and McGlynn *et al.* (2012) showed, that replication and transcription of the DNA have to be spatially separated. Collisions of those two processes lead to the disruption of the proper cell function. So, during the cell cycle arrest caused by the aphidicolin, no new RNA is produced (also, the existing one has limited half-life). This explains the cessation of the protein production and reduction of the cell size.

Summary

The interior of the human cells is an extremely intricate and complex environment. Numerous structures of varying size and complexity are confined by cellular organelles. Also, long biopolymers intertwine with each other creating a vast meshwork of molecular pathways and openings between them. In-between the organelles and the cytoskeleton myriad of proteins, nucleic acids, ions and complexes of each are solvated with the intercellular water molecules. Together all of them create a crowded environment in which chemical characteristics of such solution differ significantly from those observed in the uncrowded water solutions.

Majority of biochemical and biophysical processes are preferentially measured under simpler conditions of a buffered water in test tubes. Only recently, clearly visible discrepancies between *in vitro* and *in vivo* conditions are receiving increased attention. Still, the uniform descriptions of the conditions present in the cellular environment remain scarce. This thesis aimed to elucidate one of the key physical characteristics of the living crowded systems – the viscosity.

We used previous works reporting the length-scale dependence of the viscosity on the size of tracer travelling through the cytoplasm of living human cells as a starting point of our investigations. We studied the length-scale dependent viscosity improving the accuracy and precision of its determination. We used the fluorescence correlation spectroscopy (FCS) for this study. This technique allowed for the precise, quantitative measurements of the diffusion coefficients of fluorescent or fluorescently tagged probes of different sizes. We chose the tested tracers for their reported inertness with respect to the cytoplasmic contents. Among the tested molecules were small dyes, complex branched sugars (dextrans), proteins and nanoparticles, all ranging from 1-100 nm in the radius. During our experiments, we used several distinct cell lines. Most of our research focused on two model cell lines: the HeLa cells (cervical cancer) and the fibroblasts (coming from healthy skin). Plus, healthy human primary small airway epithelial cells (HSAEC) and their cancerous counterparts A549, both coming from lung, were used. Additionally, we also tested U2OS (bone osteoblastoma), Hep G2 (liver cancer) and MCF-7 (breast cancer). We did not simply apply the model of the length-scale dependent viscosity of the cytoplasm for the study of the different cell types. To prove the usefulness of the model and our approach, we studied the oligomerization of the dynamin-related protein 1

(Drp1). Additionally, we monitored the changes of the nanoviscosity (experienced by the EGFP) of the cell cytoplasm during the HeLa cell cycle.

During our meticulous studies, we measured the diffusion of different kinds of tracers inside the living HeLa cells and confirmed the previously described model of the length-scale dependent viscosity. We observed, that depending on the size of the probe, the cytosol of HeLa cells crosses from the nanoviscosity regime, through the moderate region of rapid change into the macroviscosity. Then, through a series of theoretical calculations, we proved, that the relation of the size and the experienced viscosity in the cytosol of the living cells, can be utilised for the studies of oligomerization of the Drp1. Thanks to the application of different mutated variants of the Drp1-EGFP fusion protein, we quantitatively monitored the diffusive motion of the monomers, the dimers, and the tetramers. Basing on the investigations of the mutant Drp1 variants, we also convincingly described the behaviour of the wild-type Drp1. Furthermore, we were able to calculate the kinetic parameters of the equilibrium between the dimeric and the tetrameric forms of the Drp1.

After the creation of the model of the length-scale dependent viscosity of the cytoplasm of the HeLa cells and testing its functionality during the investigations concerning the oligomerization of the Drp1 protein, we checked whether all human cells conform to the same model. First, we meticulously investigated the human skin fibroblasts. Then, we further expanded our approach by including cancerous cell lines (Hep G2, MCF-7). We also used two closely related cell types (HSAEC and A549) representing healthy and cancerous lung. Finally, we tested U2OS line, as an example of the cancerous connective tissue. From all those investigations, we made unexpected observations. Apart from fibroblasts, all cell lines, no matter their origin, or character, resembled HeLa cells. We propose an explanation for this observation: the fibroblasts have differently organised actin cytoskeleton than other cells. Our hypothesis is further supported by the noticeably distinct shape of the fibroblasts and different behaviour of the biggest objects tested when compared to the results obtained for the HeLa cells.

Our last experiment concerned the changes of the nanoviscosity of the cell cytoplasm during the cell cycle. Every living cell has to divide, and the cell cycle is a series of processes designated to do so. Before every division, all cell content has to be duplicated. That should impact the physiological conditions inside the

cytosol. Our results coming from the monitoring of the diffusion of the EGFP in the HeLa cells for 30 hours disprove this assumption. Apart from the slight, but statistically significant, transient increase during the S phase (the DNA synthesis), the nanoviscosity of the cytoplasm in the living cells experienced by the EGFP remains on a constant level. This result may indicate, that previously unknown mechanism maintains the physiological viscosity of the cytosol. Our hypothesis is supported by different works showing how changes of viscosity could prove disastrous for the well-being of the cell. We also observed the side effect of the cell cycle arrest by an external agent – the aphidicolin. We discussed two possible explanations of the inhibiting action of the aphidicolin.

In summary, this thesis provides a meticulous description of the studies concerning the subject of the viscosity of living human cells. Our data show, how important it is to take into consideration the viscosity when performing any experiments *in vivo*. Disregarding the impact of viscosity may lead to immense miscalculations and misinterpretations. We provided explanations of different phenomena, which open up many different paths to be followed. We proved, that the fluorescence correlation spectroscopy is an effective tool for investigations of diffusion inside living cells. Similar investigations could be performed in the distinct sub-cellular compartments and organelles. The FCS allows measuring the kinetics of different biochemical complexation reactions. More ambitious plans could extend to the tracing the action of drugs after their introduction into the cells.

Bibliography

Al-Habori, M. (1995) Microcompartmentation, metabolic channelling and carbohydrate metabolism, *Int. J. Biochem. Cell Biol.*, 27(2), pp. 123–132. doi: 10.1016/1357-2725(94)00079-Q.

Alberts, B., Johnson, A., Lewis, J., Raff, M., Roberts, K. and Walter, P. (2008) *Molecular Biology of the Cell*. Garland Science.

Anders, L., Ke, N., Hydbring, P., Choi, Y. J., Widlund, H. R., Chick, J. M., Zhai, H., Vidal, M., Gygi, S. P., Braun, P., *et al.* (2011) A Systematic Screen for CDK4/6 Substrates Links FOXM1 Phosphorylation to Senescence Suppression in Cancer Cells, *Cancer Cell*. Elsevier Inc., 20(5), pp. 620–634. doi: 10.1016/j.ccr.2011.10.001.

Anderson, S., Bankier, A. T., Barrell, B. G., de Bruijn, M. H., Coulson, A. R., Drouin, J., Eperon, I. C., Nierlich, D. P., Roe, B. A., Sanger, F., *et al.* (1981) Sequence and organization of the human mitochondrial genome, *Nature*, 290(5806), pp. 457–465. doi: 10.1038/290457a0.

Angiolini, J., Plachta, N., Mocskos, E. and Levi, V. (2015) Exploring the Dynamics of Cell Processes through Simulations of Fluorescence Microscopy Experiments, *Biophys. J.* Biophysical Society, 108(11), pp. 2613–2618. doi: 10.1016/j.bpj.2015.04.014.

Antonny, B., Burd, C., De Camilli, P., Chen, E., Daumke, O., Faelber, K., Ford, M., Frolov, V. A., Frost, A., Hinshaw, J. E., *et al.* (2016) Membrane fission by dynamin: what we know and what we need to know, *EMBO J.*, 35(21), pp. 2270–2284. doi: 10.15252/embj.201694613.

Arrio-Dupont, M., Foucault, G., Vacher, M., Devaux, P. F. and Cribier, S. (2000) Translational diffusion of globular proteins in the cytoplasm of cultured muscle cells, *Biophys. J.* Elsevier, 78(2), pp. 901–907. doi: 10.1016/S0006-3495(00)76647-1.

Atkins, P. W. and De Paula, J. (2010) *Atkins' Physical Chemistry*. Oxford University Press.

Bancaud, A., Huet, S., Daigle, N., Mozziconacci, J., Beaudouin, J. and Ellenberg, J. (2009) Molecular crowding affects diffusion and binding of nuclear proteins in heterochromatin and reveals the fractal organization of chromatin, *EMBO J.*, 28(24), pp. 3785–3798. doi: 10.1038/emboj.2009.340.

Baranovskiy, A. G., Babayeva, N. D., Suwa, Y., Gu, J., Pavlov, Y. I. and Tahirov, T. H. (2014) Structural basis for inhibition of DNA replication by aphidicolin, *Nucleic Acids Res.*, 42(22), pp. 14013–14021. doi: 10.1093/nar/gku1209.

Bedessem, B. and Ruphy, S. (2015) SMT or TOFT? How the Two Main Theories of Carcinogenesis are Made (Artificially) Incompatible, *Acta Biotheor.* Springer Netherlands, 63(3), pp. 257–267. doi: 10.1007/s10441-015-9252-1.

Bedessem, B. and Ruphy, S. (2017) SMT and TOFT Integrable After All: A Reply to Bizzarri and Cucina, *Acta Biotheor.* Springer Netherlands, 65(1), pp. 81–85. doi: 10.1007/s10441-016-9286-z.

van den Berg, B., Ellis, R. J. and Dobson, C. M. (1999) Effects of macromolecular crowding on protein folding and aggregation, *EMBO J.*, 18(24), pp. 6927–6933. doi: 10.1093/emboj/18.24.6927.

Berland, K. M., So, P. T. and Gratton, E. (1995) Two-photon fluorescence

correlation spectroscopy: method and application to the intracellular environment, *Biophys. J.*, 68(2), pp. 694–701. doi: 10.1016/S0006-3495(95)80230-4.

Bizzarri, M. and Cucina, A. (2016) SMT and TOFT: Why and How They are Opposite and Incompatible Paradigms, *Acta Biotheor.* Springer Netherlands, 64(3), pp. 221–239. doi: 10.1007/s10441-016-9281-4.

Borel, F., Lacroix, F. B. and Margolis, R. L. (2002) Prolonged arrest of mammalian cells at the G1/S boundary results in permanent S phase stasis., *J. Cell Sci.*, 115(Pt 14), pp. 2829–2838.

Brock, R. (2006) Fluorescence correlation spectroscopy in cell biology, in *Fluoresc. Spectrosc. Biol.*, pp. 245–262. doi: 10.1007/3-540-27004-3_14.

Brock, R., Hink, M. A. and Jovin, T. M. (1998) Fluorescence correlation microscopy of cells in the presence of autofluorescence, *Biophys. J.*, 75(5), pp. 2547–2557. doi: 10.1016/S0006-3495(98)77699-4.

Broderick, R., Ramadurai, S., Tóth, K., Togashi, D. M., Ryder, A. G., Langowski, J. and Nasheuer, H. P. (2012) Cell cycle-dependent mobility of Cdc45 determined in vivo by Fluorescence Correlation Spectroscopy, *PLoS One*, 7(4). doi: 10.1371/journal.pone.0035537.

Brown, R. (1828) XXVII. A brief account of microscopical observations made in the months of June, July and August 1827, on the particles contained in the pollen of plants; and on the general existence of active molecules in organic and inorganic bodies, *Philos. Mag. Ser. 2*, 4(21), pp. 161–173. doi: 10.1080/14786442808674769.

Brown, R. (1829) XXIV. Additional remarks on active molecules, *Philos. Mag.*, 6(33), pp. 161–166. doi: 10.1080/14786442908675115.

Brücher, B. L. D. M. and Jamall, I. S. (2016) Somatic Mutation Theory - Why it's Wrong for Most Cancers, *Cell. Physiol. Biochem.*, 38(5), pp. 1663–1680. doi: 10.1159/000443106.

Busser, J., Geldmacher, D. S. and Herrup, K. (1998) Ectopic Cell Cycle Proteins Predict the Sites of Neuronal Cell Death in Alzheimer's Disease Brain, *J. Neurosci.*, 18(8), pp. 2801–2807. doi: 10.1523/JNEUROSCI.18-08-02801.1998.

Capoulade, J., Wachsmuth, M., Hufnagel, L. and Knop, M. (2011) Quantitative fluorescence imaging of protein diffusion and interaction in living cells, *Nat. Biotechnol.*, 29(9), pp. 835–839. doi: 10.1038/nbt.1928.

Cappell, S. D., Chung, M., Jaimovich, A., Spencer, S. L. and Meyer, T. (2016) Irreversible APCCdh1 Inactivation Underlies the Point of No Return for Cell-Cycle Entry, *Cell.* Elsevier Inc., 166(1), pp. 167–180. doi: 10.1016/j.cell.2016.05.077.

Chang, C. R., Manlandro, C. M., Arnoult, D., Stadler, J., Posey, A. E., Hill, R. B. and Blackstone, C. (2010) A lethal de novo mutation in the middle domain of the dynamin-related GTPase Drp1 impairs higher order assembly and mitochondrial division, *J. Biol. Chem.*, 285(42), pp. 32494–32503. doi: 10.1074/jbc.M110.142430.

Chiu, W. L., Niwa, Y., Zeng, W., Hirano, T., Kobayashi, H. and Sheen, J. (1996) Engineered GFP as a vital reporter in plants, *Curr. Biol.*, 6(3), pp. 325–330. doi:

10.1016/S0960-9822(02)00483-9.

Cognet, L., Leduc, C. and Lounis, B. (2014) Advances in live-cell single-particle tracking and dynamic super-resolution imaging, *Curr. Opin. Chem. Biol.*, 20(1), pp. 78–85. doi: 10.1016/j.cbpa.2014.04.015.

Crank, J. (1975) *The Mathematics of Diffusion*. doi: 10.1016/0306-4549(77)90072-X.

Cuervo, a M. and Dice, J. F. (1998) Lysosomes, a meeting point of proteins, chaperones, and proteases., *J. Mol. Med. (Berl).*, 76(1), pp. 6–12. doi: 10.1007/s001090050185.

Dauty, E. and Verkman, A. S. (2005) Actin Cytoskeleton as the Principal Determinant of Size-dependent DNA Mobility in Cytoplasm, *J. Biol. Chem.*, 280(9), pp. 7823–7828. doi: 10.1074/jbc.M412374200.

Davis, P. K., Ho, A. and Dowdy, S. F. (2001) Biological methods for cell-cycle synchronization of mammalian cells, *Biotechniques*, 30(6), pp. 1322–1331.

Dittrich, P., Malvezzi-Campeggi, F., Jahnz, M. and Schwille, P. (2001) Accessing molecular dynamics in cells by fluorescence correlation spectroscopy, *Biol. Chem.*, 382(3), pp. 491–494. doi: 10.1515/BC.2001.061.

Dix, J. A. and Verkman, A. S. (2008) Crowding effects on diffusion in solutions and cells, *Annu. Rev. Biophys.*, 37(1), pp. 247–263. doi: 10.1146/annurev.biophys.37.032807.125824.

Doi, M. and Edwards, S. F. (1986) *The theory of polymer dynamics*. Clarendon Press.

Doye, V. and Hurt, E. (1997) From nucleoporins to nuclear pore complexes, *Curr. Opin. Cell Biol.*, 9, pp. 401–411.

Dross, N., Spriet, C., Zwerger, M., Müller, G., Waldeck, W. and Langowski, J. (2009) Mapping eGFP oligomer mobility in living cell nuclei, *PLoS One*, 4(4), pp. 1–13. doi: 10.1371/journal.pone.0005041.

Duchen, M. R. (2004) Mitochondria in health and disease: Perspectives on a new mitochondrial biology, *Mol. Aspects Med.*, 25(4), pp. 365–451. doi: 10.1016/j.mam.2004.03.001.

De Duve, C. (1996) The peroxisome in retrospect, *Ann. N. Y. Acad. Sci.*, 804, pp. 1–10. doi: 10.1111/j.1749-6632.1996.tb18603.x.

Einstein, A. (1905) Über die von der molekularkinetischen Theorie der Wärme geforderte Bewegung von in ruhenden Flüssigkeiten suspendierten Teilchen, *Ann. Phys.*, 322(8), pp. 549–560. doi: 10.1002/andp.19053220806.

Einstein, A. and Fürth, R. (1956) *Investigations on the theory of Brownian movement*. Dover Publications.

Eliezer, D., Jennings, P. A., Wright, P. E., Doniach, S., Hodgson, K. O. and Tsuruta, H. (1995) The radius of gyration of an apomyoglobin folding intermediate, *Science (80-.).*, 270(5235), p. 487. doi: 10.1126/science.270.5235.487.

Ellis, R. J. (2001) Macromolecular crowding: Obvious but underappreciated, *Trends Biochem. Sci.*, 26(10), pp. 597–604. doi: 10.1016/S0968-0004(01)01938-7.

Ellis, R. J. and Minton, A. P. (2003) Join the crowd, *Nature*. Nature Publishing Group, 425(6953), pp. 27–28. doi: 10.1038/425027a.

Elowitz, M. B., Surette, M. G., Wolf, P. E., Stock, J. B. and Leibler, S. (1999) Protein mobility in the cytoplasm of Escherichia coli, *J. Bacteriol.*, 181(1), pp. 197–203. doi: 0021-9193/99/$04.00-0.

Elsner, M., Hashimoto, H., Simpson, J. C., Cassel, D., Nilsson, T. and Weiss, M. (2003) Spatiotemporal dynamics of the COPI vesicle machinery, *EMBO Rep.*, 4(10), pp. 1000–1005. doi: 10.1038/sj.embor.embor942.

Elson, E. L., Schlessinger, J., Koppel, D. E., Axelrod, D. and Webb, W. W. (1976) Measurement of lateral transport on cell surfaces., *Prog. Clin. Biol. Res.*, 9, pp. 137–47.

Elson, E. L. (2011) Fluorescence correlation spectroscopy: Past, present, future, *Biophys. J.*, 101(12), pp. 2855–2870. doi: 10.1016/j.bpj.2011.11.012.

Elson, E. L. and Magde, D. (1974) Fluorescence correlation spectroscopy. I. Conceptual basis and theory, *Biopolymers*, 13(1), pp. 1–27. doi: 10.1002/bip.1974.360130102.

Engel, B. D., Schaffer, M., Albert, S., Asano, S., Plitzko, J. M. and Baumeister, W. (2015) In situ structural analysis of Golgi intracisternal protein arrays., *Proc. Natl. Acad. Sci. U. S. A.*, 112(36), pp. 11264–9. doi: 10.1073/pnas.1515337112.

Feng, G., Mellor, R. H., Bernstein, M., Keller-Peck, C., Nguyen, Q. T., Wallace, M., Nerbonne, J. M., Lichtman, J. W. and Sanes, J. R. (2000) Imaging neuronal sets in transgenic mice expressing multiple spectral variants of GFP, *Neuron*, 28(1), pp. 41–51.

Fick, A. (1855) V. On liquid diffusion, *London, Edinburgh, Dublin Philos. Mag. J. Sci.* Taylor & Francis Group, 10(63), pp. 30–39. doi: 10.1080/14786445508641925.

Finka, A., Sood, V., Quadroni, M., De Los Rios, P. D. L. and Goloubinoff, P. (2015) Quantitative proteomics of heat-treated human cells show an across-the-board mild depletion of housekeeping proteins to massively accumulate few HSPs, *Cell Stress Chaperones*, 20(4), pp. 605–620. doi: 10.1007/s12192-015-0583-2.

Foo, Y. H., Naredi-Rainer, N., Lamb, D. C., Ahmed, S. and Wohland, T. (2012) Factors affecting the quantification of biomolecular interactions by fluorescence cross-correlation spectroscopy, *Biophys. J.*, 102(5), pp. 1174–1183. doi: 10.1016/j.bpj.2012.01.040.

Frank, S., Gaume, B., Bergmann-Leitner, E. S., Leitner, W. W., Robert, E. G., Catez, F., Smith, C. L. and Youle, R. J. (2001) The Role of Dynamin-Related Protein 1, a Mediator of Mitochondrial Fission, in Apoptosis, *Dev. Cell*, 1(4), pp. 515–525. doi: 10.1016/S1534-5807(01)00055-7.

Frey, E. and Kroy, K. (2005) Brownian motion: A paradigm of soft matter and biological physics, *Ann. der Phys.*, 14(1–3), pp. 20–50. doi: 10.1002/andp.200410132.

Fröhlich, C., Grabiger, S., Schwefel, D., Faelber, K., Rosenbaum, E., Mears, J., Rocks, O. and Daumke, O. (2013) Structural insights into oligomerization and mitochondrial remodelling of dynamin 1-like protein, *EMBO J.*, 32(9), pp. 1280–

1292. doi: 10.1038/emboj.2013.74.

García-Pérez, A. I., López-Beltrán, E. A., Klüner, P., Luque, J., Ballesteros, P. and Cerdán, S. (1999) Molecular crowding and viscosity as determinants of translational diffusion of metabolites in subcellular organelles, *Arch. Biochem. Biophys.*, 362(2), pp. 329–338. doi: 10.1006/abbi.1998.1051.

Gennerich, A. and Schild, D. (2000) Fluorescence correlation spectroscopy in small cytosolic compartments depends critically on the diffusion model used, *Biophys. J.*, 79(6), pp. 3294–3306. doi: 10.1016/S0006-3495(00)76561-1.

Gerken, M., Krippner-Heidenreich, A., Steinert, S., Willi, S., Neugart, F., Zappe, A., Wrachtrup, J., Tietz, C. and Scheurich, P. (2010) Fluorescence correlation spectroscopy reveals topological segregation of the two tumor necrosis factor membrane receptors, *Biochim. Biophys. Acta - Biomembr.* Elsevier B.V., 1798(6), pp. 1081–1089. doi: 10.1016/j.bbamem.2010.02.021.

Glover, T. W., Berger, C., Coyle, J. and Echo, B. (1984) DNA polymerase α inhibition by aphidicolin induces gaps and breaks at common fragile sites in human chromosomes, *Hum. Genet.*, 67(2), pp. 136–142. doi: 10.1007/BF00272988.

Gorisch, S. M. (2005) Histone acetylation increases chromatin accessibility, *J. Cell Sci.*, 118(24), pp. 5825–5834. doi: 10.1242/jcs.02689.

Graham, T. (1829) A short account of experimental researches on the diffusion of gases through each other, and their separation by mechanical means, *Q. J. Sci. Lit. Art*, 27, pp. 74–83.

Griffith, L. G. and Swartz, M. A. (2006) Capturing complex 3D tissue physiology in vitro, *Nat. Rev. Mol. Cell Biol.*, 7(3), pp. 211–224. doi: 10.1038/nrm1858.

Guigas, G., Kalla, C. and Weiss, M. (2007a) Probing the nanoscale viscoelasticity of intracellular fluids in living cells, *Biophys. J.*, 93(1), pp. 316–323. doi: 10.1529/biophysj.106.099267.

Guigas, G., Kalla, C. and Weiss, M. (2007b) The degree of macromolecular crowding in the cytoplasm and nucleoplasm of mammalian cells is conserved, *FEBS Lett.*, 581(26), pp. 5094–5098. doi: 10.1016/j.febslet.2007.09.054.

Guillouzo, A. and Guguen-Guillouzo, C. (2008) Evolving concepts in liver tissue modeling and implications for in vivo toxicology, *Expert Opin. Drug Metab. Toxicol.* Taylor & Francis, 4(10), pp. 1279–1294. doi: 10.1517/17425255.4.10.1279.

Guo, M., Ehrlicher, A. J., Jensen, M. H., Renz, M., Moore, J. R., Goldman, R. D., Lippincott-Schwartz, J., Mackintosh, F. C. and Weitz, D. A. (2014) Probing the stochastic, motor-driven properties of the cytoplasm using force spectrum microscopy, *Cell*. Elsevier Inc., 158(4), pp. 822–832. doi: 10.1016/j.cell.2014.06.051.

Hahn, A. T., Jones, J. T. and Meyer, T. (2009) Quantitative analysis of cell cycle phase durations and PC12 differentiation using fluorescent biosensors, *Cell Cycle*, 8(7), pp. 1044–1052. doi: 10.4161/cc.8.7.8042.

Hanahan, D. and Weinberg, R. A. (2000) The hallmarks of cancer., *Cell*, 100(1), pp. 57–70. doi: 10.1007/s00262-010-0968-0.

Hanahan, D. and Weinberg, R. A. (2011) Hallmarks of cancer: The next

generation, *Cell*. Elsevier Inc., 144(5), pp. 646–674. doi: 10.1016/j.cell.2011.02.013.

Haupts, U., Maiti, S., Schwille, P. and Webb, W. W. (1998) Dynamics of fluorescence fluctuations in green fluorescent protein observed by fluorescence correlation spectroscopy., *Proc. Natl. Acad. Sci. U. S. A.*, 95, pp. 13573–13578. doi: 10.1073/pnas.95.23.13573.

Haustein, E. and Schwille, P. (2003) Ultrasensitive investigations of biological systems by fluorescence correlation spectroscopy, *Methods*, 29(2), pp. 153–166. doi: 10.1016/S1046-2023(02)00306-7.

Hell, S., Reiner, G., Cremer, C. and Stelzer, E. H. K. (1993) Aberrations in confocal fluorescence microscopy induced by mismatches in refractive index, *J. Microsc.*, 169(3), pp. 391–405. doi: 10.1111/j.1365-2818.1993.tb03315.x.

Helmrich, A., Ballarino, M. and Tora, L. (2011) Collisions between Replication and Transcription Complexes Cause Common Fragile Site Instability at the Longest Human Genes, *Mol. Cell*. Elsevier, 44(6), pp. 966–977. doi: 10.1016/j.molcel.2011.10.013.

Hendil, K. B., Hartmann-Petersen, R. and Tanaka, K. (2002) 26 S proteasomes function as stable entities, *J. Mol. Biol.*, 315(4), pp. 627–636. doi: 10.1006/jmbi.2001.5285.

Hess, S. T., Huang, S., Heikal, A. A. and Webb, W. W. (2002) Biological and chemical applications of fluorescence correlation spectroscopy: A review, *Biochemistry*, 41(3), pp. 697–705. doi: 10.1021/bi0118512.

Hinde, E., Cardarelli, F., Digman, M. a and Gratton, E. (2010) In vivo pair correlation analysis of EGFP intranuclear diffusion reveals DNA-dependent molecular flow., *Proc. Natl. Acad. Sci. U. S. A.*, 107, pp. 16560–16565. doi: 10.1073/pnas.1006731107.

Hinde, E., Cardarelli, F., Digman, M. A. and Gratton, E. (2012) Changes in chromatin compaction during the cell cycle revealed by micrometer-scale measurement of molecular flow in the nucleus, *Biophys. J.*, 102(3), pp. 691–697. doi: 10.1016/j.bpj.2011.11.4026.

Hinde, E. and Cardarelli, F. (2011) Measuring the flow of molecules in cells, *Biophys. Rev.*, 3(3), pp. 119–129. doi: 10.1007/s12551-011-0051-x.

Holtzer, L., Meckel, T. and Schmidt, T. (2007) Nanometric three-dimensional tracking of individual quantum dots in cells, *Appl. Phys. Lett.*, 90(5), p. 053902. doi: 10.1063/1.2437066.

Hołyst, R., Bielejewska, A., Szymański, J., Wilk, A., Patkowski, A., Gapiński, J., Żywociński, A., Kalwarczyk, T., Kalwarczyk, E., Tabaka, M., *et al.* (2009) Scaling form of viscosity at all length-scales in poly(ethylene glycol) solutions studied by fluorescence correlation spectroscopy and capillary electrophoresis, *Phys. Chem. Chem. Phys.*, 11(40), p. 9025. doi: 10.1039/b908386c.

Hong, J. and Gierasch, L. M. (2010) Macromolecular crowding remodels the energy landscape of a protein by favoring a more compact unfolded state, *J. Am. Chem. Soc.*, 132(30), pp. 10445–10452. doi: 10.1021/ja103166y.

Hou, S., Ziebacz, N., Kalwarczyk, T., Kaminski, T. S., Wieczorek, S. A. and Holyst, R. (2011) Influence of nano-viscosity and depletion interactions on

cleavage of DNA by enzymes in glycerol and poly(ethylene glycol) solutions: qualitative analysis, *Soft Matter*, 7(7), pp. 3092–3099. doi: 10.1039/C0SM00899K.

Hou, S., Sun, L., Wieczorek, S. A., Kalwarczyk, T., Kaminski, T. S. and Holyst, R. (2014) Fluorescence correlation spectroscopy analysis for accurate determination of proportion of doubly labeled DNA in fluorescent DNA pool for quantitative biochemical assays, *Biosens. Bioelectron.*, 51, pp. 8–15. doi: 10.1016/j.bios.2013.07.010.

Hu, J., Jafari, S., Han, Y., Grodzinsky, A. J., Cai, S. and Guo, M. (2017) Size- and speed-dependent mechanical behavior in living mammalian cytoplasm, *Proc. Natl. Acad. Sci.*, 114(36), pp. 9529–9534. doi: 10.1073/pnas.1702488114.

Huang, R., Chavez, I., Taute, K. M., Lukić, B., Jeney, S., Raizen, M. G. and Florin, E.-L. (2011) Direct observation of the full transition from ballistic to diffusive Brownian motion in a liquid, *Nat. Phys.*, 7(7), pp. 576–580. doi: 10.1038/nphys1953.

Illaste, A., Laasmaa, M., Peterson, P. and Vendelin, M. (2012) Analysis of molecular movement reveals latticelike obstructions to diffusion in heart muscle cells, *Biophys. J.*, 102(4), pp. 739–748. doi: 10.1016/j.bpj.2012.01.012.

Ingram, N., Macnab, S. A., Marston, G., Scott, N., Carr, I. M., Markham, A. F., Whitehouse, A. and Coletta, P. L. (2013) The use of high-frequency ultrasound imaging and biofluorescence for in vivo evaluation of gene therapy vectors, *BMC Med. Imaging*. BMC Medical Imaging, 13(1), p. 1. doi: 10.1186/1471-2342-13-35.

Janson, L. W., Ragsdale, K. and Luby-Phelps, K. (1996) Mechanism and size cutoff for steric exclusion from actin-rich cytoplasmic domains, *Biophys. J.* Elsevier, 71(3), pp. 1228–1234. doi: 10.1016/S0006-3495(96)79367-0.

Jasnin, M., Moulin, M., Haertlein, M., Zaccai, G. and Tehei, M. (2008) Down to atomic-scale intracellular water dynamics, *EMBO Rep.*, 9(6), pp. 543–547. doi: 10.1038/embor.2008.50.

Jordan, M. a, Thrower, D. and Wilson, L. (1992) Effects of vinblastine, podophyllotoxin and nocodazole on mitotic spindles. Implications for the role of microtubule dynamics in mitosis., *J. Cell Sci.*, 102 (Pt 3, pp. 401–416.

Juan, G., Hernando, E. and Cordon-Cardo, C. (2002) Separation of live cells in different phases of the cell cycle for gene expression analysis, *Cytometry*, 49(4), pp. 170–175. doi: 10.1002/cyto.10173.

Kalwarczyk, T., Ziębacz, N., Bielejewska, A., Zaboklicka, E., Koynov, K., Szymański, J., Wilk, A., Patkowski, A., Gapiński, J., Butt, H. J., *et al.* (2011) Comparative analysis of viscosity of complex liquids and cytoplasm of mammalian cells at the nanoscale, *Nano Lett.*, 11(5), pp. 2157–2163. doi: 10.1021/nl2008218.

Kalwarczyk, T., Sozanski, K., Jakiela, S., Wisniewska, A., Kalwarczyk, E., Kryszczuk, K., Hou, S. and Holyst, R. (2014) Length-scale dependent transport properties of colloidal and protein solutions for prediction of crystal nucleation rates, *Nanoscale*, 6(17), pp. 10340–10346. doi: 10.1039/c4nr00647j.

Kalwarczyk, T., Sozanski, K., Ochab-Marcinek, A., Szymanski, J., Tabaka, M., Hou, S. and Holyst, R. (2015) Motion of nanoprobes in complex liquids within

the framework of the length-scale dependent viscosity model, *Adv. Colloid Interface Sci.* Elsevier B.V., 223, pp. 55–63. doi: 10.1016/j.cis.2015.06.007.

Kalwarczyk, T., Kwapiszewska, K., Szczepanski, K., Sozanski, K., Szymanski, J., Michalska, B., Patalas-Krawczyk, P., Duszynski, J. and Holyst, R. (2017) Apparent Anomalous Diffusion in the Cytoplasm of Human Cells: The Effect of Probes' Polydispersity, *J. Phys. Chem. B*, 121(42), pp. 9831–9837. doi: 10.1021/acs.jpcb.7b07158.

Kalwarczyk, T., Tabaka, M. and Hołyst, R. (2012) Biologistics-Diffusion coefficients for complete proteome of Escherichia coli, *Bioinformatics*, 28(22), pp. 2971–2978. doi: 10.1093/bioinformatics/bts537.

Kao, H. P., Abney, J. R. and Verkman, A. S. (1993) Determinants of the translational diffusion of a small solute in cytoplasm, *J. Cell Biol.*, 120(1), pp. 175–184.

Kerr, R. A., Bartol, T. M., Kaminsky, B., Dittrich, M., Chang, J.-C. J., Baden, S. B., Sejnowski, T. J. and Stiles, J. R. (2008) Fast Monte Carlo Simulation Methods for Biological Reaction-Diffusion Systems in Solution and on Surfaces., *SIAM J Sci Comput*, 30(6), p. 3126. doi: http://dx.doi.org/10.1137/070692017.

Keyomarsi, K., Sandoval, L., Band, V., Band, M. and Pardee, A. B. (1991) Synchronization of Tumor and Normal Cells from G 1 to Multiple Cell Cycles by Lovastatin Synchronization of Tumor and Normal Cells from G , to Multiple Cell Cycles by Lovastatin1, pp. 3602–3609.

Kim, S. A., Heinze, K. G. and Schwille, P. (2007) Fluorescence correlation spectroscopy in living cells, *Nat. Methods*, 4(11), pp. 963–973. doi: 10.1038/nmeth1104.

Kinjo, A. R. and Takada, S. (2002) Effects of macromolecular crowding on protein folding and aggregation studied by density functional theory: Dynamics, *Phys. Rev. E - Stat. Physics, Plasmas, Fluids, Relat. Interdiscip. Top.*, 66(5), p. 10. doi: 10.1103/PhysRevE.66.051902.

Koirala, S., Guo, Q., Kalia, R., Bui, H. T., Eckert, D. M., Frost, A. and Shaw, J. M. (2013) Interchangeable adaptors regulate mitochondrial dynamin assembly for membrane scission, *Proc. Natl. Acad. Sci.*, 110(15), pp. E1342–E1351. doi: 10.1073/pnas.1300855110.

Kosar, T. F. and Phillips, R. J. (1995) Measurement of protein diffusion in Dextran solutions by holographic interferometry, *AIChE J.*, 41(3), pp. 701–711. doi: 10.1002/aic.690410327.

Krude, T. (1999) Mimosine arrests proliferating human cells before onset of DNA replication in a dose-dependent manner, 159, pp. 148–159.

Kung, A. L., Zetterberg, A., Sherwood, S. W. and Schimke, R. T. (1990) Cytotoxic effects of the cell cycle phase specific agent: result of cell cycle perturbation, *Cancer Res*, 50, pp. 7307–7317.

Kung, A. L., Sherwood, S. W. and Schimke, R. T. (1990) Cell line-specific differences in the control of cell cycle progression in the absence of mitosis., *Proc. Natl. Acad. Sci. U. S. A.*, 87(December), pp. 9553–9557. doi: 10.1073/pnas.87.24.9553.

Kung, A. L., Sherwood, S. W. and Schimke, R. T. (1993) Differences in the

regulation of protein synthesis, cyclin B accumulation, and cellular growth in response to the inhibition of DNA synthesis in Chinese hamster ovary and HeLa S3 cells., *J. Biol. Chem.*, 268(31), pp. 23072–23080.

Lakowicz, J. R. (2006) *Principles of fluorescence spectroscopy*, *Princ. Fluoresc. Spectrosc.* Springer. doi: 10.1007/978-0-387-46312-4.

Lamond, A. I. (1998) Structure and Function in the Nucleus, *Science (80-.).*, 280(5363), pp. 547–553. doi: 10.1126/science.280.5363.547.

Langevin, D. and Rondelez, F. (1978) Sedimentation of large colloidal particles through semidilute polymer solutions, *Polymer (Guildf).*, 19(8), pp. 875–882. doi: 10.1016/0032-3861(78)90191-X.

Leduc, C., Si, S., Gautier, J., Soto-Ribeiro, M., Wehrle-Haller, B., Gautreau, A., Giannone, G., Cognet, L. and Lounis, B. (2013) A highly specific gold nanoprobe for live-cell single-molecule imaging, *Nano Lett.*, 13(4), pp. 1489–1494. doi: 10.1021/nl304561g.

Levi, V., Ruan, Q. Q. and Gratton, E. (2005) 3-D particle tracking in a two-photon microscope: Application to the study of molecular dynamics in cells, *Biophys. J.* Elsevier, 88(4), pp. 2919–2928. doi: 10.1529/biophysj.104.044230.

Li, T., Kheifets, S., Medellin, D. and Raizen, M. (2010) Measurement of the instantneous velocity of a brownian particle, *Science (80-.).*, 328(June), pp. 1673–1675.

Liang, L., Wang, X., Xing, D., Chen, T. and Chen, W. R. (2009) Noninvasive determination of cell nucleoplasmic viscosity by fluorescence correlation spectroscopy, *J. Biomed. Opt.*, 14(2), p. 024013. doi: 10.1117/1.3088141.

Lillemeier, B. F., Mörtelmaier, M. A., Forstner, M. B., Huppa, J. B., Groves, J. T. and Davis, M. M. (2010) TCR and Lat are expressed on separate protein islands on T cell membranes and concatenate during activation, *Nat. Immunol.*, 11(1), pp. 90–96. doi: 10.1038/ni.1832.

Lodish, H., Berk, A., Zipursky, S. L., Matsudaira, P., Baltimore, D. and Darnell, J. (2000) *Molecular Cell Biology*. 4th edn. W. H. Freeman.

Lodish, H., Berk, A., Kaiser, C. A., Krieger, M., Bretscher, A., Ploegh, H., Amon, A. and Scott, M. P. (2013) *Molecular Cell Biology (7th Edition)*. W. H. Freeman. doi: 10.1016/S1470-8175(01)00023-6.

Long, M. S., Jones, C. D., Helfrich, M. R., Mangeney-Slavin, L. K. and Keating, C. D. (2005) Dynamic microcompartmentation in synthetic cells, *Proc. Natl. Acad. Sci.*, 102(17), pp. 5920–5925. doi: 10.1073/pnas.0409333102.

Lu, H., Xue, Y., Yu, G. K., Arias, C., Lin, J., Fong, S., Faure, M., Weisburd, B., Ji, X., Mercier, A., *et al.* (2015) Compensatory induction of MYC expression by sustained CDK9 inhibition via a BRD4-dependent mechanism, *Elife*, 4(JUNE2015), pp. 1–26. doi: 10.7554/eLife.06535.

Luby-Phelps, K. (1999) Cytoarchitecture and Physical Properties of Cytoplasm: Volume, Viscosity, Diffusion, Intracellular Surface Area, 192, pp. 189–221. doi: 10.1016/S0074-7696(08)60527-6.

Luby-Phelps, K. (2013) The physical chemistry of cytoplasm and its influence on cell function: an update, *Mol. Biol. Cell*, 24(17), pp. 2593–2596. doi: 10.1091/mbc.E12-08-0617.

Luby-Phelps, K., Taylor, D. L. and Lanni, F. (1986) Probing the structure of cytoplasm., *J. Cell Biol.*, 102(6), pp. 2015–22. doi: 10.1083/jcb.102.6.2015.

Lukacs, G. L., Haggie, P., Seksek, O., Lechardeur, D., Freedman, N. and Verkman, A. S. (2000) Size-dependent DNA mobility in cytoplasm and nucleus, *J. Biol. Chem.*, 275(3), pp. 1625–1629. doi: 10.1074/jbc.275.3.1625.

Macdonald, P. J., Stepanyants, N., Mehrotra, N., Mears, J. A., Qi, X., Sesaki, H. and Ramachandran, R. (2014) A dimeric equilibrium intermediate nucleates Drp1 reassembly on mitochondrial membranes for fission, *Mol. Biol. Cell*, 25(12), pp. 1905–1915. doi: 10.1091/mbc.E14-02-0728.

Macháň, R. and Wohland, T. (2014) Recent applications of fluorescence correlation spectroscopy in live systems, *FEBS Lett.*, 588(19), pp. 3571–3584. doi: 10.1016/j.febslet.2014.03.056.

Maertens, G., Vercammen, J., Debyser, Z. and Engelborghs, Y. (2005) Measuring protein-protein interactions inside living cells using single color fluorescence correlation spectroscopy. Application to human immunodeficiency virus type 1 integrase and LEDGF/p75, *FASEB J.*, 19(8), pp. 1039–1041. doi: 10.1096/fj.04-3373fje.

Magde, D., Elson, E. L. and Webb, W. W. (1974) Fluorescence correlation spectroscopy. II. An experimental realization, *Biopolymers*, 13(1), pp. 29–61. doi: 10.1002/bip.1974.360130103.

Magde, D., Elson, E. and Webb, W. W. (1972) Thermodynamic fluctuations in a reacting system measurement by fluorescence correlation spectroscopy, *Phys. Rev. Lett.*, 29(11), pp. 705–708. doi: 10.1103/PhysRevLett.29.705.

Mahen, R., Jeyasekharan, A. D., Barry, N. P. and Venkitaraman, A. R. (2011) Continuous polo-like kinase 1 activity regulates diffusion to maintain centrosome self-organization during mitosis, *Proc. Natl. Acad. Sci.*, 108(22), pp. 9310–9315. doi: 10.1073/pnas.1101112108.

McGlynn, P., Savery, N. J. and Dillingham, M. S. (2012) The conflict between DNA replication and transcription, *Mol. Microbiol.*, 85(1), pp. 12–20. doi: 10.1111/j.1365-2958.2012.08102.x.

McShea, A., Harris, P. L., Webster, K. R., Wahl, A. F. and Smith, M. A. (1997) Abnormal expression of the cell cycle regulators P16 and CDK4 in Alzheimer's disease., *Am. J. Pathol.*, 150(6), pp. 1933–9.

Michalska, B. M., Kwapiszewska, K., Szczepanowska, J., Kalwarczyk, T., Patalas-Krawczyk, P., Szczepański, K., Hołyst, R., Duszyński, J. and Szymański, J. (2018) Insight into the fission mechanism by quantitative characterization of Drp1 protein distribution in the living cell, *Sci. Rep.*, 8(1), p. 8122. doi: 10.1038/s41598-018-26578-z.

Mika, J. T. and Poolman, B. (2011) Macromolecule diffusion and confinement in prokaryotic cells, *Curr. Opin. Biotechnol.* Elsevier Ltd, 22(1), pp. 117–126. doi: 10.1016/j.copbio.2010.09.009.

Minton, a P. (2000) Implications of macromolecular crowding for protein assembly [Review], *Curr. Opin. Struct. Biol.*, 10(1), pp. 34–39. doi: 10.1016/S0959-440X(99)00045-7.

Minton, A. P. (2001) The Influence of Macromolecular Crowding and

Macromolecular Confinement on Biochemical Reactions in Physiological Media, *J. Biol. Chem.*, 276(14), pp. 10577–10580. doi: 10.1074/jbc.R100005200.

Minton, A. P. (2006) How can biochemical reactions within cells differ from those in test tubes?, *J. Cell Sci.*, 119(14), pp. 2863–2869. doi: 10.1242/jcs.03063.

Montessuit, S., Somasekharan, S. P., Terrones, O., Lucken-Ardjomande, S., Herzig, S., Schwarzenbacher, R., Manstein, D. J., Bossy-Wetzel, E., Basañez, G., Meda, P., *et al.* (2010) Membrane Remodeling Induced by the Dynamin-Related Protein Drp1 Stimulates Bax Oligomerization, *Cell*, 142(6), pp. 889–901. doi: 10.1016/j.cell.2010.08.017.

Morelli, M. J., Allen, R. J. and Rein Ten Wolde, P. (2011) Effects of macromolecular crowding on genetic networks, *Biophys. J.* Biophysical Society, 101(12), pp. 2882–2891. doi: 10.1016/j.bpj.2011.10.053.

Mueller, V., Ringemann, C., Honigmann, A., Schwarzmann, G., Medda, R., Leutenegger, M., Polyakova, S., Belov, V. N., Hell, S. W. and Eggeling, C. (2011) STED nanoscopy reveals molecular details of cholesterol- and cytoskeleton-modulated lipid interactions in living cells, *Biophys. J.*, 101(7), pp. 1651–1660. doi: 10.1016/j.bpj.2011.09.006.

Mütze, J., Ohrt, T. and Schwille, P. (2011) Fluorescence correlation spectroscopy in vivo, *Laser Photon. Rev.*, 5(1), pp. 52–67. doi: 10.1002/lpor.200910041.

Nenninger, A., Mastroianni, G. and Mullineaux, C. W. (2010) Size dependence of protein diffusion in the cytoplasm of Escherichia coli, *J. Bacteriol.*, 192(18), pp. 4535–4540. doi: 10.1128/JB.00284-10.

Odijk, T. (2000) Depletion Theory of Protein Transport in Semi-Dilute Polymer Solutions, *Biophys. J.*, 79(5), pp. 2314–2321. doi: 10.1016/S0006-3495(00)76477-0.

Ohrt, T., Mütze, J., Staroske, W., Weinmann, L., Höck, J., Crell, K., Meister, G. and Schwille, P. (2008) Fluorescence correlation spectroscopy and fluorescence cross-correlation spectroscopy reveal the cytoplasmic origination of loaded nuclear RISC in vivo in human cells, *Nucleic Acids Res.*, 36(20), pp. 6439–6449. doi: 10.1093/nar/gkn693.

Ortega, A., Amorós, D. and García De La Torre, J. (2011) Prediction of hydrodynamic and other solution properties of rigid proteins from atomic- and residue-level models, *Biophys. J.*, 101(4), pp. 892–898. doi: 10.1016/j.bpj.2011.06.046.

Padilla-Parra, S., Audugé, N., Coppey-Moisan, M. and Tramier, M. (2011) Dual-color fluorescence lifetime correlation spectroscopy to quantify protein-protein interactions in live cell., *Microsc. Res. Tech.*, 74(8), pp. 788–93. doi: 10.1002/jemt.21015.

Panton, R. L. (Ronald L. (2013) *Incompressible flow*. Hoboken, NJ, USA: John Wiley & Sons, Inc. doi: 10.1002/9781118713075.

Patterson, G. H. (2002) A photoactivatable GFP for selective photolabeling of proteins and cells, *Science (80-.).*, 297(5588), pp. 1873–1877. doi: 10.1126/science.1074952.

Pavlova, N. N. and Thompson, C. B. (2016) The Emerging Hallmarks of Cancer Metabolism, *Cell Metab.* Elsevier Inc., 23(1), pp. 27–47. doi: 10.1016/j.cmet.2015.12.006.

Pawar, N., Donth, C. and Weiss, M. (2014) Anisotropic diffusion of macromolecules in the contiguous nucleocytoplasmic fluid during eukaryotic cell division, *Curr. Biol.* Elsevier Ltd, 24(16), pp. 1905–1908. doi: 10.1016/j.cub.2014.06.072.

Pedrali-Noy, G., Spadari, S., Miller-Faurès, a, Miller, a O., Kruppa, J. and Koch, G. (1980) Synchronization of HeLa cell cultures by inhibition of DNA polymerase alpha with aphidicolin., *Nucleic Acids Res.*, 8(2), pp. 377–387. doi: 10.1093/nar/8.2.377.

Perrin, J. (1913) *Les atomes*. Librairie Felix Alcan.

Philibert, J. (2005) One and a half century of diffusion: Fick, Einstein, before and beyond, *Diffus. Fundam.*, 4, pp. 1–19. doi: 10.1093/ajcn/29.2.205.

Phillip, Y., Kiss, V. and Schreiber, G. (2012) Protein-binding dynamics imaged in a living cell, *Proc. Natl. Acad. Sci.*, 109(5), pp. 1461–1466. doi: 10.1073/pnas.1112171109.

Pielak, G. J., Li, C., Miklos, A. C., Schlesinger, A. P., Slade, K. M., Wang, G. F. and Zigoneanu, I. G. (2009) Protein nuclear magnetic resonance under physiological conditions, *Biochemistry*, 48(2), pp. 226–234. doi: 10.1021/bi8018948.

Pollard, T. D. (2010) A Guide to Simple and Informative Binding Assays, *Mol. Biol. Cell*, 21(23), pp. 4061–4067. doi: 10.1091/mbc.E10-08-0683.

Posakony, J. W., England, J. M. and Attardi, G. (1977) Mitochondrial growth and division during the cell cycle in HeLa cells., *J. Cell Biol.*, 74(2), pp. 468–91. doi: 10.1083/jcb.74.2.468.

Potma, E. O., De Boeij, W. P. and Wiersma, D. A. (2001) Femtosecond dynamics of intracellular water probed with nonlinear optical Kerr effect microspectroscopy, *Biophys. J.* Elsevier, 80(6), pp. 3019–3024. doi: 10.1016/S0006-3495(01)76267-4.

Puck, T. T. and Steffen, J. (1963) Life Cycle Analysis of Mammalian Cells: I. A Method for Localizing Metabolic Events within the Life Cycle, and Its Application to the Action of Colcemide and Sublethal Doses of X-Irradiation, *Biophys. J.* Elsevier, 3(5), pp. 379–397. doi: 10.1016/S0006-3495(63)86828-9.

Pusey, P. N. (2011) Brownian motion goes ballistic, *Science (80-.).*, 332(6031), pp. 802–803. doi: 10.1126/science.1192222.

Radko, S. P. and Chrambach, A. (1996) Mechanisms of retardation of rigid spherical particles with 3 to 1,085 nm radius in capillary electrophoresis, using buffered polyacrylamide (molecular weight 5 × 106) solutions, *Electrophoresis*, 17(6), pp. 1094–1102. doi: 10.1002/elps.1150170619.

Reuel, N. F., Dupont, A., Thouvenin, O., Lamb, D. C. and Strano, M. S. (2012) Three-dimensional tracking of carbon nanotubes within living cells, *ACS Nano*, 6(6), pp. 5420–5428. doi: 10.1021/nn301298e.

Ridgway, D., Broderick, G., Lopez-Campistrous, A., Ru'Aini, M., Winter, P., Hamilton, M., Boulanger, P., Kovalenko, A. and Ellison, M. J. (2008) Coarse-

grained molecular simulation of diffusion and reaction kinetics in a crowded virtual cytoplasm, *Biophys. J.* Elsevier, 94(10), pp. 3748–3759. doi: 10.1529/biophysj.107.116053.

Rigler, R., Mets, Ü., Widengren, J. and Kask, P. (1993) Fluorescence correlation spectroscopy with high count rate and low background: analysis of translational diffusion, *Eur. Biophys. J.*, 22(3), pp. 169–175. doi: 10.1007/BF00185777.

Ringemann, C., Harke, B., Von Middendorff, C., Medda, R., Honigmann, A., Wagner, R., Leutenegger, M., Schönle, A., Hell, S. W. and Eggeling, C. (2009) Exploring single-molecule dynamics with fluorescence nanoscopy, *New J. Phys.*, 11, pp. 103054–103083. doi: 10.1088/1367-2630/11/10/103054.

Rodbard, D. and Chrambach, A. (1971) Estimation of molecular radius, free mobility, and valence using polyacrylamide gel electrophoresis, *Anal. Biochem.*, 40(1), pp. 95–134. doi: 10.1016/0003-2697(71)90086-8.

Sarkar, M., Li, C. and Pielak, G. J. (2013) Soft interactions and crowding, *Biophys. Rev.*, 5(2), pp. 187–194. doi: 10.1007/s12551-013-0104-4.

Sasahara, K., McPhie, P. and Minton, A. P. (2003) Effect of dextran on protein stability and conformation attributed to macromolecular crowding, *J. Mol. Biol.*, 326(4), pp. 1227–1237. doi: 10.1016/S0022-2836(02)01443-2.

Sasaki, Y., Miyoshi, D. and Sugimoto, N. (2006) Effect of molecular crowding on DNA polymerase activity, *Biotechnol. J.*, 1(4), pp. 440–446. doi: 10.1002/biot.200500032.

Sasaki, Y., Miyoshi, D. and Sugimoto, N. (2007) Regulation of DNA nucleases by molecular crowding, *Nucleic Acids Res.*, 35(12), pp. 4086–4093. doi: 10.1093/nar/gkm445.

Schachman, H. K. and Harrington, W. F. (1952) On viscosity measurement in the ultracentrifuge, *J. Am. Chem. Soc.*, 74(15), pp. 3965–3966. doi: 10.1021/ja01135a533.

Schafer, K. A. (1998) The cell cycle: a review., *Vet. Pathol.*, 35(6), pp. 461–78. doi: 10.1177/030098589803500601.

Schärtl, W. (2010) *Light Scattering from Polymer Solutions and Nanoparticle Dispersions*. 1st edn. Berlin: Springer.

Schutter, E. de. (2001) *Computational neuroscience : realistic modeling for experimentalists*. CRC Press.

Schütz, G. J., Schindler, H. and Schmidt, T. (1997) Single-molecule microscopy on model membranes reveals anomalous diffusion, *Biophys. J.*, 73(2), pp. 1073–1080. doi: 10.1016/S0006-3495(97)78139-6.

Segrè, P. N., Meeker, S. P., Pusey, P. N. and Poon, W. C. K. (1995) Viscosity and structural relaxation in suspensions of hard-sphere colloids, *Phys. Rev. Lett.*, 75(5), pp. 958–961. doi: 10.1103/PhysRevLett.75.958.

Seksek, O. and Verkman, a S. (1997) Translational diffusion of macromolecule-size solutes in cytoplasm and nucleus: Evidence for diffusion-restricting compartments without sieving., *Biophys. J.*, 72(2), pp. Tu372-Tu372. doi: 10.1083/jcb.138.1.131.

Sharma, M. and Yashonath, S. (2006) Breakdown of the Stokes-Einstein

relationship: Role of interactions in the size dependence of self-diffusivity, *J. Phys. Chem. B*, 110(34), pp. 17207–17211. doi: 10.1021/jp064364a.

Smirnova, E., Griparic, L., Shurland, D.-L. and van der Bliek, A. M. (2001) Dynamin-related Protein Drp1 Is Required for Mitochondrial Division in Mammalian Cells, *Mol. Biol. Cell*, 12(8), pp. 2245–2256. doi: 10.1091/mbc.12.8.2245.

von Smoluchowski, M. (1906) Zur kinetischen Theorie der Brownschen Molekularbewegung und der Suspensionen, *Ann. Phys.*, 326(14), pp. 756–780. doi: 10.1002/andp.19063261405.

Sodeik, B. (2000) Mechanisms of viral transport in the cytoplasm, *Trends Microbiol.*, 8(10), pp. 465–472. doi: 10.1016/S0966-842X(00)01824-2.

Sonnenschein, C. and Soto, A. M. (2000) Somatic mutation theory of carcinogenesis: Why it should be dropped and replaced, *Mol. Carcinog.*, 29(4), pp. 205–211. doi: 10.1002/1098-2744(200012)29:4<205::AID-MC1002>3.0.CO;2-W.

Sonnenschein, C. and Soto, A. M. (2013) The aging of the 2000 and 2011 Hallmarks of Cancer reviews: a critique., *J. Biosci.*, 38(3), pp. 651–63. doi: 10.1038/nature12213.

Soto, A. M. and Sonnenschein, C. (2014) One hundred years of somatic mutation theory of carcinogenesis: Is it time to switch?, *BioEssays*, 36(1), pp. 118–120. doi: 10.1002/bies.201300160.

Sozański, K., Ruhnow, F., Wiśniewska, A., Tabaka, M., Diez, S. and Hołyst, R. (2015) Small Crowders Slow Down Kinesin-1 Stepping by Hindering Motor Domain Diffusion, *Phys. Rev. Lett.*, 115(21), pp. 1–5. doi: 10.1103/PhysRevLett.115.218102.

Spadari, S., Sala, F. and Pedrali-Noy, G. (1982) Aphidicolin: a specific inhibitor of nuclear DNA replication in eukaryotes, *Trends Biochem. Sci.*, 7(1), pp. 29–32. doi: 10.1016/0968-0004(82)90061-5.

Sparks, J. S., Schelly, R. C., Smith, W. L., Davis, M. P., Tchernov, D., Pieribone, V. A. and Gruber, D. F. (2014) The covert world of fish biofluorescence: A phylogenetically widespread and phenotypically variable phenomenon, *PLoS One*, 9(1). doi: 10.1371/journal.pone.0083259.

Stadler, A. M., Embs, J. P., Digel, I., Artmann, G. M. and Unruh, T. (2008) Cytoplasmic Water and Hydration Layer Dynamics in Human Red Blood Cells, pp. 12–13.

Stepanenko, O., Verkhusha, V., Kuznetsova, I., Uversky, V. and Turoverov, K. (2008) Fluorescent proteins as biomarkers and biosensors: Throwing color lights on molecular and cellular processes, *Curr. Protein Pept. Sci.*, 9(4), pp. 338–369. doi: 10.2174/138920308785132668.

Stiles, J. R., Van Helden, D., Bartol, T. M., Salpeter, E. E. and Salpeter, M. M. (1996) Miniature endplate current rise times less than 100 microseconds from improved dual recordings can be modeled with passive acetylcholine diffusion from a synaptic vesicle., *Proc. Natl. Acad. Sci.*, 93(12), pp. 5747–5752. doi: 10.1073/pnas.93.12.5747.

Stokes, G. G. (1852) On the change of refrangibility of light, *Philos. Trans. R.*

Soc. London, 142, pp. 463–562. doi: 10.1098/rstl.1852.0022.

Strack, S. and Cribbs, J. T. (2012) Allosteric modulation of Drp1 mechanoenzyme assembly and mitochondrial fission by the variable domain, *J. Biol. Chem.*, 287(14), pp. 10990–11001. doi: 10.1074/jbc.M112.342105.

Sutherland, W. (1905) LXXV. A dynamical theory of diffusion for non-electrolytes and the molecular mass of albumin, *London, Edinburgh, Dublin Philos. Mag. J. Sci.*, 9(54), pp. 781–785. doi: 10.1080/14786440509463331.

Szymański, J., Patkowski, A., Wilk, A., Garstecki, P. and Holyst, R. (2006) Diffusion and viscosity in a crowded environment: From nano- to macroscale, *J. Phys. Chem. B*, 110(51), pp. 25593–25597. doi: 10.1021/jp0666784.

Tabaka, M., Kalwarczyk, T., Szymanski, J., Hou, S. and Holyst, R. (2014) The effect of macromolecular crowding on mobility of biomolecules, association kinetics, and gene expression in living cells, *Front. Phys.*, 2(September), pp. 1–14. doi: 10.3389/fphy.2014.00054.

Teraoka, I. (2002) *Polymer Solutions*. John Wiley & Sons. doi: 10.1002/0471224510.

Triffo, S. B., Huang, H. H., Smith, A. W., Chou, E. T. and Groves, J. T. (2012) Monitoring lipid anchor organization in cell membranes by PIE-FCCS, *J. Am. Chem. Soc.*, 134(26), pp. 10833–10842. doi: 10.1021/ja300374c.

Tsien, R. (1998) The Green Fluorescent Protein, *Biochemistry*, 67, pp. 509–544. doi: 10.1146/annurev.biochem.67.1.509.

Twig, G., Elorza, A., Molina, A. J. A., Mohamed, H., Wikstrom, J. D., Walzer, G., Stiles, L., Haigh, S. E., Katz, S., Las, G., *et al.* (2008) Fission and selective fusion govern mitochondrial segregation and elimination by autophagy, *EMBO J.*, 27(2), pp. 433–446. doi: 10.1038/sj.emboj.7601963.

Valeur, B. and Berberan-Santos, M. N. (2011) A brief history of fluorescence and phosphorescence before the emergence of quantum theory, *J. Chem. Educ.*, 88(6), pp. 731–738. doi: 10.1021/ed100182h.

Verkman, A. S. (2002) Solute and macromolecule diffusion in cellular aqueous compartments, *Trends Biochem. Sci.*, 27(1), pp. 27–33. doi: 10.1016/S0968-0004(01)02003-5.

Vermeulen, K., Van Bockstaele, D. R. and Berneman, Z. N. (2003) The cell cycle:a review of regulation,deregulation and therapeutic targets in cancer, *Cell Prolif.*, 36(3), pp. 131–149. doi: 10.1306/74D715D2-2B21-11D7-8648000102C1865D.

Wachsmuth, M., Waldeck, W. and Langowski, J. (2000) Anomalous diffusion of fluorescent probes inside living cell investigated by spatially-resolved fluorescence correlation spectroscopy, *J. Mol. Biol.*, 298(4), pp. 677–689. doi: 10.1006/jmbi.2000.3692.

Wahl, A. F., Geis, A. M., Spain, B. H., Wong, S. W., Korn, D. and Wang, T. S.-F. (1988) Gene Expression of Human DNA polymerase a during Cell Proliferation and the Cell Cycle, *M.C. B.*, 8(11), pp. 5016–5025.

Walter, H. and Brooks, D. E. (1995) Phase separationin cytoplasm, due to macromolecular crowding, is the basis for microcompartmentation, *FEBS.Lett*, 361, pp. 135–139.

Wang, Y., Sarkar, M., Smith, A. E., Krois, A. S. and Pielak, G. J. (2012) Macromolecular crowding and protein stability, *J. Am. Chem. Soc.*, 134(40), pp. 16614–16618. doi: 10.1021/ja305300m.

Wang, Z., Jiang, H., Chen, S., Du, F. and Wang, X. (2012) The mitochondrial phosphatase PGAM5 functions at the convergence point of multiple necrotic death pathways, *Cell*. Elsevier Inc., 148(1–2), pp. 228–243. doi: 10.1016/j.cell.2011.11.030.

Warburg, O., Wind, F. and Negelein, E. (1927) The metabolism of tumors in the body, *J. Gen. Physiol.* The Rockefeller University Press, 8(6), pp. 519–30.

Wattenbarger, M. R., Bloomfield, V. A., Bu, Z. and Russo, P. S. (1992) Tracer diffusion of proteins in DNA solutions, *Macromolecules*, 25(20), pp. 5263–5265. doi: 10.1021/ma00046a024.

Weiss, M. (2014) Crowding, diffusion, and biochemical reactions, *Int. Rev. Cell Mol. Biol.*, 307, pp. 383–417. doi: 10.1016/B978-0-12-800046-5.00011-4.

Wenner, J. R. and Bloomfield, V. A. (1999) Crowding effects on EcoRV kinetics and binding, *Biophys. J.*, 77(6), pp. 3234–3241. doi: 10.1016/S0006-3495(99)77154-7.

Youle, R. J. and van der Bliek, A. M. (2012) Mitochondrial fission, fusion, and stress, *Science (80-.).*, 337(6098), pp. 1062–1065. doi: 10.1126/science.1219855.Mitochondrial.

van der Zand, A., Braakman, I., Geuze, H. J. and Tabak, H. F. (2006) The return of the peroxisome, *J. Cell Sci.*, 119(6), p. 989 LP-994. doi: 10.1242/jcs.02893.

Zeng, X. R., Hao, H., Jiang, Y. and Lee, M. Y. (1994) Regulation of human DNA polymerase delta during the cell cycle., *J. Biol. Chem.*, 269(39), pp. 24027–33.

Zhdanov, V. P. (2009) Conditions of appreciable influence of microRNA on a large number of target mRNAs, *Mol. Biosyst.*, 5(6), p. 638. doi: 10.1039/b808095j.

Ziębacz, N., Wieczorek, S. A., Kalwarczyk, T., Fiałkowski, M. and Hołyst, R. (2011) Crossover regime for the diffusion of nanoparticles in polyethylene glycol solutions: influence of the depletion layer, *Soft Matter*, 7(16), pp. 7181–7186. doi: 10.1039/c0sm01357a.

Zieve, G. W., Turnbull, D., Mullins, J. M. and McIntosh, J. R. (1980) Production of large numbers of mitotic mammalian cells by use of the reversible microtubule inhibitor Nocodazole: Nocodazole accumulated mitotic cells, *Exp. Cell Res.* Academic Press, 126(2), pp. 397–405. doi: 10.1016/0014-4827(80)90279-7.

Zimmerman, S. B. and Harrison, B. (1987) Macromolecular crowding increases binding of DNA polymerase to DNA: An adaptive effect, *Biochemistry*, 84(April), pp. 1871–1875. doi: 10.1073/pnas.84.7.1871.

Zimmerman, S. B. and Pheiffer, B. H. (1983) Macromolecular crowding allows blunt-end ligation by DNA ligases from rat liver or Escherichia coli., *Proc. Natl. Acad. Sci.*, 80(19), pp. 5852–5856. doi: 10.1073/pnas.80.19.5852.